DEVELOPMENT OF A LUNG CANCER TARGETING PEPTIDE FOR IMAGING AND DRUG DELIVERY

APPROVED BY SUPERVISORY COMMITTEE

Kathlynn C. Brown, Ph.D.

Ian Corbin, Ph.D.

John Minna, M.D.

Jennifer Kohler Ph.D.

DEDICATION

I would like to first thank my mentor Dr. Kathlynn Brown. Through hard times and moves, she was always encouraging and found the positive in any situation. We could always discuss difficult experiments and come up with new ways to approach the problem. I will be forever grateful of the consistent advice and correction when presenting data. She encourages a healthy workplace where the motto is "Work hard and be nice"

I also need to give thanks to Dr. Michael McGuire for patiently answering my constant questions. He always made time for scientific discussion no matter how busy his own schedule. The waters I waded through would have been much muddier if not for his knowledge, experience, and willingness to share both.

I thank my loving wife Kelsey. Ever supportive of late nights, long hours and moving across country… twice. She always encourages me, despite failures and setbacks, to keep going and to never give up. I thank my kids for waving goodbye to me every morning and giant bear hugs every night when I got back. Finally, I thank God for his gentle guiding hand and tender mercies.

DEVELOPMENT OF A LUNG CANCER TARGETING PEPTIDE FOR IMAGING AND DRUG DELIVERY

by

CURTIS ALLRED

DISSERTATION / THESIS

Presented to the Faculty of the Graduate School of Biomedical Sciences

The University of Texas Southwestern Medical Center at Dallas

In Partial Fulfillment of the Requirements

For the Degree of

DOCTOR OF PHILOSOPHY

The University of Texas Southwestern Medical Center at Dallas

Dallas, Texas

May, 2018

DEVELOPMENT OF A LUNG CANCER TARGETING PEPTIDE FOR

IMAGING AND DRUG DELIVERY

Curtis Allred

The University of Texas Southwestern Medical Center at Dallas, 2017

Kathlynn Brown, Ph.D.

Lung cancer kills more people in the United Stated than the next three biggest cancer killers combined. Non-small cell lung cancer (NSCLC) accounts for 85% of lung cancer patients and has an overall estimated 5-year survival of 18% in 2017. The emergence of targeted therapies (molecularly guided treatment) has improved the overall survival and quality of life of ~20% of NSCLC patients. A different molecularly guided treatment modality, targeting therapy, has shown success in other cancer types, but has not yet been successfully applied in NSCLC.

Peptides are a class of molecules that have demonstrated exquisite targeting of cancer cells. HCC15.2 peptide was identified from a phage display library screen on NSCLC cells. It

binds to an unknown receptor on a specific subset of NSCLC patient samples (24%) and cell lines (50%), which is not present in immortalized but non-transformed human bronchial epithelial cells (HBEC). Not only does HCC15.2 have a high affinity of ~5 nM and high specificity, it also triggers internalization and delivers its cargo into the cancer cell.

HCC15.2 was optimized by altering the multimerization and amino acid content and protecting it from serum degradation. After the optimizations, HCC15.2 was shown to deliver many cargo types into cancer cells which traffic to and accumulate in lysosomes. HCC15.2 also demonstrated its ability to home to a subcutaneous xenograft in mice ~30-fold better than non-targeted dye after systemic delivery. This peptide used in molecular imaging could aid in earlier tumor detection, which correlates with better patient survival. HCC15.2 conjugated to saporin, a ribosome inactivating protein, showed an IC50 of 5.4 nM in *in vitro* viability assays. Delivery of saporin by HCC15.2 significantly slowed the growth of tumor xenografts. HCC15.2 is a perfect candidate for molecularly guided imaging and therapy.

Table of Contents

Table of Figures

List of Tables

List of Abbreviations

A – Alanine

Ac – Acetylated

ADC – Antibody-drug conjugate

ADCC – Antibody dependent cell cytotoxicity

AJCC – American Joint Committee on Cancer

ALK – Anaplastic lymphoma kinase

ALL – Acute lymphoblastic leukemia

Arf6 – ADP-ribosylation factor 6

ATA – Anti-toxin antibodies

Cav1 – caveolin-1

CHC1 – Clathrin heavy chain 1

CHC2 – Clathrin heavy chain 2

CIE – Clathrin-independent endocytic

CLIC – Clathrin-independent carrier

CME – Clathrin mediated endocytosis

c-MET – Tyrosine-protein kinase Met

CT – Computed tomography

CTXB – Cholera toxin B

DCM – Dichloromethane

DMF – N,N-Dimethylmethanamide

EDT – 1,2-Ethanedithiol

EFS – Event free survival

EGFR – Epidermal growth factor receptor

EIPA – 5-(N-Ethyl-N-isopropyl) amiloride

F – Phenylalanine

GEEC – GPI-enriched endocytic compartment

GPI_AP – Glycosylphosphatidylinositol-anchored protein

HBEC – Human bronchial epithelial cell

HCTU – 2-(6-Chloro-1H-benzotriazole-1-yl)-1,1,3,3-tetramethylaminium hexafluorophosphate

HER2 – Human epidermal growth factor receptor

HGF – Hepatocyte growth factor

HGFR – Hepatocyte growth factor receptor

HL – Hodgkin's lymphoma

Ldct – Low-dose computed tomography

LRP1 – Low-density lipoprotein receptor-related protein 1

mc – Maleimide caproic acid

MMAE – Monomethyl auristatin E

MMAF – Monomethyl auristatin F

MMPP – Magnesium monoperoxyphthalate hexahydrate

MβCD – Methyl-beta-cyclodextrin

NIR – Near-infrared imaging

NK-1R – Neurokinin-1 receptor

NSCLC – Non-small cell lung cancer

ORR – Overall response rate

OS – Overall survival

P – Proline

PAB – Para-amino benzyl alcohol

PD-1 – Programmed cell death 1

PDC – Peptide drug conjugate

PDI – Protein disulfide-isomerase

PD-L1 – Programmed cell death ligand 1

PE – Pseudomonas exotoxin A

PEG – Polyethylnene glycol

PET – Positron emission tomography

PFS – Progression free survival

PI3K – Phosphoinositide 3 kinase

RIP – Ribosome inactivating proteins

ROI – Region of interest

ROS-1 – c-ros oncogene 1

RTK – Receptor tyrosine kinase

SA – Streptavidin

T – Threonine

T-DM1 – Trastuzumab-emtansine

TFA – 2,2,2-Trifluoroacetic acid

TIPS – Triisopropylsilane

TMA – Tissue microarray

TNM – Tumor, Nodes, Metastases

TRE – Total radiant efficiency

VC – Valine citrulline

VEGF – Vascular endothelial growth factor

VEGFR – Vascular endothelial growth factor Receptor

VLS – Vascular leak syndrome

WGA – Wheat germ agglutinin

Chapter 1 Current State of Lung Cancer Treatments

1.1 Introduction

Smoking remains the single largest preventable cause of death among Americans. Anti-smoking public health campaigns have successfully decreased the prevalence of smoking, which in turn has decreased lung cancer rates in America. However, lung cancer was still responsible for 26.5% of cancer deaths in 2016, killing as many people as the next four biggest cancer killers combined; breast, prostate, colorectal, and pancreatic [2]. Further, the incidence of lung cancer in those who have never smoked is on the rise.

There are two main contributing factors to the deadliness of lung cancer. First, patients often do not present symptoms until the cancer is advanced. Nearly 60% of patients already have metastatic disease upon diagnosis, which corresponds to a dismal 4% 5-year survival rate (Figure 1-1). The NIH NCI home page for lung cancer says it best "For most patients with lung cancer, current treatments do not cure the cancer." Only 16% of patients are diagnosed when the disease is localized and considered

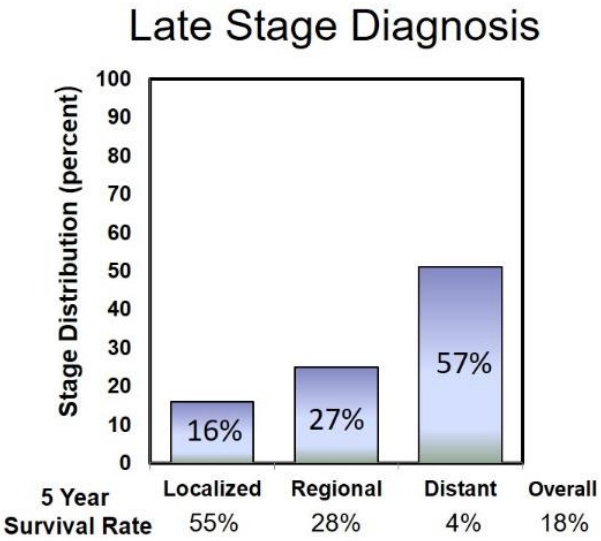

Figure 1-1 Late Stage Diagnosis Correlates with Poor Prognosis
Statistics from ACS Cancer Facts and Figures 2017 [1]. 57% of NSCLC patients are diagnosed after cancer is metastatic.

curable. These patients have a 55% 5-year survival rate. The earlier the cancer is detected, the better the patient outcome.

The second major problem facing NSCLC patients is that lung cancer is a collection of heterogeneous diseases. Lung cancer is divided into two major types, small cell (13%) and non-small cell (NSCLC) (83%). NSCLC is pathologically subdivided further to adenocarcinoma (40%), squamous (25%), large cell (15%) and a few others [4]. Complicating matters further, is the wide range of mutations and oncogenic drivers present in the different subtypes. Figure 1-2, demonstrates the spectra of known mutations that commonly occur in adenocarcinomas and squamous cell carcinomas. For example, Ras and EGFR are mutated in ~30% and ~15% of adenocarcinoma cases respectively and both are rarely found in squamous cell carcinoma cases. Even though cancers may be grouped together, patients can respond differently to treatments depending on the pathological grouping and mutational status.

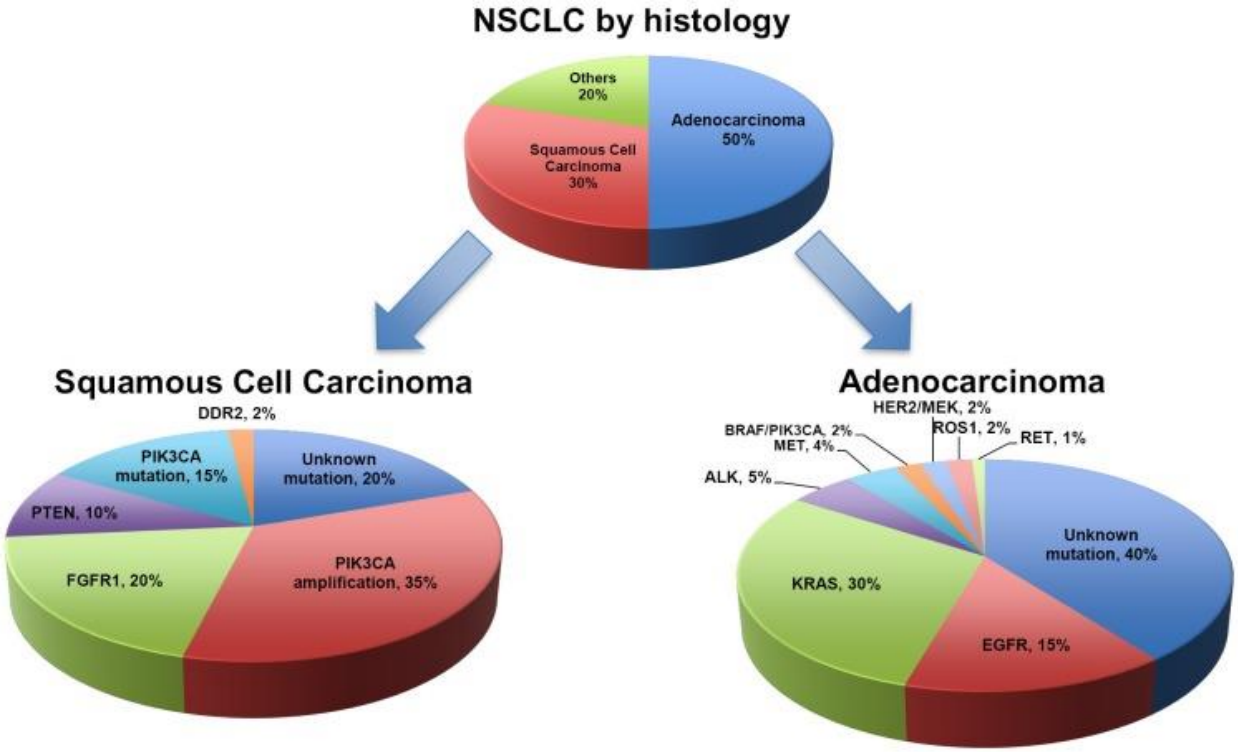

Figure 1-2 Lung Cancer is a Collection of Heterogeneous Diseases
Mutational status of NSCLC patients varies, especially between pathological subgroups [3].

However, both of these problems, late stage diagnosis and heterogeneity, could be solved in part by identifying and exploiting novel biomarkers. Molecular imaging using biomarkers or ligands could greatly increase the contrast between cancer and other non-cancerous tissues for diagnosing lung cancer earlier during screening. Molecular targeting using biomarkers or ligands has already demonstrated efficacy in a small percentage of patients in the form of targeted and targeting therapies. This highlights an urgent need for new biomarkers and ligands that can be developed into effective imaging agents and targeting therapies. Peptides are a class of targeting molecules ideal for both applications.

1.2 Current Clinical Practices in NSCLC

1.2.1 Diagnostic Procedures

Chest x-rays were the standard diagnostic procedure for many years as computed tomography (CT) scans expose the patient to more radiation. Low-dose computed tomography (LDCT) is now the standard diagnostic procedure, which produces better resolution than x-rays and less radiation than standard CT. In an effort to detect cancer earlier among those at high risk, a widespread annual LDCT screen resulted in a 15–20% increase in survival [5]. However, about 95% of scans and follow-up x-rays ended up being false positives. A new study, UKLS, solved this problem with a more structured protocol for the management of nodules and reduced the false positive rate to 3.6% [6].

If metastases are suspected, further imaging as well as guided biopsies will likely be required for confirmation. In this case, contrast CT combined with FDG PET imaging is a very sensitive way to find metastases in the liver or bone. If CNS metastases are suspected, MRI will likely be required [7]. Practically all patients who present with possible lung cancer require

verification by tissue biopsy. This can help guide molecularly based treatments. Fiberoptic bronchoscopy, endobronchial ultrasound or endoscopic ultrasound-guided needle aspirations, CT-guided coaxial core biopsy, cervical mediastinoscopy, or thoracoscopy-guided biopsies are all used depending on where the tumor is located. Generally, the least invasive procedures are preferred as long as the required amount of tissue can be acquired. Lymph nodes and possible metastases are also biopsied for staging purposes [8].

1.2.2 Current Staging Practices

Therapies are guided by a number of different factors. First and most important is the stage of disease as described by the Tumor, Nodes, Metastasized (TNM) system from the American Joint Committee on Cancer (AJCC). Next is the pathology, then molecular profile, and lastly the fitness of the patient. All of these factors guide the treatment of the patient.

In the TNM system, the tumor is ranked from 0–4; T0 being no evidence of tumor, to T4 where the tumor is large and/or causing significant problems, such as growing in and around the airways or aorta. The nodes are measured from 0–3; N0 being no evidence in lymph nodes, to N3 where far lymph nodes contain cancer, such as the opposite lung or in the supraclavicular lymph nodes. Metastasis is measured from 0–1b. M0 is no metastasis, M1a cancer has spread within the pleural cavity, M1b is spread to other organs. For lung cancer, M1b metastases are commonly found in the brain, bones, or liver [9].

Staging a tumor depends on all three factors. Stage IA tumors are defined as up to T1b, N0, M0 and can be resected with no adjuvant therapy. Stage II patients are defined as T2b, N1, M0 or T3, N0, M0. This corresponds to a moderately sized tumor with very little or no lymph node involvement, no metastasis, and is generally treated with surgery and adjuvant chemotherapy.

Stage IIIA patients are defined as T1-3, N2, M0; T3, N1, M0; or T4, N0-1, M0. The surrounding lymph nodes are removed and chemotherapy, radiation therapy, or both are administered. Because of the complexity of other factors, such as where the tumor is growing, each case at this point is looked at separately. A patient may even receive chemotherapy, then surgical resection, then radiotherapy.

Stage IIIB-IV treatment is almost always non-curative and meant to prolong and improve quality of life. These stages have major lymph node involvement and/or metastasis, up to T4, N3, M1b. The majority (nearly 60%) of patients are diagnosed in these stages. There are many approved therapies for these patients and treatment options get complicated, each prolonging life by months [10].

1.2.3 Chemotherapies Currently Used in NSCLC

Chemotherapies are a class of molecules that target all rapidly growing and actively dividing cells. Cancer cells are rapidly dividing, but so are many other healthy cell types, such as skin, hair, gut, and blood cells. Chemotherapies also affect these other cell types and have serious adverse side effects for the patient. Because of the toxicity to normal cells, patients are treated at a maximal tolerable dose and not necessarily at the maximal effective dose to kill the cancer. Virtually all cancers have the phenotype of rapid division, therefore chemotherapies can be broadly applied to most cancers and are the only treatment available for many cancer patients.

1.2.3.1 Platinum

For standard of care, NSCLC patients are provided with combination therapy consisting of one platinum drug and one other small molecule chemotherapeutic. The platinum drugs, cisplatin (Platinol) and carboplatin (Paraplatin, Bristol-Myers Squibb, New York City, NY) are

both DNA alkylating agents and cause DNA damage to rapidly dividing cells. They are especially toxic to cancers deficient in DNA repair [11].

1.2.3.2 Chemotherapy

The cytotoxic drugs are more varying in function. Vinorelbine (Navelbine, Pierre Fabre, Parsippany, NJ) belongs to a class of molecules called vinca alkaloids, which destabilize microtubule formation. Docetaxel (Docefrez, Sun Pharma Global, Mumbai, India) (Taxotere, Sanofi-Aventis, Paris, France), and Paclitaxel (Taxol, Bristol-Myers Squibb, New York City, NY), belong to the family of taxanes which also act to stabilize tubulin, which inhibits cell division [12]. Pemetrexed (Alimta, Eli Lilly, Indianapolis, IN) is an antifolate which halts purine and pyrimidine synthesis [13]. Gemcitabine (Gemzar, Pfizer, New York City, NY) is a nucleoside which is incorporated into DNA in place of cytosine and halts further synthesis. Etoposide (Etopophos, Bristol-Myers Squibb, New York City, NY) is a podophyllotoxin which inhibits topoisomerase [12]. While different in toxicity profiles, these drugs all have very similar efficacies in patients A study in 2002 determined that different combinations of platinum with certain cytotoxics were statistically the same [14].

1.2.4 Current FDA Approved Targeted Therapies Against the Tumors

Targeted therapies have created a paradigm shift in the way cancer is treated. Molecularly based subgroups are now becoming the most important classification. Oncogenes and driver mutations are proteins that the cancer has become dependent upon (addiction). Overexpression or mutations in these proteins open a therapeutic window between cancer and normal cells. This allows reagents such as monoclonal antibodies and small molecule inhibitors to target cancer with less off-target effects to healthy cells. Patients who receive targeted therapies generally have fewer and less severe side effects during treatment and a longer progression free survival.

Targeted therapies address some of the major problems associated with cytotoxic chemotherapy. They effectively treat patients who have already received chemotherapy and relapsed with resistance. Many also work well as first line therapies, and the toxicity profiles are generally less severe compared to general cytotoxic chemotherapy. However, these treatments have some of their own drawbacks as well. Targeted therapies apply only to patients whose cancer contains a specific target. In lung cancer, targeted therapies apply to less than 10% of patients. Another hurdle that all targeted therapy treatments face is the development of resistance. This has partially been countered by next generation therapeutics to the same target. In some cases, second and third line treatments are now available, but only to the same small subpopulation of patients.

1.2.4.1 EGFR

Epidermal growth factor receptor (EGFR) is mutated in ~15% of adenocarcinoma tumors and rarely in squamous. These mutations are also more common in those of Asian descent, women and never smokers. The most seen mutations are deletions of exon 19 and L858R point mutation [15]. These changes constitutively activate EGFR signaling, which results in uncontrolled growth. EGFR has multiple generations of tyrosine kinase inhibitors (TKIs) available to target mutant EGFR and resistant forms that arise from EGFR inhibition.

Erlotinib (Tarceva, Genentech, San Fransisco CA) and Gefitinib (Iressa, AstraZeneca, Cambridge, United Kingdom) were the first targeted therapies in NSCLC. In 2004 the FDA approved erlotinib as a second line therapy. This decision was based on results from a clinical trial that showed increase in the median overall survival (OS) by 2 months. Upon retroactive analysis, it was found that among the EGFR-mutant-positive patients, the difference in median OS was even greater, 10.7 vs 3.8 months in the EGFR negative group [16]. In 2006 a phase III

clinical trial in east Asia showed the 12-month progression-free survival (PFS) was significantly higher for the gefitinib treated vs the chemo groups (24.9% vs 6.7% respectively). Both of these studies did not have stunning results, but in retrospective analysis, patients in whom EGFR was mutated responded to gefitinib with a significantly longer PFS than chemotherapy. Those who had no mutations and received gefitinib had significantly shorter PFS than chemo. Gefitinib and erlotinib both had reduced toxic side effects compared to standard of care chemotherapy. These FDA approvals were as second line treatment only for both drugs, irrespective of EGFR mutational status.

Guided by these results, the OPTIMAL trial in China compared erlotinib and chemotherapy groups of patients who had EGFR mutations. They found a PFS of 13.1 months for erlotinib vs 4.6 for chemotherapy, a significant improvement [17]. EURTAC or NCT00446225 was similarly set up in Europe, and they saw an improvement of 4.5 months in PFS in the erlotinib arm vs chemotherapy (9.7 months vs 5.2 months respectively) [18]. These results led to the FDA approval of erlotinib as a first line treatment for patients with either the exon 19 deletion or L858R point mutation in 2013. Gefitinib was similarly tried in molecularly selected patients in clinical trials NEJ002 and WJTOG3405. They reported 5.4-month and 2.9-month PFS benefit, respectively, over chemotherapy treated groups [19]. Gefitinib was also approved in 2015 for first line use in patients with specific mutations.

Afatinib (Gilotrif, Boehringer Ingelheim, Ingelheim am Rhein, Germany) is a second-generation EGFR TKI that differs from erlotinib and gefitinib in a few important ways. Afatinib has activity against HER2 and EGFR, and more importantly against the T790M mutant that confers resistance to first generation EGFR inhibitors [20]. It is also a covalent suicide inhibitor instead of reversible like the first generation [21]. Afatinib was approved in 2013 based on the

results from the LUX-Lung 6 trial where it was found that afatinib increased the PFS from 5.6 months to 11 months [22]

Osimertinib (Tagrisso, AstraZeneca, Cambridge, United Kingdom) is a third generation irreversible EGFR TKI that targets the T790M mutant and does not bind the wild-type EGFR. This confers the benefit of less off target toxicities [23]. In AURA3, a phase III clinical trial, osimertinib increased the PFS from 4.4 months to 10.1 months in patients with T790M mutations [24].

Necitumumab (Portrazza, Eli Lilly, Indianapolis, IN) was approved in November 2015 for the first line treatment of metastatic squamous cell carcinoma in conjunction with combination chemotherapy. This monoclonal anti-EGFR antibody received approval based on results from a phase III clinical trial where portrazza plus gemcitabine and cisplatin increased the OS of patients by 1.6 months compared to chemotherapy alone. In this case both minor and major adverse reactions were higher in the portrazza group, but deemed acceptable [25].

1.2.4.2 ALK/ROS-1 Rearrangements

Anaplastic lymphoma kinase (ALK) and c-ros oncogene 1 (ROS-1) are related receptor tyrosine kinases that can be oncogenic drivers. Chromosomal rearrangements, which lead to fusion proteins, constitutively activate these proteins in ~4% (ALK) and ~1–2% (ROS-1) of NSCLC patients. ALK often fuses with EML4 and ROS-1 often fuses with CD74 [26]. Crizotinib (Xalkori, Pfizer, New York City, NY) is a first line tyrosine kinase inhibitor (TKI), with FDA approval for use first with ALK (2011) and more recently with ROS-1 (2016). It also inhibits tyrosine-protein kinase Met (c-MET) or hepatocyte growth factor receptor (HGFR), but NSCLC rarely contains c-MET kinase activating mutations [27]. Crizotinib competitively binds the ATP pocket of the fusion protein, causing G1-S phase cell cycle arrest and apoptosis [28].

While patients respond favorably, most cases progress after 8–12 months either due to further changes in ALK or to compensatory pathway activation, such as EGFR or Ras [29]. It is also noted that crizotinib has little or no effect on CNS metastasis as it has poor blood-brain barrier penetration [30].

Two clinical trials showed the efficacy of crizotinib in patients with ALK fusions, after which it gained FDA approval. Profile-1007 was a phase III trial for patients that had progressed after chemotherapy and had the ALK rearrangement. The PFS for the crizotinib group was 7.7 months compared to 3 months for those on chemotherapy. In a phase III clinical trial (PROFILE 1014) patients with ALK fusion and no previous treatments were either treated with crizotinib or cytotoxic chemotherapy. The PFS for crizotinib again showed a significant improvement over standard of care at 10.9 to 7 months respectively [31].

In 2014, the FDA approved ceritinib (Zykadia, Novartis, East Hanover, NJ) for relapsed patients after crizotinib treatment, which was expanded to first line treatment in May 2017 [32]. In a phase 3 clinical trial, NCT01828099, ceritinib showed a PFS of 16.6 months compared to the 8.1 months in the chemotherapy group[33]. Ceritinib is able to treat most patients who stop responding to crizotinib and is more effective at treating CNS lesions.

Alectinib (Alecensa, Genentech, San Fransisco, CA) was approved as a second line therapy after crizotinib treatment relapse in 2015 and also shows good efficacy against CNS metastasis [34]. In a recent phase III trial, alectinib was assessed to have a higher PFS vs crizotinib in first line treatment as measured at 12 months (68.4% vs 48.7%), but has yet to be approved as a first line therapy.

Brigatinib (Alunbrig, Ariad, Cambridge, MA) recently received accelerated approval as a second line therapy in 2017 based on preliminary results from a phase II trial showing tumor

shrinkage in about 50% of patients [35, 36]. These drugs could conceivably be used one after the other after patients stop responding to previous treatments, which could significantly improve survival. However, these treatments are only for the same ~5% of all adenocarcinoma cases.

1.2.4.3 B-Raf

B-Raf is mutated in 1–2% of adenocarcinoma cases. This mutation occurs on amino acid 599 where a valine is mutated to a glutamic acid (V599E). This mutation acts to destabilize the inactive form of the protein, likely by mimicking an activating phosphorylation [37]. This allows B-Raf to signal downstream to MEK and ERK1/2 independently of Ras signaling. B-Raf activating mutations corresponds with a poorer prognosis in those that receive standard of care, highlighting the need for targeted therapies for these patients.

In 2 arms of a multicenter phase (II) clinical trial NCT01336634, two drugs previously approved for treatment of B-Raf-positive tumors in melanoma were tested in B-Raf -positive NSCLC patients. B-Raf (V600E) inhibitor Dabrafenib (Tafinlar, Novartis, East Hanover, NJ) as a monotherapy or in combination with MEK inhibitor Tramentinib (Mekinist, Novartis, East Hanover, NJ). While final results still remain unpublished, the combination therapy had an OR of 63% with a PFS of 9.7 months, and the dabrafenib monotherapy group had an OR of 33% with a PFS of 5.5 months[38]. Patients with the same mutations that received standard of care chemotherapy had an OR of 9% and PFS of 3.1 months [38, 39]. This led to the approval of the combination therapy in June 2017 for patients testing positive for the B-Raf V600E mutation. However, in an editorial, the authors noted the difficulty in running such a trial. Approximately 6000 patients were screened to recruit 59 patients.

1.2.5 Targeted Therapies also Target Tumor Environment

1.2.5.1 Angiogenesis

Angiogenesis is a crucial part of tumorigenesis. As the tumor grows, it requires more and more oxygen and nutrients. It begins releasing vascular endothelial growth factor (VEGF) to recruit new blood vessels to the site of the tumor. There is no order and the vessels are described as “leaky” and their course “torturous.” This makes tumors susceptible to anti-angiogenic treatments. With poor vasculature and nutrients to begin with, any perturbation can help starve the tumor.

Bevacizumab (Avastin®, Genentech, South San Francisco, CA) was approved in 2006 for the first line treatment of non-squamous NSCLC in combination with carboplatin and paclitaxel. It was the first angiogenesis treatment available and is an anti VEGF-A monoclonal antibody. This decision came mainly from a phase III clinical trial, ECOG E4599. Bevacizumab was given in combination with carboplatin and paclitaxel to non-squamous NSCLC patients, where an increased OS was seen in the bevacizumab group, 12.3 months vs 10.3 months, and the PFS was 6.2 months vs 4.5 months compared to chemotherapy alone. There was also a 4.4% serious adverse event rate of hemoptysis despite the precautions of excluding squamous-type cancers and others at risk for bleeding [40].

Ramucirumab (CYRAMZA, Eli Lilly, Indianapolis, IN) is a monoclonal antibody that binds to VEGF receptor 2, blocking VEGF from signaling. It was approved in December 2014 for second line use in combination with docetaxel. In a phase III clinical trial, REVEL, relapsed patients were treated with ramucirumab plus docetaxel or with docetaxel alone. Ramucirumab was able to increase the OS by 1.4 months (10.5 months vs 9.1 months)[41]. This met some

needs left by bevacizumab, namely for squamous and second line patients. It is also currently being tested as a first line therapy.

1.2.5.2 Immunotherapies

Immunotherapies are a class of targeted therapies that essentially take the brakes off the immune system in patients with cancer. Programmed cell death 1 (PD-1) is a cell surface receptor found on t-cells that when activated by its ligand programmed cell death ligand 1, (PD-L1) which is often overexpressed in tumors, will produce an inhibitory signal. It is an important pathway in avoiding autoimmunity in the body. Cancer cells that express PD-L1 are more likely to survive when cancer neo-antigens arise.

Pembrolizumab (Keytruda, Merck, Darmstadt, Germany) received accelerated approval in October 2015 for the second line treatment of PD-L1 positive tumors. KEYNOTE-010 showed that the PD-L1 positive patients responded to Keytruda treatment with an OS of 14.9 months vs 8.2 months, a significant increase [42]. 1 year later, this approval was expanded to a firstline treatment for those who have 50% or more PD-L1 expression on the tumor. In the phase III clinical trial KEYNOTE-024, pembrolizumab treatment extended the PFS by 4.3 months (10.3 months vs 6 months in the chemotherapy alone) [43]. Most recently, in May 2017, Pembrolizumab was granted accelerated approval for use in combination with carboplatin and pemetrexed as a first line therapy regardless of PD-L1 expression, as long as mutations that can be treated with other targeted therapies are absent. KEYNOTE-021 showed a 55% objective response OR compared to 29% for the chemotherapy alone. The PFS was 13 months vs 8.9 months respectively.

Nivolumab (OPDIVO®, Bristol-Myers Squibb, New York City, NY) is an anti PD-1 IgG4 monoclonal antibody that gained approval as a second line therapy for relapsed patients in

March 2015. This immunotherapy was approved based on the results of 2 clinical trials checkmate 057 and checkmate 017 which both improved OS by nearly 3 months [44, 45]. The FDA also cited checkmate 063, a phase II clinical trial showing the safety of the treatment [46]. It was also noted that this treatment helped no matter the PD-L1 expression of the tumor.

Atezolizumab (TECENTRIQ, Genentech, South San Francisco, CA), an anti-PD-L1 monoclonal IgG1, was approved for second line use in October 2016. This was based on 2 clinical trials, POPLAR and OAK. In these phase III trials, the OS was 12.6 months vs 9.7 months (atezolizumab vs chemotherapy) and 13.8 months vs 9.6 months respectively [47, 48]. These patients also had less abundant and less severe adverse events.

1.2.6 Potential Targeted Therapies for NSCLC

1.2.6.1 Angiogenesis

Nintedanib (Vargatef®, Boehringer Ingelheim, Ingelheim am Rhein, Germany) is a triple angiokinase inhibitor that has been approved in the EU since 2014 but is still not approved in the US. There have been other TKIs for VEGFR in many trials that have shown little or no effect in the patient populations tried despite extensive testing. Vandetanib (Caprelsa, Sanofi Genzyme, Paris, France) and sorafenib (NEXAVAR, Bayer Pharmaceuticals, Berlin, Germany) being the most extensively tested [49].

1.2.6.2 Immunotherapies

There are 4 more ongoing phase III trials for other immune checkpoint-inhibiting antibodies that could soon receive FDA approval. Ipilimumab (YERVOY, Bristol-Meyers Squibb, New York City, NY), and Tremelimumab (AstraZeneca, Cambridge, United Kingdom) are both anti-CTLA4 monoclonal antibodies. Durvalumab (Imfinzi, AstraZeneca, Cambridge,

United Kingdom), and Avelumab (Bavencio, Merck KGaA & Pfizer) are anti-PD-L1 antibodies similar to atezolizumab [50].

1.2.6.3 HER2/ERBB2/NEU

Human epidermal growth factor receptor (HER2) has been developed as a target extensively in breast cancer patients. Due to its success in HER2 positive breast cancer, Trastuzumab (Herceptin, Genentech, San Francisco, CA) has also been tested on HER2 positive NSCLC. HER2 overexpression occurs in 6–35%, amplification in 10–20%, and mutations in ≤4% of NSCLC cases [51]. Targeted therapies for HER2 have so far been unsuccessful in significantly meeting endpoints in clinical trials [52]. However it has been noted that patients with very high HER2 overexpression did see benefit from trastuzumab plus chemotherapy treatment [53]. HER2 targeted therapy might also have some benefit for those who harbor HER2 mutations [54]. Both scenarios have yet to be further studied in NSCLC. There are currently several clinical trials for Trastuzumab-emtansine (T-DM1) for patients with HER2 positive NSCLC.

1.2.6.4 MET/c-MET/HGFR

MET is the natural RTK of the hepatocyte growth factor (HGF) and can be overexpressed or mutated in 2–4% of previously untreated NSCLC. MET overexpression is also a common mechanism of acquiring resistance to EGFR TKIs and is present in 5–20% of patients previously treated with EGFR TKIs [55]. Two phase II studies using erlotinib plus tivantinib (Arqule, Burlington, MA) (a MET selective TKI) vs erlotinib failed to meet primary endpoints of improvement in OS and PFS. However retrospective analysis of MET-high patients showed substantial improvement [56]. NCT01580735 also failed to meet primary endpoints, but also showed benefit to MET-high patients [57]. In a case study, a single patient that had MET

amplification was treated with crizotinib, showing a major partial response despite having no ALK rearrangement or MET mutations [58]. This has good potential for use in a fewer number of patients that express very high levels of MET.

1.2.6.5 Ras

Ras is the most commonly mutated oncogenic driver in NSCLC, and 78% of those mutations happen at the twelfth amino acid glycine [59]. Ras mutations are common not only in lung cancer but also in many others such as pancreatic cancer (95%) [60]. Despite decades of research, no targeted therapy is yet available for Ras. It is difficult to find good small molecule inhibition to RAS for a number of reasons. First, it is a small protein with poor "binding pockets" for small molecules to bind to, and small molecules are generally poor at disrupting protein-protein interactions. Second, RAS is required for normal cell function and disruption of normal RAS causes high toxicities in patients. Much research has also been devoted to downstream effectors such as RAF, MEK, ERK, AKT, mTOR, and PI3K. But none of these have effectively treated patients with RAS mutant cancers [61].

1.3 Targeting Therapies

Targeted therapies began a new focus on molecularly guided treatments. Patients respond more quickly, for longer, and with fewer side effects. Current targeted therapies for cancer are generally either antibodies or small molecule drugs. Development for both requires a known target and lots of difficult and expensive optimizations. Only 15 protein targets across all types of cancer have clinically approved antibody targeted therapies [62], and most of these are only present on a fraction of cancer cases. EGFR activating mutations have a host of small molecule inhibitors and an inactivating antibody in clinical use [63], but these treatments only apply to 5–10% of NSCLC patients[64]. There are only so many oncogenic drivers that are targetable by

small molecules or antibodies. Despite decades of research, Ras has no clinically useful small molecule inhibitors, and is not targetable by antibodies because it is intracellular.

While targeted therapies focus on treating a certain molecular feature on which the cancer is dependent, such as protein overexpression or mutation, targeting therapies focus on using that feature to deliver a toxic payload to cancer. This is a significant advantage over targeted therapies, as the target does not need to be critical to the tumors functionality, potentially increasing the number of biomarkers available for targeting. So far, most targeting therapies being developed are in the form of antibody-drug conjugates (ADCs). There are only 4 clinically approved targeting therapies available for cancer treatment, none of which are approved for use in lung cancer. All of these targeting therapies are ADCs and have similar mechanisms of action to one another. An antibody to an overexpressed protein is conjugated to a highly toxic molecule via a cleavable or non-cleavable linker. After internalization of the ADC, the therapeutic is released from the antibody inside the cell, where it seeks its target and destroys the cell.

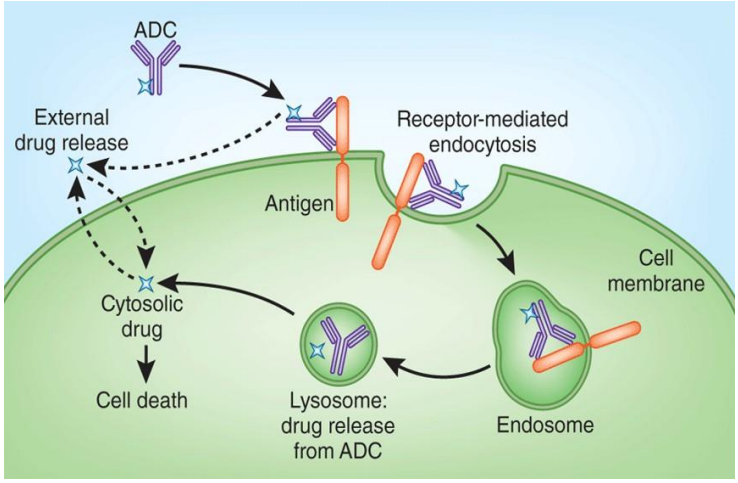

Figure 1-3 Antibody Drug Conjugates are Examples of Targeting Therapies
Mechanism of Action of Adcetris for the treatment of Hodgkin's lymphoma [67].

1.3.1 Clinically Approved Antibody-Drug Conjugates

1.3.1.1 Mylotarg (Gemtuzumab Ozogamicin)

Gemtuzumab ozogamicin (Mylotarg, Pfizer, New York City, NY) is an anti-CD33 monoclonal antibody conjugated to ozogamicin, a calicheamicin analog. This therapeutic causes

DNA strand scission [65]. It was initially given accelerated approval as a second line therapy for CD33 positive AML in 2000. It failed to meet endpoints in later clinical trials and even caused some high toxicities and early deaths. For these reasons Pfizer voluntarily pulled the drug from the market in 2010 [66]. After redesigning dosing and population treatment strategies, Mylotarg again received FDA approval in October 2017. It was tested in newly diagnosed AML patients with high CD33 expression and it was given in combination with chemotherapy vs chemotherapy alone. The median event free survival (EFS) was nearly double that of chemotherapy alone, 17.3 months vs 9.5 respectively [67]. Two other trials also showed limited benefit to select patients as a single agent. Median OS was improved from 3.6 months to 4.9 months. The other trial had no randomized control group, and the median PFS was 11.6 months. While it received approval for those patients, it needs to be more thoroughly studied [68, 69]. The initial toxicities found are still of concern, but the dosage was lowered and they are only giving it to patients they predict will respond. In these cases, the benefits outweigh the risk.

1.3.1.2 Adcetris (Brentuximab Vedotin)

Brentuximab vedotin (Adcetris, Seattle Genetics, Bothell, WA) is an anti-CD30 monoclonal antibody conjugated to monomethyl auristatin E (MMAE), a potent microtubule inhibitor. A pivotal phase II trial in CD30-positive patients with Hodgkin's lymphoma (HL) gained it accelerated approval in 2011. Relapsed patients were treated with adcetris and had an ORR of 73% with a complete remission rate of 32% and partial remission of 40%. [70] A second trial gained it accelerated approval in the second line treatment of CD30 positive ALCL patients. Relapsed patients treated with adcetris had an ORR of 86% with a complete remission rate of 57% and a partial remission rate of 29% [71].

1.3.1.3 Kadcyla® (T-DM1, Trastuzumab Emtansine)

T-DM1 (Kadcyla, Genentech, South San Francisco, CA) is the first and only current ADC approved for solid tumor treatment. Trastuzumab (Herceptin, Genentech, South San Francisco, CA) has been a targeted therapy in HER2-positive breast cancers since 2010, but patients relapse and become resistant to trastuzumab therapy. Trastuzumab was conjugated to emtansine, which is a microtubule destabilizer [12], and tested in patients who had relapsed after previous HER2 targeted therapies. Results from a phase III clinical trial increased OS from 25.1 months to 30.9 months with T-DM1 single therapy treatment vs standard of care [72]. Based on these results, the FDA granted approval in February 2013. Two later clinical trials showed significant improvement in the median OS of patients treated with T-DM1 as a single agent vs standard of care. The EMILIA trial showed a 4-month improvement (29.9 months vs 25.9 months respectively) and the TH3RESA trial showed a 6.9-month improvement (22.7 months vs 15.8 months respectively) [73, 74]. It is very well tolerated in patients and benefits those who have relapsed previously, significantly extending life. T-DM1 is currently being tested in clinical trials in patients with HER2-positive NSCLC

1.3.1.4 Besponsa (Inotuzumab-ozogamicin)

Inotuzumab-ozogamicin (Besponsa, Pfizer, New York City, NY) is an anti-CD22 monoclonal antibody conjugated to ozogamicin. Acute lymphoblastic leukemia (ALL) patients whose cancer contains the Philadelphia chromosome and who have already progressed after other targeted therapies can be treated with Besponsa as of September 2017. In a phase III clinical trial called INO-VATE ALL, 80.7% of patients who received Besponsa had a complete remission compared to 29.4% in the standard of care. The PFS was also significantly higher at 5 months vs 1.8 months [75].

1.3.2 Peptide Drug Conjugates

Because of the success of the approved ADC's, there are over one hundred current clinical trials testing different ADC's, most of which are still phase I or II. Ten are currently being tested in NSCLC patients. ADCs suffer from some of the same disadvantages as targeted therapies, such as development of resistance. A major drawback of ADCs is that these treatments are incredibly expensive, in excess of $100,000 for a single course. This is because antibodies themselves are expensive to develop, but ADCs also require additional development, such as drug conjugation, linker, uniformity, etc. However, they offer some important benefits unaddressed by the targeted therapies. Targeting therapies are not limited to oncogenic drivers. They can target nearly any protein that is expressed specifically on the surface of the tumor and can internalize with the therapeutic. They are just a vehicle to get inside the cell; then the payload is released and the cell is killed. This significantly increases the number of proteins targets available. While antibodies are the only currently approved targeting molecules, peptides offer an alternative class of cancer targeting molecules that have other advantages.

Peptides represent another class of targeting molecule with affinity and specificity on par with monoclonal antibodies. There are currently only two peptide drug conjugates (PDCs), being tested in clinical trials. GRN1005 consists of a low-density lipoprotein receptor-related protein 1 (LRP1) targeting peptide Angiopep-2, conjugated to ~3 paclitaxel molecules. GRN1005 is being tested for efficacy against brain metastasis from NSCLC and breast cancer. LRP1 binding allows for transcytosis across the blood-brain barrier, and is often overexpressed in gliomas [76].

The second PDC is not for treating the cancer itself, but for pain in terminal cancer patients. Substance P is an 11-amino acid peptide that is the natural ligand of neurokinin-1 receptor (NK-1R). NK-1R is expressed on neurons associated with pain transduction and anxious

behavior. Saporin was conjugated to substance P and delivered intrathecally, where it kills the pain neurons. As nerve damage is permanent, this treatment is only for terminally ill patients with uncontrolled pain.

1.4 Peptides Offer Advantages in Targeting Therapies

Despite many useful qualities, peptides fell out of favor and antibodies became the gold standard for specific targeting. Antibodies have two distinct advantages for targeting therapy. They are stable molecules with a long serum half-life, which makes administration easier and less frequent than peptides. They also contain other functional domains that recruit immune system involvement, such as antibody dependent cell cytotoxicity (ADCC), that aid in cancer treatment. These advantages are likely why antibodies came to be the preferred targeting molecule, but they come at a cost. Antibody engineering, development, and production is expensive and time consuming. Modifications and conjugations are tricky and inexact, leaving ADCs conjugated to a distribution of therapeutics.

Peptides match antibodies in terms of specificity and affinity to a target but can be synthesized, modified, and optimized relatively cheaply and easily compared to antibodies. Peptides are much smaller and penetrate tumor tissue more deeply, which is critical in delivery to solid tumors. Because they are synthesized, PDCs can be uniform with exact stoichiometric peptide to drug ratios. They could also be produced biologically such as being cloned onto a protein toxin for cancer targeting.

	Advantages	Disadvantages
Peptides	High Affinity High Specificity Tumor Penetration Easily Modified Streamlined Optimization Relatively Inexpensive Chemically Synthesized or Biologically Produced	Rapid Clearance
Antibodies	High Affinity High Specificity Immune Functionality (ADCC) Long Serum Half-life	Difficult to Modify Expensive Less Conjugation Control

Table 1-1 Peptides Offer Many Advantages in Targeting Therapy

Phage display biopanning has successfully been employed to select many peptidic ligands for novel biomarkers present in cancer [77]. These peptides have been used to target dyes and therapeutics specifically to cancer in *in vitro* and *in vivo* studies [78-80]. HCC15.2 is a peptide isolated from phage display that bound to ~54% (21/39) of cell lines tested [81]. It binds to an undetermined molecular biomarker present on a specific subset of NSCLC lines, that is not present on immortalized non-transformed human bronchial epithelial cells. Then binding triggers internalization of HCC15.2 and any cargo it carries, including large nanoparticles. HCC15.2 can act as a perfect targeting molecule, delivering with high affinity virtually any cargo, specifically to a large subset of NSCLC patients.

1.5 Conclusion

Targeted therapies have produced a fundamental shift in the way we treat cancers. This shift has put the focus on molecular targets, in addition to pathology and organ of origination. Targeted therapies increase the survival and quality of life of patients whom they benefit.

Unfortunately, that is only a fraction of cancer patients. Targeting therapies will expand the number of biomarkers we can target, also increasing the number of patients that can benefit from these therapies. Both targeted and targeting therapies cause less severe and less frequent side effects in the patients while increasing the time until relapse.

Peptides are an upcoming class of targeting molecules that increase the toolbox of targeting molecules specific to cancer. Targeting peptides can help alleviate two of the major problems with lung cancer, late stage diagnosis and disease heterogeneity. Imaging agents can be delivered specifically to cancer cells for earlier detection. Then those patients that show positive for peptide binding could receive a targeted peptide therapeutic.

1.6 References

[1] ACS. Cancer Facts and Figures 2017. In: Society AC, editor. Cancer Facts and Figures. Atlanta, GA USA: American Cancer Society; 2017.

[2] ACS. American Cancer Society, Cancer Facts & Figures 2016. 2016.

[3] Chan BA, Hughes BGM. Targeted therapy for non-small cell lung cancer: current standards and the promise of the future. Translational Lung Cancer Research. 2015;4:36-54.

[4] Travis W.D. CTV, Corrin B., Shimosato Y., Brambilla E. Histological Classification of Lung and Pleural Tumours. In: Histological Typing of Lung and Pleural Tumours. Berlin, Heidelberg: Springer; 1999.

[5] The National Lung Screening Trial Research T. Reduced Lung-Cancer Mortality with Low-Dose Computed Tomographic Screening. The New England journal of medicine. 2011;365:395-409.

[6] Blandin Knight S, Crosbie PA, Balata H, Chudziak J, Hussell T, Dive C. Progress and prospects of early detection in lung cancer. Open Biology. 2017;7.

[7] Novello S, Barlesi F, Califano R, Cufer T, Ekman S, Levra MG, et al. Metastatic non-small-cell lung cancer: ESMO Clinical Practice Guidelines for diagnosis, treatment and follow-up†. Annals of Oncology. 2016;27:v1-v27.

[8] Dietel M, Bubendorf L, Dingemans A-MC, Dooms C, Elmberger G, García RC, et al. Diagnostic procedures for non-small-cell lung cancer (NSCLC): recommendations of the European Expert Group. Thorax. 2016;71:177-84.

[9] team TACSmaec. Non-Small Cell Lung Cancer Stages. American Cancer Society; Feb 2016.

[10] Zarogoulidis K, Zarogoulidis P, Darwiche K, Boutsikou E, Machairiotis N, Tsakiridis K, et al. Treatment of non-small cell lung cancer (NSCLC). Journal of Thoracic Disease. 2013;5:S389-S96.

[11] Dasari S, Tchounwou PB. Cisplatin in cancer therapy: molecular mechanisms of action. European journal of pharmacology. 2014;0:364-78.

[12] Weinberg RA. The Biology of Cancer Second Edition. 2 ed. New York: Garland Science, Taylor & Francis Group, LLC; 2014.

[13] Adjei AA. Pharmacology and Mechanism of Action of Pemetrexed. Clinical Lung Cancer. 2004;5:S51-S5.

[14] Schiller JH, Harrington D, Belani CP, Langer C, Sandler A, Krook J, et al. Comparison of Four Chemotherapy Regimens for Advanced Non–Small-Cell Lung Cancer. New England Journal of Medicine. 2002;346:92-8.

[15] Zhang Z, Stiegler AL, Boggon TJ, Kobayashi S, Halmos B. EGFR-mutated lung cancer: a paradigm of molecular oncology. Oncotarget. 2010;1:497-514.

[16] Shepherd FA, Rodrigues Pereira J, Ciuleanu T, Tan EH, Hirsh V, Thongprasert S, et al. Erlotinib in Previously Treated Non–Small-Cell Lung Cancer. New England Journal of Medicine. 2005;353:123-32.

[17] Zhou C, Wu Y-L, Chen G, Feng J, Liu X-Q, Wang C, et al. Erlotinib versus chemotherapy as first-line treatment for patients with advanced EGFR mutation-positive non-small-cell lung cancer (OPTIMAL, CTONG-0802): a multicentre, open-label, randomised, phase 3 study. The Lancet Oncology.12:735-42.

[18] Rosell R, Carcereny E, Gervais R, Vergnenegre A, Massuti B, Felip E, et al. Erlotinib versus standard chemotherapy as first-line treatment for European patients with advanced EGFR mutation-positive non-small-cell lung cancer (EURTAC): a multicentre, open-label, randomised phase 3 trial. The Lancet Oncology. 2012;13:239-46.

[19] Ellis PM, Coakley N, Feld R, Kuruvilla S, Ung YC. Use of the epidermal growth factor receptor inhibitors gefitinib, erlotinib, afatinib, dacomitinib, and icotinib in the treatment of non-small-cell lung cancer: a systematic review. Current Oncology. 2015;22:e183-e215.

[20] Pao W, Miller VA, Politi KA, Riely GJ, Somwar R, Zakowski MF, et al. Acquired Resistance of Lung Adenocarcinomas to Gefitinib or Erlotinib Is Associated with a Second Mutation in the EGFR Kinase Domain. PLoS Medicine. 2005;2:e73.

[21] Yu HA, Riely GJ. Second Generation Epidermal Growth Factor Receptor Tyrosine Kinase Inhibitors In Lung Cancers. Journal of the National Comprehensive Cancer Network : JNCCN. 2013;11:161-9.

[22] Wu Y-L, Zhou C, Hu C-P, Feng J, Lu S, Huang Y, et al. Afatinib versus cisplatin plus gemcitabine for first-line treatment of Asian patients with advanced non-small-cell lung cancer harbouring EGFR mutations (LUX-Lung 6): an open-label, randomised phase 3 trial. The Lancet Oncology.15:213-22.

[23] Barnes TA, O'Kane GM, Vincent MD, Leighl NB. Third-Generation Tyrosine Kinase Inhibitors Targeting Epidermal Growth Factor Receptor Mutations in Non-Small Cell Lung Cancer. Frontiers in Oncology. 2017;7.

[24] Mok TS, Wu Y-L, Ahn M-J, Garassino MC, Kim HR, Ramalingam SS, et al. Osimertinib or Platinum–Pemetrexed in EGFR T790M–Positive Lung Cancer. New England Journal of Medicine. 2016;376:629-40.

[25] Thatcher N, Hirsch FR, Luft AV, Szczesna A, Ciuleanu TE, Dediu M, et al. Necitumumab plus gemcitabine and cisplatin versus gemcitabine and cisplatin alone as first-line therapy in patients with stage IV squamous non-small-cell lung cancer (SQUIRE): an open-label, randomised, controlled phase 3 trial. The Lancet Oncology.16:763-74.

[26] Suryavanshi M, Panigrahi M, Kumar D, Verma H, Saifi M, Dabas B, et al. ROS1 rearrangement and response to crizotinib in Stage IV non-small cell lung cancer. Lung India. 2017;34:411-4.

[27] Salgia R. Role of c-Met in Cancer: Emphasis on Lung Cancer. Seminars in Oncology. 2009;36:S52-S8.

[28] Sahu A, Prabhash K, Noronha V, Joshi A, Desai S. Crizotinib: A comprehensive review2013.

[29] Leprieur EG, Fallet V, Cadranel J, Wislez M. Spotlight on crizotinib in the first-line treatment of ALK-positive advanced non-small-cell lung cancer: patients selection and perspectives. Lung Cancer: Targets and Therapy. 2016;7:83-90.

[30] Awad MM, Shaw AT. ALK Inhibitors in Non–Small Cell Lung Cancer: Crizotinib and Beyond. Clinical advances in hematology & oncology : H&O. 2014;12:429-39.

[31] Solomon BJ, Mok T, Kim D-W, Wu Y-L, Nakagawa K, Mekhail T, et al. First-Line Crizotinib versus Chemotherapy in ALK-Positive Lung Cancer. New England Journal of Medicine. 2014;371:2167-77.

[32] Staff N. FDA Expands Approval of Ceritinib for ALK-Positive Non-Small Cell Lung Cancer. Cancer Currents Blog: NIH; 2017.

[33] Soria J-C, Tan DSW, Chiari R, Wu Y-L, Paz-Ares L, Wolf J, et al. First-line ceritinib versus platinum-based chemotherapy in advanced ALK-rearranged non-small-cell lung cancer (ASCEND-4): a randomised, open-label, phase 3 study. The Lancet.389:917-29.

[34] Gandhi L, Ou S-HI, Shaw AT, Barlesi F, Dingemans A-MC, Kim D-W, et al. Efficacy of alectinib in central nervous system metastases in crizotinib-resistant ALK-positive non–small-cell lung cancer: Comparison of RECIST 1.1 and RANO-HGG criteria. European Journal of Cancer. 2017;82:27-33.

[35] Kim D-W, Tiseo M, Ahn M-J, Reckamp KL, Hansen KH, Kim S-W, et al. Brigatinib in Patients With Crizotinib-Refractory Anaplastic Lymphoma Kinase–Positive Non–Small-Cell Lung Cancer: A Randomized, Multicenter Phase II Trial. Journal of Clinical Oncology. 2017;35:2490-8.

[36] Staff N. FDA Grants Brigatinib Accelerated Approval for Metastatic Non-Small Cell Lung Cancer. Cancer Currents Blog: NIH; 2017.

[37] Wan PTC, Garnett MJ, Roe SM, Lee S, Niculescu-Duvaz D, Good VM, et al. Mechanism of Activation of the RAF-ERK Signaling Pathway by Oncogenic Mutations of B-RAF. Cell.116:855-67.

[38] Planchard D, Kim TM, Mazieres J, Quoix E, Riely G, Barlesi F, et al. Dabrafenib in BRAF V600E–Mutant Advanced Non-Small Cell Lung Cancer: an Open-label, Single arm, Multicenter, Phase 2 Trial. The Lancet Oncology. 2016;17:642-50.

[39] Planchard D, Besse B, Groen HJM, Souquet P-J, Quoix E, Baik CS, et al. An open-label phase 2 trial of dabrafenib plus trametinib in patients with previously treated BRAF V600E–mutant metastatic non-small cell lung cancer. The Lancet Oncology. 2016;17:984-93.

[40] Sandler A, Gray R, Perry MC, Brahmer J, Schiller JH, Dowlati A, et al. Paclitaxel–Carboplatin Alone or with Bevacizumab for Non–Small-Cell Lung Cancer. New England Journal of Medicine. 2006;355:2542-50.

[41] Garon EB, Cao D, Alexandris E, John WJ, Yurasov S, Perol M. A Randomized, Double-Blind, Phase III Study of Docetaxel and Ramucirumab Versus Docetaxel and Placebo in the Treatment of Stage IV Non–Small-Cell Lung Cancer After Disease Progression After 1 Previous Platinum-Based Therapy (REVEL): Treatment Rationale and Study Design. Clinical Lung Cancer.13:505-9.

[42] Herbst RS, Baas P, Kim D-W, Felip E, Pérez-Gracia JL, Han J-Y, et al. Pembrolizumab versus docetaxel for previously treated, PD-L1-positive, advanced non-small-cell lung cancer (KEYNOTE-010): a randomised controlled trial. The Lancet.387:1540-50.

[43] Reck M, Rodríguez-Abreu D, Robinson AG, Hui R, Csőszi T, Fülöp A, et al. Pembrolizumab versus Chemotherapy for PD-L1–Positive Non–Small-Cell Lung Cancer. New England Journal of Medicine. 2016;375:1823-33.

[44] Borghaei H, Paz-Ares L, Horn L, Spigel DR, Steins M, Ready NE, et al. Nivolumab versus Docetaxel in Advanced Nonsquamous Non–Small-Cell Lung Cancer. New England Journal of Medicine. 2015;373:1627-39.

[45] Brahmer J, Reckamp KL, Baas P, Crinò L, Eberhardt WEE, Poddubskaya E, et al. Nivolumab versus Docetaxel in Advanced Squamous-Cell Non–Small-Cell Lung Cancer. New England Journal of Medicine. 2015;373:123-35.

[46] Rizvi NA, Mazières J, Planchard D, Stinchcombe TE, Dy GK, Antonia SJ, et al. Activity and safety of nivolumab, an anti-PD-1 immune checkpoint inhibitor, for patients with advanced, refractory squamous non-small-cell lung cancer (CheckMate 063): a phase 2, single-arm trial. The Lancet Oncology.16:257-65.

[47] Fehrenbacher L, Spira A, Ballinger M, Kowanetz M, Vansteenkiste J, Mazieres J, et al. Atezolizumab versus docetaxel for patients with previously treated non-small-cell lung cancer (POPLAR): a multicentre, open-label, phase 2 randomised controlled trial. The Lancet.387:1837-46.

[48] Rittmeyer A, Barlesi F, Waterkamp D, Park K, Ciardiello F, von Pawel J, et al. Atezolizumab versus docetaxel in patients with previously treated non-small-cell lung cancer (OAK): a phase 3, open-label, multicentre randomised controlled trial. The Lancet. 2017;389:255-65.

[49] Manzo A, Montanino A, Carillio G, Costanzo R, Sandomenico C, Normanno N, et al. Angiogenesis Inhibitors in NSCLC. International Journal of Molecular Sciences. 2017;18.

[50] Malhotra J, Jabbour SK, Aisner J. Current state of immunotherapy for non-small cell lung cancer. Translational Lung Cancer Research. 2017;6:196-211.

[51] Garrido-Castro AC, Felip E. HER2 driven non-small cell lung cancer (NSCLC): potential therapeutic approaches. Translational Lung Cancer Research. 2013;2:122-7.

[52] Krug LM, Miller VA, Patel J, Crapanzano J, Azzoli CG, Gomez J, et al. Randomized phase II study of weekly docetaxel plus trastuzumab versus weekly paclitaxel plus trastuzumab in patients with previously untreated advanced nonsmall cell lung carcinoma. Cancer. 2005;104:2149-55.

[53] Gatzemeier U, Groth G, Butts C, Van Zandwijk N, Shepherd F, Ardizzoni A, et al. Randomized phase II trial of gemcitabine–cisplatin with or without trastuzumab in HER2-positive non-small-cell lung cancer. Annals of Oncology. 2004;15:19-27.

[54] Mazières J, Peters S, Lepage B, Cortot AB, Barlesi F, Beau-Faller M, et al. Lung Cancer That Harbors an HER2 Mutation: Epidemiologic Characteristics and Therapeutic Perspectives. Journal of Clinical Oncology. 2013;31:1997-2003.

[55] Solomon BJ. MET Amplification in Non-Small Cell Lung Cancer. My Cancer Genome: Vanderbilt-Ingram Cancer Center; 2015. p. https://www.mycancergenome.org/content/disease/lung-cancer/met/59/.

[56] Agwa ES, Ma PC. Targeting the MET receptor tyrosine kinase in non-small cell lung cancer: emerging role of tivantinib. Cancer Management and Research. 2014;6:397-404.

[57] Azuma K, Hirashima T, Yamamoto N, Okamoto I, Takahashi T, Nishio M, et al. Phase II study of erlotinib plus tivantinib (ARQ 197) in patients with locally advanced or metastatic EGFR mutation-positive non-small-cell lung cancer just after progression on EGFR-TKI, gefitinib or erlotinib. ESMO Open. 2016;1:e000063.

[58] Schwab R, Petak I, Kollar M, Pinter F, Varkondi E, Kohanka A, et al. Major partial response to crizotinib, a dual MET/ALK inhibitor, in a squamous cell lung (SCC) carcinoma patient with de novo c-MET amplification in the absence of ALK rearrangement. Lung Cancer.83:109-11.

[59] Bhattacharya S, Socinski MA, Burns TF. KRAS mutant lung cancer: progress thus far on an elusive therapeutic target. Clinical and Translational Medicine. 2015;4:35.

[60] Zeitouni D, Pylayeva-Gupta Y, Der CJ, Bryant KL. KRAS Mutant Pancreatic Cancer: No Lone Path to an Effective Treatment. Cancers. 2016;8:45.

[61] Cox AD, Fesik SW, Kimmelman AC, Luo J, Der CJ. Drugging the undruggable Ras: mission possible? Nature reviews Drug discovery. 2014;13:828-51.

[62] Shepard HM, Phillips GL, Thanos CD, Feldmann M. Developments in therapy with monoclonal antibodies and related proteins. Clinical Medicine. 2017;17:220-32.

[63] Jackman D, Pao W, Riely GJ, Engelman JA, Kris MG, Jänne PA, et al. Clinical Definition of Acquired Resistance to Epidermal Growth Factor Receptor Tyrosine Kinase Inhibitors in Non–Small-Cell Lung Cancer. Journal of Clinical Oncology. 2010;28:357-60.

[64] Boch C, Kollmeier J, Roth A, Stephan-Falkenau S, Misch D, Grüning W, et al. The frequency of EGFR and KRAS mutations in non-small cell lung cancer (NSCLC): routine screening data for central Europe from a cohort study. BMJ Open. 2013;3:e002560.

[65] Walker S, Landovitz R, Ding WD, Ellestad GA, Kahne D. Cleavage behavior of calicheamicin gamma 1 and calicheamicin T. Proceedings of the National Academy of Sciences of the United States of America. 1992;89:4608-12.

[66] Staff N. Gemtuzumab Receives New FDA Approval for Acute Myeloid Leukemia. In: NCI, editor. Cancer Currents Blog: NIH; 2017.

[67] Castaigne S, Pautas C, Terré C, Raffoux E, Bordessoule D, Bastie J-N, et al. Effect of gemtuzumab ozogamicin on survival of adult patients with de-novo acute myeloid leukaemia (ALFA-0701): a randomised, open-label, phase 3 study. The Lancet.379:1508-16.

[68] Amadori S, Suciu S, Selleslag D, Aversa F, Gaidano G, Musso M, et al. Gemtuzumab Ozogamicin Versus Best Supportive Care in Older Patients With Newly Diagnosed Acute Myeloid Leukemia Unsuitable for Intensive Chemotherapy: Results of the Randomized Phase III EORTC-GIMEMA AML-19 Trial. Journal of Clinical Oncology. 2016;34:972-9.

[69] Taksin AL, Legrand O, Raffoux E, de Revel T, Thomas X, Contentin N, et al. High efficacy and safety profile of fractionated doses of Mylotarg as induction therapy in patients with relapsed acute myeloblastic leukemia: a prospective study of the alfa group. Leukemia. 2006;21:66-71.

[70] Younes A, Gopal AK, Smith SE, Ansell SM, Rosenblatt JD, Savage KJ, et al. Results of a Pivotal Phase II Study of Brentuximab Vedotin for Patients With Relapsed or Refractory Hodgkin's Lymphoma. Journal of Clinical Oncology. 2012;30:2183-9.

[71] Pro B, Advani R, Brice P, Bartlett NL, Rosenblatt JD, Illidge T, et al. Brentuximab Vedotin (SGN-35) in Patients With Relapsed or Refractory Systemic Anaplastic Large-Cell Lymphoma: Results of a Phase II Study. Journal of Clinical Oncology. 2012;30:2190-6.

[72] Verma S, Miles D, Gianni L, Krop IE, Welslau M, Baselga J, et al. Trastuzumab Emtansine for HER2-Positive Advanced Breast Cancer. New England Journal of Medicine. 2012;367:1783-91.

[73] Diéras V, Miles D, Verma S, Pegram M, Welslau M, Baselga J, et al. Trastuzumab emtansine versus capecitabine plus lapatinib in patients with previously treated HER2-positive advanced breast cancer (EMILIA): a descriptive analysis of final overall survival results from a randomised, open-label, phase 3 trial. The Lancet Oncology. 2017;18:732-42.

[74] Krop IE, Kim S-B, Martin AG, LoRusso PM, Ferrero J-M, Badovinac-Crnjevic T, et al. Trastuzumab emtansine versus treatment of physician's choice in patients with previously treated HER2-positive metastatic breast cancer (TH3RESA): final overall survival results from a randomised open-label phase 3 trial. The Lancet Oncology. 2017;18:743-54.

[75] Kantarjian HM, DeAngelo DJ, Stelljes M, Martinelli G, Liedtke M, Stock W, et al. Inotuzumab Ozogamicin versus Standard Therapy for Acute Lymphoblastic Leukemia. New England Journal of Medicine. 2016;375:740-53.

[76] Demeule M, Currie J-C, Bertrand Y, Ché C, Nguyen T, Régina A, et al. Involvement of the low-density lipoprotein receptor-related protein in the transcytosis of the brain delivery vector Angiopep-2. Journal of Neurochemistry. 2008;106:1534-44.

[77] McGuire MJ, Li S, Brown KC. Biopanning of Phage Displayed Peptide Libraries for the Isolation of Cell-Specific Ligands. Methods in molecular biology (Clifton, NJ). 2009;504:291-321.

[78] Umlauf BJ, Chung C-Y, Brown KC. Modular Three-component Delivery System Facilitates HLA Class I Antigen Presentation and CD8(+) T-cell Activation Against Tumors. Molecular Therapy. 2015;23:1092-102.

[79] Gray BP, Li S, Brown KC. From Phage Display to Nanoparticle Delivery: Functionalizing Liposomes with Multivalent Peptides Improves Targeting to a Cancer Biomarker. Bioconjugate chemistry. 2013;24:85-96.

[80] Singh AN, McGuire MJ, Li S, Hao G, Kumar A, Sun X, et al. Dimerization of a Phage-Display Selected Peptide for Imaging of α(v)β(6)- Integrin: Two Approaches to the Multivalent Effect. Theranostics. 2014;4:745-60.

[81] McGuire MJ, Gray BP, Li S, Cupka D, Byers LA, Wu L, et al. Identification and Characterization of a Suite of Tumor Targeting Peptides for Non-Small Cell Lung Cancer. Scientific Reports. 2014;4:4480.

Chapter 2 HCC15.2 Optimizations for Imaging and Drug Delivery

2.1 Introduction and Previous Work

Previously published work describes the isolation and characterization of a cancer-targeting peptide HCC15.2 [1]. HCC15.2 was isolated from the Ph.D.™-12 Phage Display Peptide Library purchased from NEB, on HCC15 cells. HCC15 cells are derived from a NSCLC tumor, subtype squamous cell carcinoma, of a 47-year-old male patient. One round of phage display panning consists of incubating the library with live HCC15 cells for 1 hour. Uninternalized phage are washed away and the cells are lysed to collect and amplify internalized phage. After 5 rounds of panning, the phage clones converged on two sequences, with HCC15.2

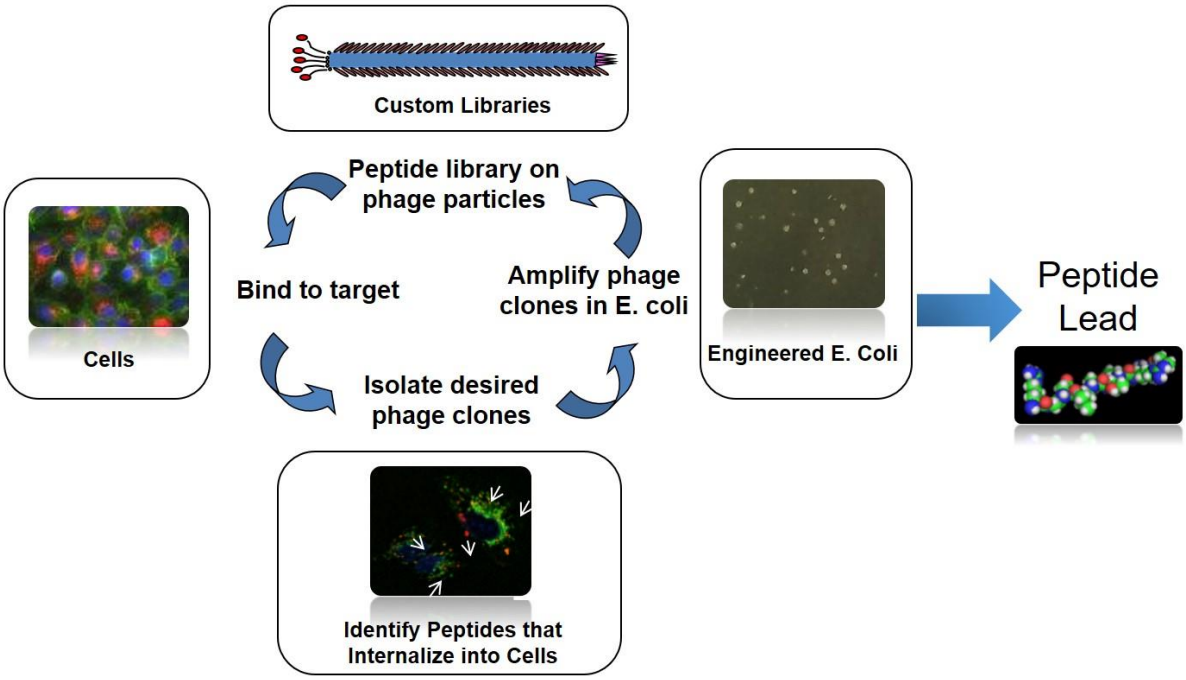

Figure 2-1 Phage Display Biopanning Produces High Affinity Peptides
Diagram of a single round of phage display bio-panning on cancer cells.

representing ~25% of the phage clones. HCC15.2 was taken out of the context of the phage and synthesized in a tetrameric format, to mimic the multimeric binding of phage [2]. The following experiments establish the specificity for cancer and not normal cells, and the broad applicability across multiple cancer types.

2.1.1 HCC15.2 Specifically Binds and Internalizes into Cancer

To avoid loss of library content and potentially useful peptides, a negative selection is not used. Because there is no negative selection, the first step after panning is to verify specificity to cancer. To address this question, the biotinylated peptide was conjugated to R-phycoerythrin via streptavidin, then incubated with two cell lines; a NSCLC line (H1299) and one that approximates normal epithelium (HBEC3). After 1 hour of incubation, uninternalized peptide is washed away and fluorescence was analyzed by flow cytometry. HCC15.2 binds to H1299 cells, but not to the HBEC3 cells (Figure2-1 A). Further, scrambling the sequence of HCC15.2 randomly as a control leads to loss of binding in H1299 cells. These results show that HCC15.2 binding is sequence specific for some feature on cancer cells that is not present in the normal epithelium.

The panning was specifically biased toward peptides that internalized into cancer cells. Fluorescent microscopy was used to visually verify peptide internalization. HCC15.2 was conjugated to streptavidin-coated QDots and incubated with H1299 cells for 1 hour, then imaged by confocal microscopy to determine if HCC15.2 was internalized. HCC15.2 clearly internalizes into cancer cells, while the control peptide does not (Figure2-1 B).

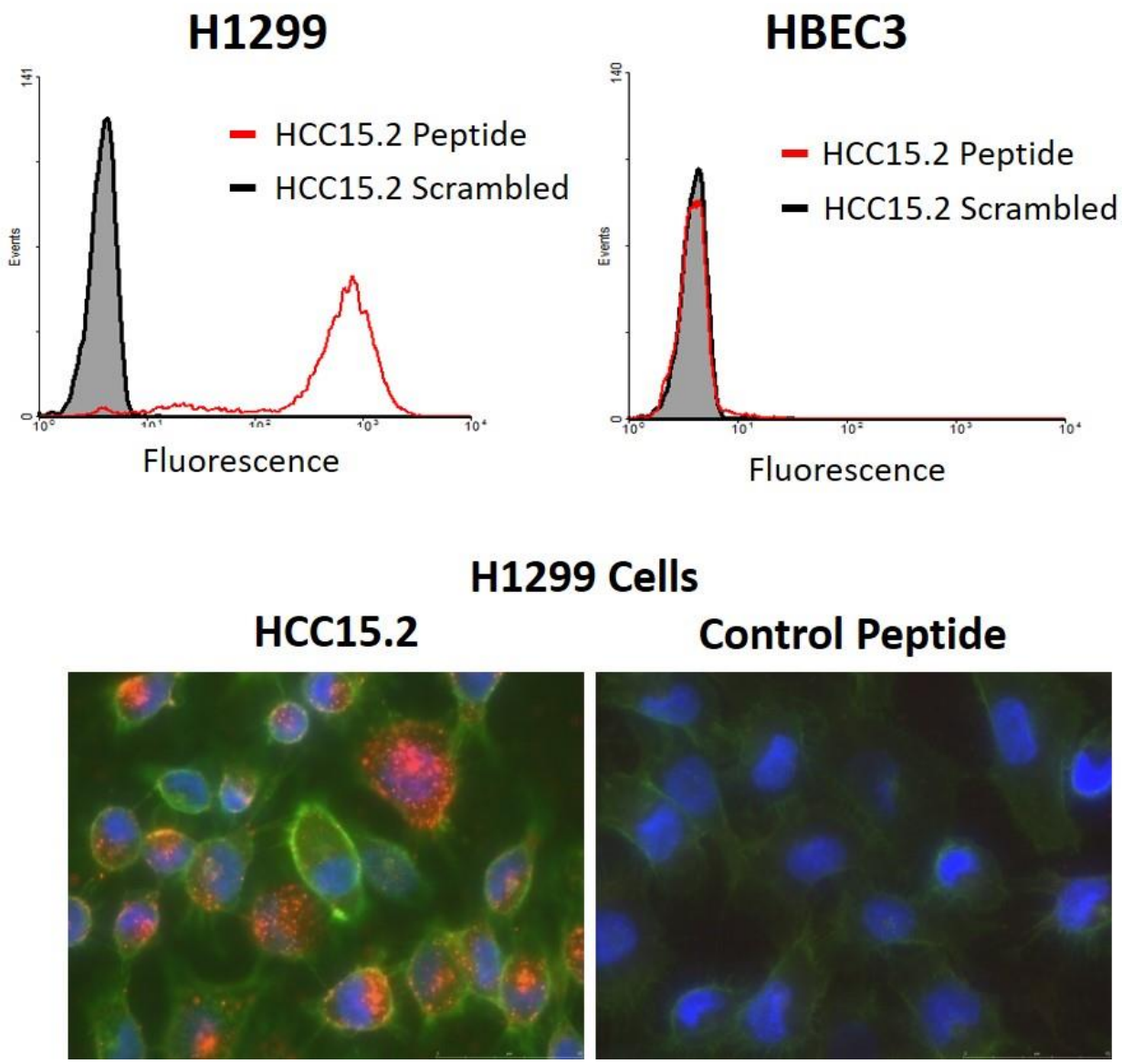

Figure 2-2 HCC15.2 Specifically Binds and Internalizes in Cancer Cells
a) Histograms from flow cytometry. HCC15.2 peptide conjugated to R-Phycoerythrin (HCC15.2-PE) and incubated with cells for 1 hour. HCC15.2 binds to H1299 cells but not to normal HBECs. b) Fluorescent microscopy in H1299 NCSLC cells of HCC15.2 peptide conjugated to Qdots (Red), Nuclei (Blue) stained with DAPI and cell membrane (green), WGA-Alexa Fluor488. HCC15.2 internalizes in cancer cells and the control peptide does not. Figure adapted from [1]

2.1.2 HCC15.2 Binds a Panel of Cell Lines

Peptides selected through phage display would be of limited use in cancer therapy if they bound very few cell lines, or conversely all cells nonspecifically. To verify the breadth of binding, HCC15.2 was tested on a panel of NSCLC lines by flow cytometry. In the context of the phage, ~54% (21/39) of cell lines internalized HCC15.2. The synthetic tetrameric peptide bound 50% (12/24) of NSCLC lines (Figure 2-2 a). This binding profile in a specific subset of lines, includes lines derived from all major pathological subgroups. Some cell lines internalize up to 1,500-fold more peptide than the control lines (Figure 2-2 b). These results suggest that HCC15.2 binds a biomarker that spans pathologic subgroups. A second, smaller panel of tumor cell lines derived from other organ sites was also tested, with 63% (7/11) that internalize HCC15.2 (Figure 2-2 c). These data suggest that the receptor that may be expressed broadly in many cancer types.

2.1.3 HCC15.2 Binds Human NSCLC Samples

There is always concern that experimentation in cell lines does not represent the *in vivo* situation, and binding may be an artifact of tissue culture. To verify that binding occurs in human tumor tissue, HCC15.2-Qdot conjugate was incubated with a tissue microarray (TMA) containing NSCLC biopsy samples. This array contained 37 squamous, 5 large cell, 8 adenocarcinoma, 7 BAC, and 2 carcinosarcomas as well as patient-matched, adjacent normal-lung tissue. 24% (14/59) of the samples stain positive for HCC15.2 binding (Figure 2-6). This data shows that HCC15.2 is capable of recognizing a clinically relevant biomarker present in human tissue samples. Further, we saw no HCC15.2 binding on patient-matched, normal-lung sections, indicating a retention of tumor specificity in human samples.

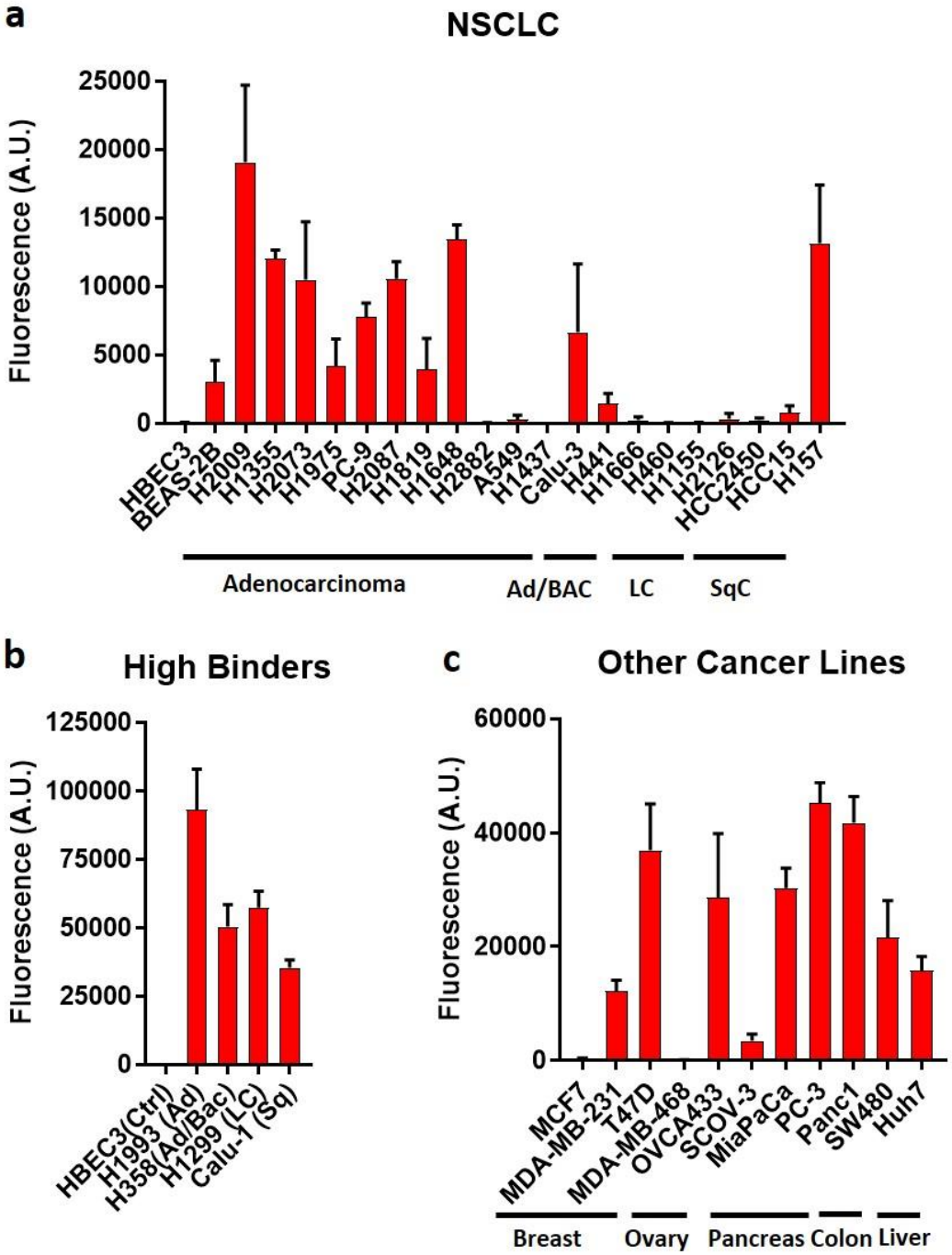

Figure 2-3 HCC15.2 Binds a Specific Subset of Cell Lines
Quantification of the peptide binding measured by flow cytometry on a panel of NSCLC lines, cutoff for positive binding is 5000 A.U. a) HCC15.2-PE is incubated with cells for 1 hour, then fluorescence is measured by flow. HCC15.2 binds 50% (12/24) of the cell lines tested, and does not bind HBEC3 cells. b) Some NSCLC lines internalize large amounts of HCC15.2 peptide. c) 63% (7/11) of cell lines derived from cancers of other organ origins also bind HCC15.2. Figure adapted from [1].

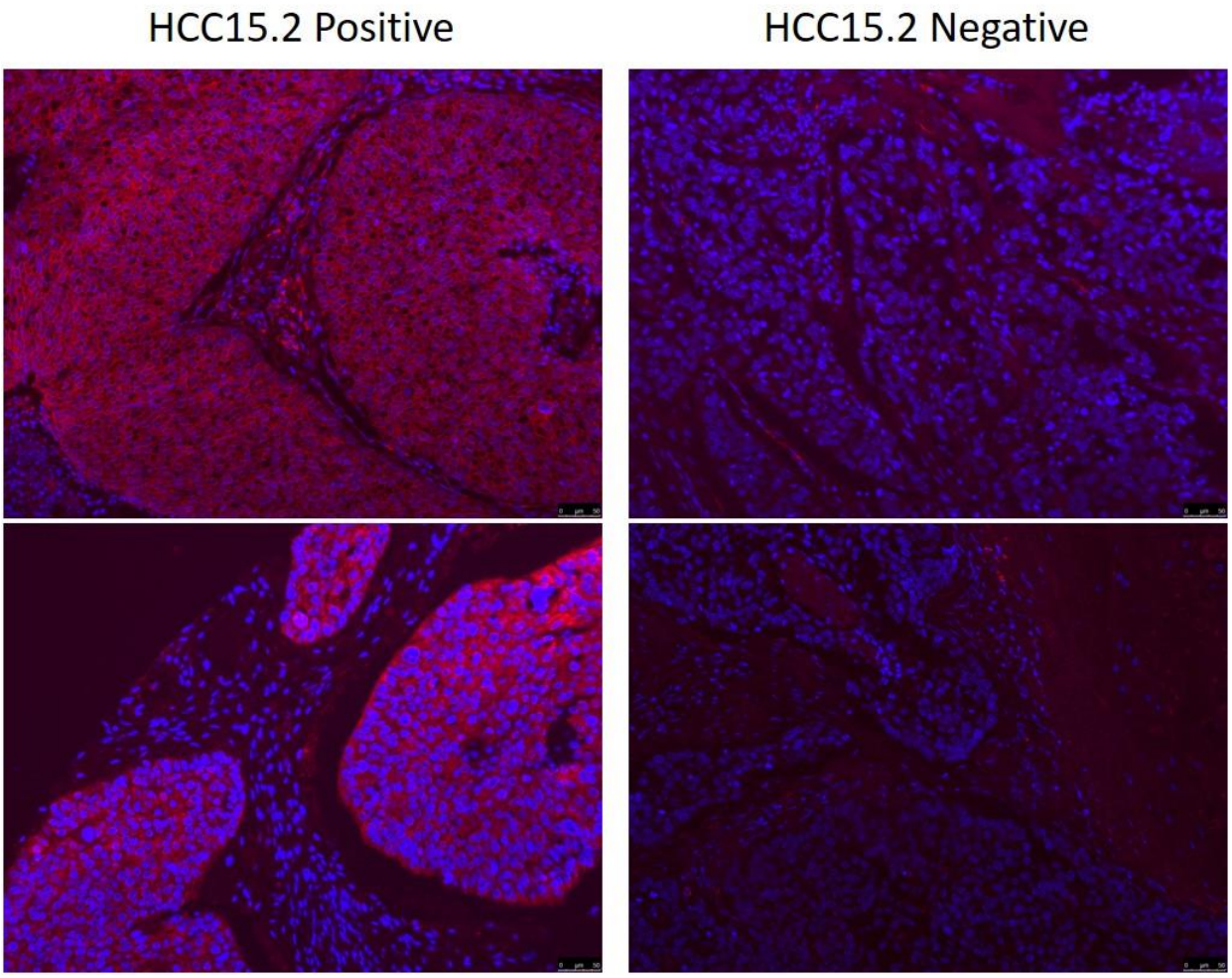

Figure 2-4 HCC15.2 Binds Human NSCLC Samples
An Imgenex NSCLC tumor array containing 59 human samples from all major subtypes of NSCLC was stained with 10 nM HCC15.2-Qdot-605 and counterstained with DAPI. Representative images of tumor sections that stained positively and negatively for HCC15.2. 24% (14/59) of the tumor samples stained HCC15.2 positive. (8 squamous, 4 adenocarcinoma, 2 large cell) Scale bar 50 µm. Figure adapted from [1].

These data together suggest that HCC15.2 is binding some biomarker that is present on a subset of human lung cancers as well as cancers from other tissues. This binding and internalization is specific to cancer, and does not occur in normal tissues. These experiments show HCC15.2 possesses qualities that are desirable for targeting ligands. More specifically, for delivery of various drugs or imaging agents to cancer. The peptide itself had not been altered other than removing it from the context of the phage. In effect, it is the “lead” candidate and

needs to be further optimized before moving to clinical applications. It was questioned whether improvements could be made to optimize HCC15.2 for downstream applications. This chapter focuses on identifying the minimal binding domain, assessing and optimizing affinity, and improving serum stability.

2.2 Results

2.2.1 HCC15.2 Monomer Binds Cancer Nearly as well as Tetramer

Peptides in our lab are selected by phage display panning on live cells. The peptide is genetically fused to the P3 coat protein allowing a single peptide to be displayed in 3-5 copies per phage. This multi-valent binding is required for many peptides when they are synthesized outside of the context of the phage. To ascertain whether multivalent binding was required,

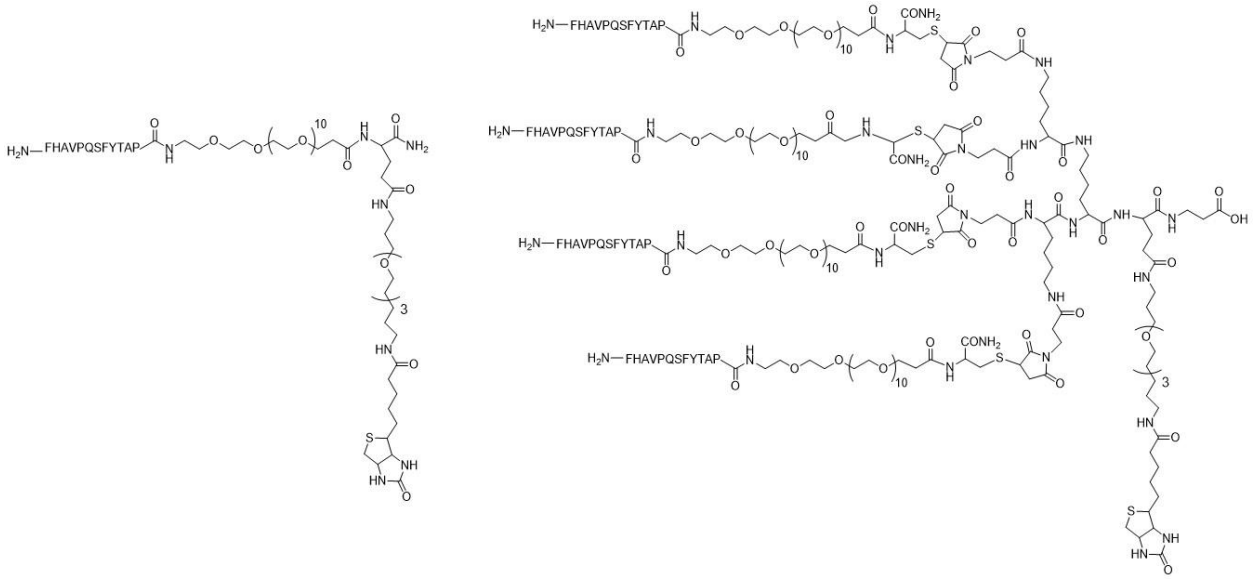

Figure 2-5 Structures of Monomeric and Tetrameric HCC15.2
HCC15.2 monomer has a free N-terminus, but contains a PEG_{11} linker to the carboxy-side of the peptide binding domain followed by a functional group (biotinylated glutamic acid shown here), and is amidated on its C-terminus. To synthesize the tetramer, monomeric peptide is synthesized with a PEG_{11} linker, then cysteine for convergent synthesis onto a branching tri-lysine core labeled with maleimide. The core contains a functional group on the C-terminus (biotinylated glutamic acid shown here)

monomeric and tetrameric HCC15.2 peptides were synthesized (Figure 2-5), and the half-maximal binding affinity was determined using a flow-based assay (Figure 2-6). HCC15.2 was conjugated to Alexa Fluor™ 555 via bitoin-streptavidin and serially diluted for incubation on live cells for 1 hour at 37˚C. Fluorescence was measured by flow cytometry and the affinity was calculated on GraphPad Prizm. Tetramerization increased binding and internalization by only 2-fold [3.73 ±0.57 nM (SEM) to 6.38±1.8 8 nM n=3], which corresponds to a less than linear increase in affinity (Figure 2-6). Many other peptides isolated in our lab require multivalent binding, the monomer having high micromolar affinities. HCC15.2 monomer binds to its target

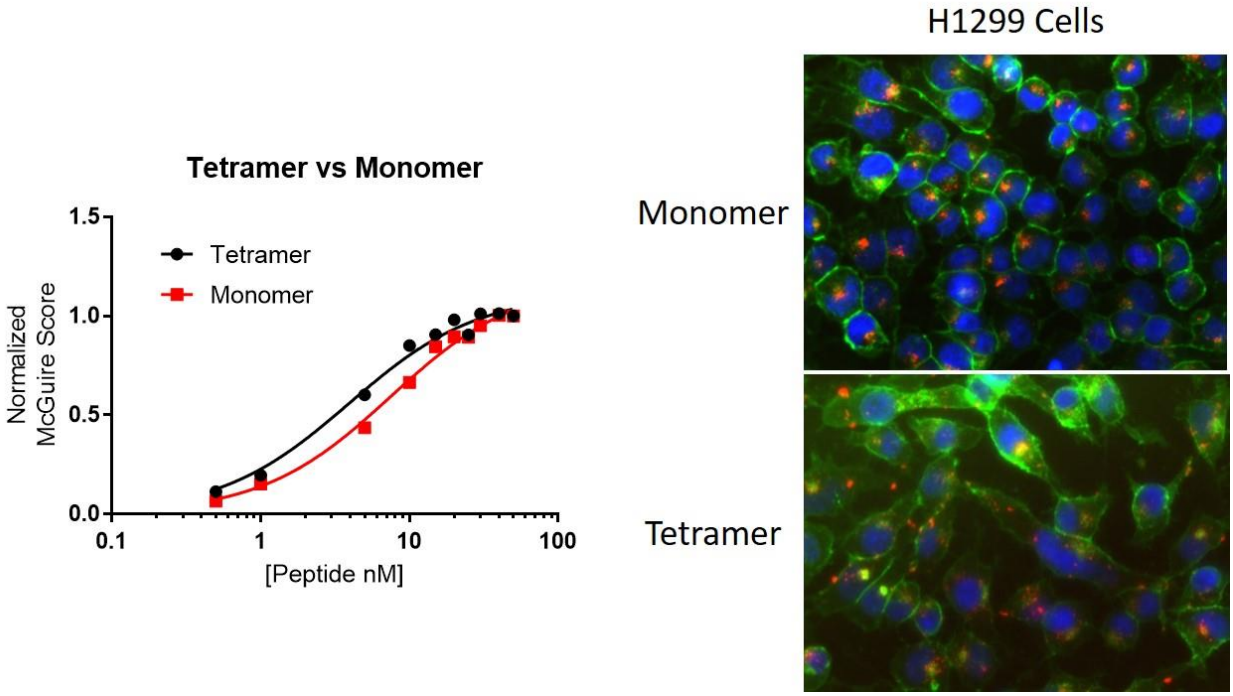

Figure 2-6 HCC15.2 Binds with Nanomolar Affinity as a Monomer
Representative binding curves of HCC15.2 monomer and tetramer. H1299 cells were incubated with increasing concentrations of HCC15.2-AF555 for 1 hour at 37˚C. The cells were washed and lifted for analysis by flow cytometry. The half-maximal binding was calculated on GraphPad Prism® software. Fluorescence microscopy images showing HCC5.2 monomer still internalizes and maintains the same perinuclear punctate staining as the tetramer. HCC15.2-dye was incubated with live cells for 1 hour then fixed and counterstained and imaged on a Zeiss LSM-700 confocal microscope. Red is peptide-AF555, green is cell membrane stained with WGA-AF488, Blue is nuclei stained with DAPI.

on the same order of magnitude as monoclonal antibodies. Multivalent binding shows a small benefit to affinity but is not required.

To visually verify that monomeric HCC15.2 still internalized, the peptide was conjugated to Alexa Fluor™ 555 and incubated with live cells for 1 hour, then fixed the cells and counter-stained the cell membrane and nuclei to look for internalization by fluorescence microscopy. HCC15.2 monomer showed clear internalization to a similar degree and localization as the tetramer. Thus, HCC15.2 monomer binds cancer cells with low nanomolar affinity and can deliver cargoes into live cells. Since synthesis of the monomeric peptide requires less than half the time and less than one-quarter of the materials to produce, monomeric HCC15.2 was used for the rest of the optimizations, which simplified and sped up experimentation.

2.2.2 HCC15.2 is Truncated to Reveal Minimal Binding Sequence

Next, we sought to address which amino acids are crucial to cell binding. Different versions of monomeric HCC15.2 were synthesized by sequentially truncating amino acids from the termini and measuring binding by flow cytometry using the same assay described in section 2.2.2. Two C-terminal amino acids, alanine (A) and proline (P) can be truncated with only ~3-fold

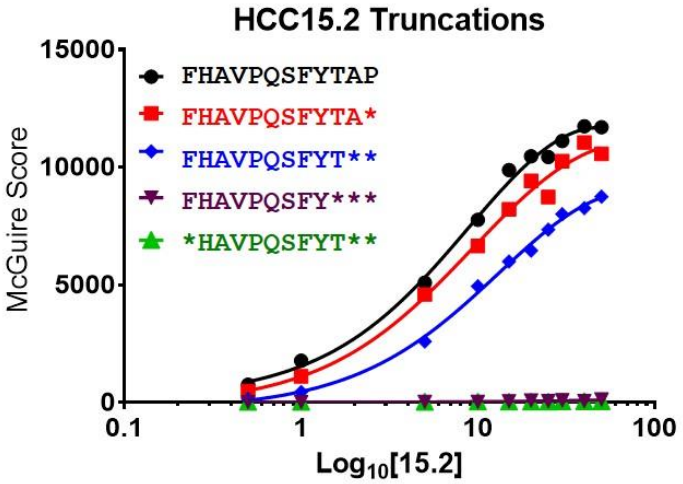

Figure 2-7 Truncations Reveal Minimum Binding Domain Representative peptide binding curves generated by flow cytometry, showing progressive truncations to HCC15.2 reveals minimal binding domain FHAVPQSFYT. Removing the C-terminal A and P (Blue) results in some loss of affinity (13.9 nM), but loss of the N-teminal F (green) or C-terminal T (purple) results in complete loss of binding. Red is 10.8 nM, black is 4.3 nM. Credit: Emily Miller.

decrease in affinity, but if the third amino acid threonine (T) is removed as well, all binding is lost. Similarly, if the first N-terminal amino acid phenylalanine (F) is truncated, binding is completely lost (Figure 2-7). While not all amino acids in between are necessarily crucial to binding, FHAVPQSFYT cannot be truncated further from the termini, as F and T are crucial to binding. While the affinity is decreased by ~3-fold with this truncation, it is advantageous to remove the P for practical purposes. The constrained nature of P, especially on the C-terminus, makes synthesis, conjugations, and modifications complex, while removal can make future modifications easier.

2.2.3 Acetylation Protects HCC15.2 From Degradation

The structure of the monomer already protects the C-terminus from protease degradation with amidation, a biotinylated amino acid, and a PEG linker (Figure 2-1). The N-terminus contains an unmodified, naturally occurring amino acid F, which if removed results in total loss of binding. Protection from degradation is therefore crucial for peptide targeting and delivery of payloads. A common, naturally occurring method for N-terminal protection is acetylation [3]. This modification adds minimal steric bulk to the peptide and removes the positive charge of the amino group. With this modification on the monomer, there are 2 separate questions to address. Can acetylation protect HCC15.2 from human serum peptidases? Does acetylation interfere with peptide binding and internalization?

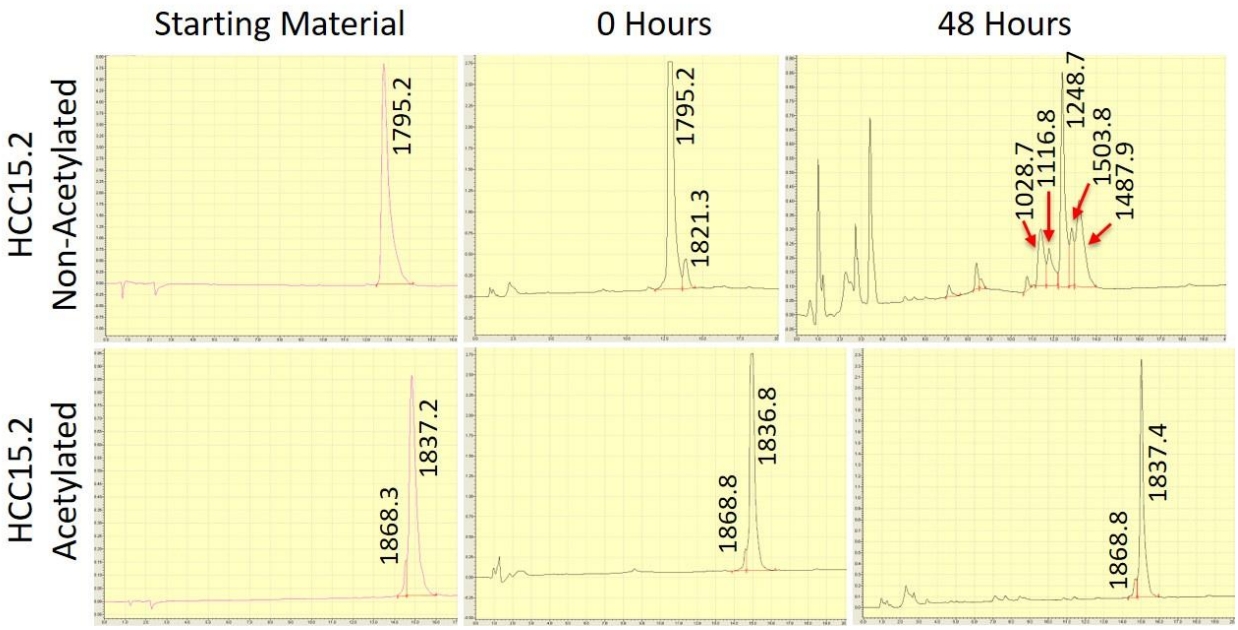

HCC15.2	Theoretical Mass	Sample	Observed Mass	Δ Mass	% of Peak
Non Acetylated	1794	Starting Material	1795	0	99.9%
		0 Hours	1795 1821	0 +26	91.8% 8.2%
		48 Hours	1488 1503 1248 1116 1028	-307 -292 -547 -679 -767	26.6% 9.1% 35.1% 8.8% 12.8%
Acetylated	1834	Starting Material	1837 1868	0 31	93.5% 6.5%
		0 Hours	1837 1868	0 31	95.1% 4.9%
		48 Hours	1837 1868	0 31	93.4% 6.6%

Figure 2-8 Acetylation Protects HCC15.2 From Degradation
AcHCC15.2 was incubated in 100% human serum for 0 and 48-hours. Serum proteins were precipitated in ethanol and peptide was run on analytical HPLC. Collected fractions were analyzed by 4800 MALDI TOF/TOF™ and the area under each peak was integrated to calculate the percentage of peptide that fraction represented At 0 hours, there is no change in the protected HCC15.2, but a small peak +26 appears in the unprotected HCC15.2. At 48 hours, no degradation of AcHCC15.2 is observed, while significant degradation of the unprotected HCC15.2 is observed, seen as multiple messy peaks on the HPLC trace. Credit: Indu Venugopal

dissolved in human serum for 0 and 48-hours, and then serum proteins were precipitated and the peptide was run on analytical HPLC. The percent of peptide degraded over time was calculated by integrating the area under the curves and verified products via 4800 MALDI TOF/TOF™ MS. The acetylation completely protects HCC15.2 from any degradation by human serum, while none of the starting material of unprotected HCC15.2 can be found (Figure 2-8). The quantification can be found in Table 2-1. The unprotected HCC15.2 began at 99.9% purity, which by 48 hours becomes a mess of peaks, none of which match the mass of the full-length peptide. Protected HCC15.2 started at ~95% purity and remained the same throughout the 48-hour treatment.

To address the second question, the binding affinity of acetylated and non-acetylated optimized HCC15.2 were compared, using the same flow cytometry assay in section 2.2.3. Acetylation did not decrease peptide binding affinity compared to non-acetylated HCC15.2 (Figure 2-9). These data show that acetylation is an effective way to protect the N-terminus with no loss in binding affinity.

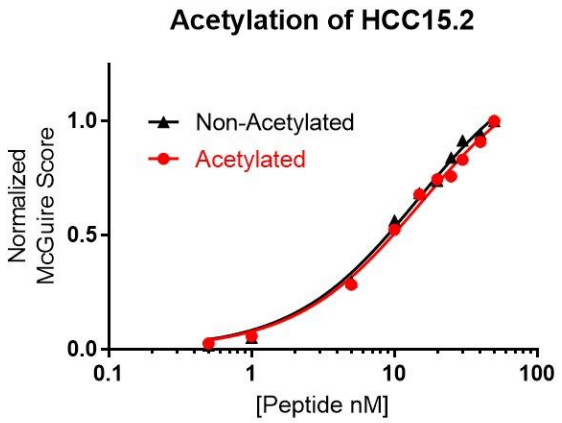

Figure 2-9 Acetylation Does Not Affect Binding AcHCC15.2 serial dilutions were incubated on H1299 cells for 1 hour, then analyzed by flow cytometry. Representative curves show no effect of acetylation on peptide binding.

2.2.4 Multimerization Linearly Increases Optimized HCC15.2 Binding

Optimizing HCC15.2 as a monomer greatly sped experimentation, but one question remained. Does multimerization of the optimized peptide further enhance desirable attributes? To address this question, optimized HCC15.2 was synthesized as a monomer, dimer, and

tetramer, and affinity was determined by flow cytometry and microscopy. HCC15.2 monomer, dimer, and tetramer were conjugated to Alexa Fluor™ 647, serially diluted, and incubated on H1299 cells for 1 hour. After the incubation, cells were washed and analyzed by flow. The tetramer bound ~2-fold better than the dimer, which bound ~2.5-fold better than the monomer (2.86±0.21 nM, 5.65±0.12 nM, 14.85±0.17 nM respectively, n≥3). This is a linear increase in binding, and no effects from avidity were observed.

Cells plated on microscope slides were incubated with 50 nM HCC15.2-Qdot605 (red) for 1 hour, then washed, and growth media was returned to the wells for 23 hours. Cells were then washed, fixed, and counterstained with DAPI and imaged by confocal microscopy. No

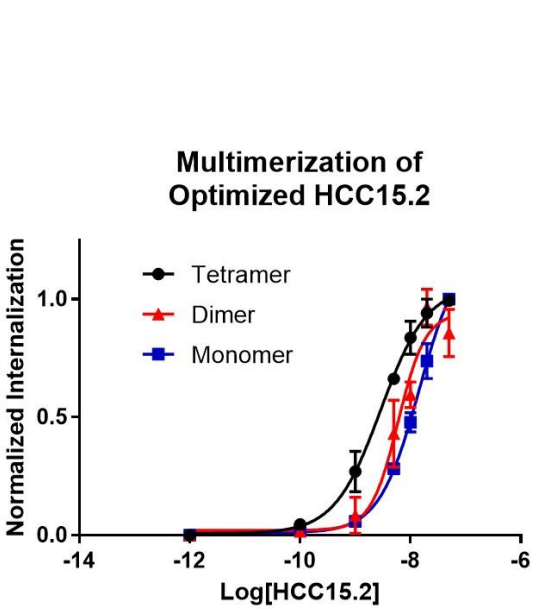

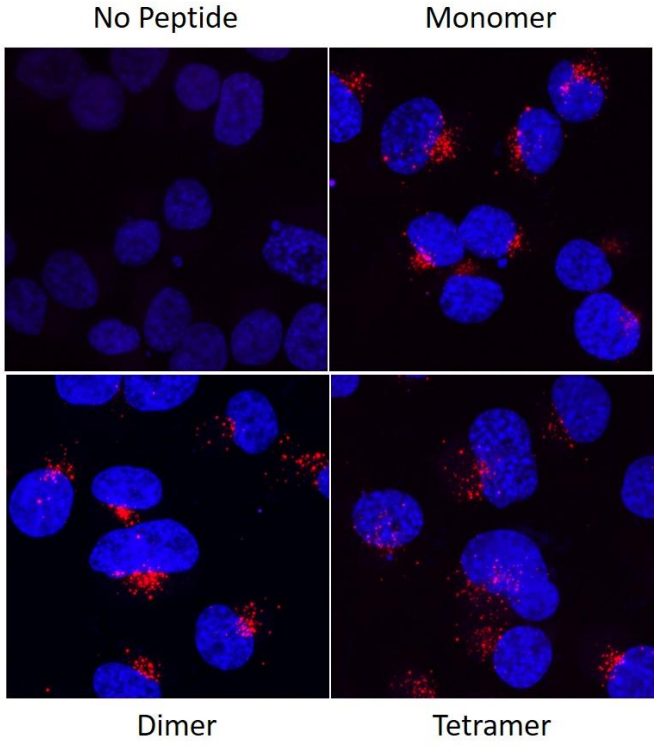

Figure 2-10 Multimerization of Optimized HCC15.2 Linearly Increases Affinity
H1299 cells were incubated with a concentration gradient of HCC15.2-Alexa Fluor 647 in the monomeric, dimeric, and tetrameric formats for 1 hour. Cells were washed and analyzed by flow cytomety. Dimer bound ~2.5-fold better than monomer, and tetramer bound ~2-fold better than dimer. H1299 cells were plated, then incubated with 50 nM HCC15.2-Qdot605 for 1 hour, removed, and then normal growth media was replaced. After 24 hours, cells were fixed, and counterstained with DAPI (blue). Representative maximally projected z-stacks for each group reveal no apparent difference in peptide internalization or localization.

apparent difference in the extent of peptide internalization or localization is observed by microscopy.

These experiments show the versatility of HCC15.2. Monomer, dimer, and tetramer all have low nanomolar binding with a nearly linear increase in binding correlating to valency. Removal of a single N-terminal amino acid, F, completely removes all binding capabilities. This acetylated peptide is identical to HCC15.2, except for one amino acid, and serves as a control for experiments in the following chapters.

Peptide	Valency	Affinity
FHAVPQSFYTAP	Tetramer	3.73 ± 0.57 nM
FHAVPQSFYTAP	Monomer	4.30 ± 0.11 nM
FHAVPQSFYTA*	Monomer	10.82 ± 0.67 nM
FHAVPQSFYT**	Monomer	13.93 ± 0.21 nM
FHAVPQSFY***	Monomer	ND
*HAVPQSFYT**	Monomer	ND
(Ac) FHAVPQSFYT**	Monomer	14.85 ± 0.17 nM
(Ac) FHAVPQSFYT**	Dimer	5.65 ± 0.12 nM
(Ac) FHAVPQSFYT**	Tetramer	2.37 ± 0.07 nM

Table 2-2 Summary of HCC15.2 Affinities on H1299 Cells.
Sequences and valency of HCC15.2 permutations are listed with the calculated affinities measured on H1299 cells.

2.2.5 HCC15.2 Does Not Stain Normal Tissue in Microarray

HCC15.2 dimer conjugated to Qdot655 was incubated with the US Biomax FDA normal TMA. This TMA contains 30 normal tissue samples from 3 patients which includes the following tissues: cerebrum, cerebellum, ovary, pancreas, pituitary gland, breast, spleen, tonsil, thymus, stomach, intestine, colon, tongue, prostate, skeletal muscle, cardiac, pericardium, lymph node, bone marrow, testis, thyroid, heart, liver, kidney, uterus, cervix, skin, peripheral nerve, esophagus, lung, and adrenal gland. Most tissues showed no staining of HCC15.2; however, 2/3 of lung cancer samples showed nonhomogeneous signal slightly above background. All 3

adrenal gland samples also showed varying degrees of signal. In both tissues, staining is abnormal and significantly less than staining observed in previous NSCLC tumor samples. Follow-up experiments in normal lung and adrenal tissue are planned.

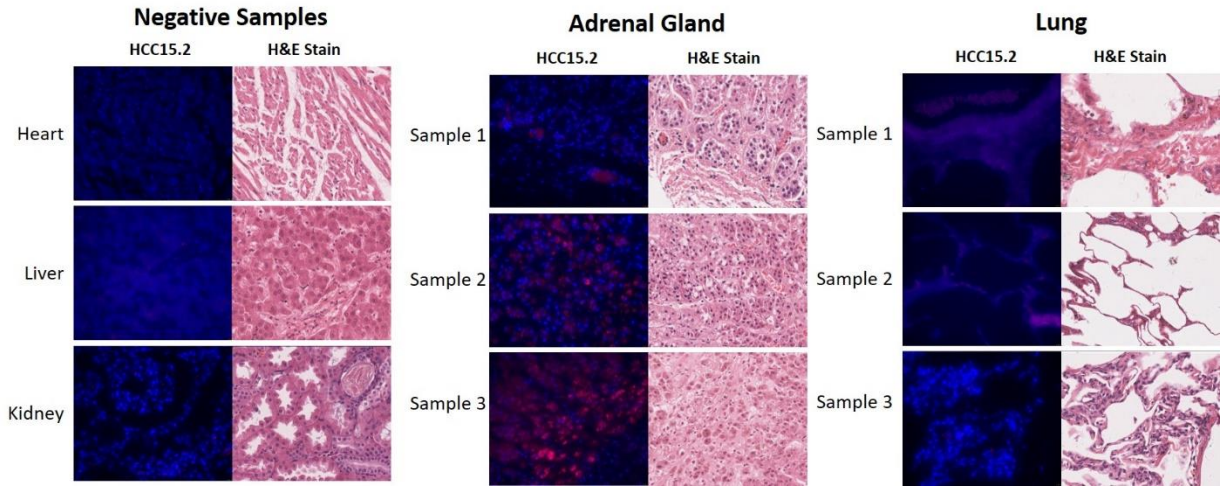

Figure 2-11 HCC15.2 Stains Negative in Normal Tissue Microarray
US Biomax FDA normal tissue array with 30 tissues from 3 patients was incubated with HCC15.2 conjugated to Qdot-655 for 1 hour, washed, and counterstained with DAPI. All tissues stained negatively for HCC15.2 binding, as shown in representative slices of heart, liver, and kidney. Lung (2/3) and adrenal gland (3/3) tissues showed abnormal, nonhomogeneous staining slightly higher than background, but significantly less than tumor samples.

2.3 Discussion

This study highlights the versatility of HCC15.2. The peptide can be used in many different formats with low nanomolar efficiency. Other than the obvious cost-reducing implications, using a monomer instead of a tetramer has several advantages. One of the main reasons for using the monomer is its flexibility in use. Everything that can be done with dimer and tetramer can be done with the monomer, but it can also be added to any protein of choice via cloning. The dimer and tetramer are limited to chemical conjugation to proteins. This has presented some difficulty in the past with non-uniform labeling or few available conjugation sites. Cloning the monomer onto a terminus of a protein would simply and easily tag the protein

with peptide 1:1. Chapter 5 details the use of HCC15.2 to target a protein toxin to cancer cells *in vitro* and *in vivo.* This was accomplished by conjugation, but future experiments will involve cloning HCC15.2 directly onto the toxin.

Another advantage of a small monomeric peptide would be in diagnostics, such as positron emission tomography (PET) in clinical settings and near-infrared imaging (NIR) in research applications. The effectiveness of imaging is based on contrast. The higher the contrast between the tumor and other tissues, the easier it is to detect small tumors. A small peptide with high tumor affinity (HCC15.2) could deliver a contrast agent to the tumor and then clear rapidly from the blood stream so other tissues do not have time to take it up. This contrast would be limited in clearance organs such as the kidneys.

Terminal truncations are the fastest way to trim the peptide and find at least two crucial amino acids. The most thorough approach would be one similar to the process of medicinal chemistry. Replacing each amino acid, one at a time with other amino acids or analogs containing similar properties, such as hydrophobicity to try to increase affinity. This process is very resource and labor intensive and it was decided not to pursue this line of experimentation.

The peptides are displayed from the N-terminus of the P3 coat protein of phage during selection. As such, the C-terminus is always bound to something and protected. This is mimicked in the synthetic peptides, where the C-terminus ends with a PEG_{11}, a functional group, and amidation. This effectively protects the C-terminus from enzyme degradation while allowing for functionalization.

The N-terminus was still susceptible, containing only unaltered amino acids. Acetylation is a common method of protecting the N-terminus of peptides from degradation. It is accomplished during synthesis, before cleavage from the resin and requires very little in the way

of time or resources. We have already shown that acetylation protects HCC15.2 tetramer from degradation in mouse serum [1] . But had it not worked there are a variety of unnatural amino acids or other modifications that could protect the peptide from serum amino peptidases. Chapter 6 details the peptide with other N-terminal modifications, such as PEG linkers which do not decrease peptide binding.

2.4 Conclusion

HCC15.2 peptide has demonstrated an ability to discriminate between cancer cell lines and the normal lung epithelium. Further it binds a certain subset of cancer lines that express a common receptor on the cell surface. The peptide can be minimized from the original selection, FHAVPQSFYTAP tetramer, to AcFHAVPQSFYT-PEG_{11}-Biotin monomer. This optimized peptide has a ~15 nM binding affinity and has demonstrated ability to deliver a variety of cargoes, from small molecule dyes, to proteins, to nanoparticles. These optimizations have broadened the versatility of HCC15.2 to be used in many formats and applications.

2.5 Materials & Methods

2.5.1 Materials and Cell Lines

NovaPEG Rink Amide resin and FMOC-Glu(biotinyl-PEG)-OH were purchased from NovaBiochem®(Millipore Sigma, Billerica, MA). 2-(6-Chloro-1H-benzotriazole-1-yl)-1,1,3,3-tetramethylaminium hexafluorophosphate (HCTU), N,N-Dimethylmethanamide (DMF), N-Methylmorpholine (NMM), 2,2,2-Trifluoroacetic acid (TFA), and all FMOC amino acids were purchased from Gyros Protein Technologies (Tucson, AZ). The FMOC-NH-$(PEG)_{11}$-COOH ($C_{42}H_{65}NO_{16}$) was purchased from Polypure (Oslo, Norway). Triisopropylsilane (TIPS) and 1,2-

Ethanedithiol (EDT) were purchased from Sigma Aldrich (Livermore, CA). Piperidine was purchased from Alfa Aesar (Tewksbury, MA), and Acetonitrile, Dichloromethane (DCM), Diethyl ether and most tissue culture supplies were purchased through VWR (Radnor, PA). Human lung cancer cell lines were kindly provided by John Minna M.D. (UT Southwestern Medical Center in Dallas) or purchased from ATCC® and maintained in RPMI + glutamine (Corning®, VWR) + 5% fetal bovine serum (FBS)(Gemini Bio-Products, Sacramento, CA) at 37˚C supplied with 5% CO_2.

2.5.2 Peptide Synthesis

Peptides were synthesized on a Prelude® synthesizer (Gyros Protein Technologies, Tuscon, AZ), according to standard FMOC solid phase synthesis procedures [4]. NovaPEG Rink Amide resin was weighed into a reaction vessel to swell in DMF twice for 30 minutes each. FMOC protected amino acids were dissolved into 0.1M, HCTU to 0.2M, NMM to .4M and piperidine to 20% vol/vol in DMF, and all added to appropriate reagent bottles. Acetylation solution is also prepared if required, 90% DMF, 5% 0.4M NMM, and 5% acetic anhydride. 5-fold excess FMOC protected peptide in activating NMM and HCTU solutions were coupled twice to the resin for 25 minutes each. The FMOC group was then removed in two 10-minute piperidine incubations, to prepare for the next amino acid coupling. For nonstandard couplings such as the biotinylated glutamic acid or the PEG_{11}, the synthesis was programmed with a pause and the reagent was added by hand, and run at 2.5-fold excess for 3 hours. If protecting the peptide, add acetylation solution for 40 minutes after final deprotection. When peptide synthesis was complete, the resin underwent a final deprotection, extra DMF washes as well as DCM washes to speed drying in a desiccator overnight. Multimerization core was synthesized in a similar manner as peptides, but on β-alanine wang resin, with double FMOC protected lysines to

create branching N-termini, to which maleimide groups were coupled. Tri-lysine tetrameric core has 4 maleimide binding sites for convergent synthesis coupling.

2.5.3 Peptide Cleavage

Cleavage solution is made with 94% TFA, 2.5% water, 2.5% EDT, and 1% TIPS. Resin is transferred to a capped filter syringe with cleavage solution and rocked at room temperature for 2-3 hours and no more than 3 hours. Cleavage solution is collected in a 50 ml centrifuge tube and resin washed with more cleavage solution twice. Reduce filtrate to less than 1 mL by evaporating TFA with nitrogen in a fume hood. Add ether to 50 mL, vortex, and chill at -80˚C for 1-2 hours. Centrifuge at 2500 g for 5 minutes at 4˚C. Carefully pour off ether and wash twice with more 10 mL ether, vortexing and centrifuging, then dry in desiccator under vacuum overnight. This yields crude monomeric peptide for purification.

2.5.4 Peptide Purification

Crude peptide was purified on a PROTO 300 C18 10µm 20 x 250mm column (Higgins Analytical, Mountain View, California) by reverse phase high performance liquid chromatography (HPLC) on a Shimadzu modular HPLC (Shimadzu, Kyoto, Japan). Water and acetonitrile solvents were prepared by adding 0.01% TFA. Crude peptide was dissolved in 90% water+0.01% TFA and 10% CAN + 0.01% TFA (90/10). The column is equilibrated with 90/10 for 10 minutes. The dissolved peptide is loaded onto the column and the run starts at 90/10 with a gradient change to 40/60 water/Acetonitrile over 60 minutes, with a flow rate of 10 mL/minute. Fractions that contain peptide products as detected by UV at 220 nm are spotted in sinapic acid and run on 4800 Plus matrix-assisted laser desorption/ionization, time of flight/time of flight (4800 MALDI TOF/TOF™) to verify mass and estimate purity (Applied Biosystems/MDS

SCIEX, Foster City, CA). Fractions corresponding with the correct peptide mass are frozen at -80˚C for at least 1 hour. Lyophilize frozen fractions and check for purity by analytical HPLC.

2.5.5 Peptide Multimerization

Peptides to be multimerized were synthesized with a C-terminal Cysteine separated from the sequence with a PEG_{11} linker. Thiol-Michael addition chemistry was used to join the cysteine from the purified monomeric peptide to the maleimide on the core. This reaction is run in phosphate-buffered saline (PBS) pH 7.4 at room temperature for 2 hours with 2 to 4-fold excess monomeric peptide. Tetrameric peptide was purified and excess monomeric peptide was recovered via HPLC using the same protocol mentioned above. Mass was verified by 4800 MALDI TOF/TOF™.

2.5.6 Flow Cytometry

Biotinylated peptide was conjugated to streptavidin-R-phycoerythrin or streptavidin-Alexa Fluor™ 647 (1:1) for 30 min at RT. The remaining binding sites on streptavidin were quenched with RPMI 1640 and solution diluted to 25 nM. Tumor cells were grown to 90% confluency in a 12 well plate, then incubated with 500 µl peptide-dye conjugate for 1 hour at 37 C. After 1 hour, peptide was removed and the cells were washed 3x with PBS for 5 min, 2x with acid rinse, and 1x PBS rinse. Trypsin (0.25%) was added until cells became suspended, then complete growth media was added to inactivate the trypsin. Cells were transferred to a flow tube, and put on ice in the dark. Flow cytometry was run on BD FACSCelesta and data were analyzed on Flowing software. A region containing < 5% of the cells in the negative control was established and the McGuire score was calculated for each sample by multiplying the percent of positive cells by the mean fluorescence intensity of those positive cells

2.5.7 Binding Affinity

A concentration curve made by serial dilutions ranging from 0.1-100 nM of HCC15.2-SAPE conjugate was prepared. Lung cancer cells were plated in 12-well tissue culture dishes for confluency and flow cytometry the next day. Each well received 1 concentration of peptide. The McGuire score was calculated for each concentration and plotted in GraphPad Prizm®. Nonlinear regression curve fitting the line and one-site-specific-binding algorithms were used to calculate half-maximal internalization (our estimate of Kd). Concentration curves for each peptide were tested at least three times and Kd was calculated from the average of the runs.

2.6 References

[1] McGuire MJ, Gray BP, Li S, Cupka D, Byers LA, Wu L, et al. Identification and Characterization of a Suite of Tumor Targeting Peptides for Non-Small Cell Lung Cancer. Scientific Reports. 2014;4:4480.

[2] Li S, McGuire MJ, Lin M, Liu Y-H, Oyama T, Sun X, et al. Synthesis and characterization of a high-affinity α(v)β(6)-specific ligand for in vitro and in vivo applications. Molecular cancer therapeutics. 2009;8:1239-49.

[3] Arnesen T. Towards a Functional Understanding of Protein N-Terminal Acetylation. PLoS Biology. 2011;9:e1001074.

[4] Behrendt R, White P, Offer J. Advances in Fmoc solid-phase peptide synthesis. Journal of Peptide Science. 2016;22:4-27.

Chapter 3 Discovery of the Mechanism of Endocytosis and Localization of HCC15.2

3.1 Introduction

With the advent of targeted therapies, the focus in cancer therapy has been shifting from general chemotherapies to more specific cancer targeting. Targeting therapies introduce greater specificity, but also greater complexity. The affinity of the targeting agent and the payload toxicity are still critical factors, but it is important to understand not only what to deliver, but how and to where inside the cell it is delivered. Receptor numbers and internalization rates, freeing of the payload by cleavage, and payload engagement with its target in sufficient amounts to kill the cell are crucial factors to account for with targeting therapies. HCC15.2 is a good candidate for targeting therapy and these factors need to be understood. This chapter addresses mechanism of endocytosis, as well as the internal trafficking of HCC15.2.

3.2 Results

3.2.1 HCC15.2 is Internalized via Receptor Mediated Endocytosis

Previous experiments demonstrate that HCC15.2 binds a specific subset of cell lines, unlabeled HCC15.2 will block internalization of labeled peptide, and binding is sequence specific (Chapter 2). This evidence indicates binding and internalization of HCC15.2 is receptor mediated. To substantiate this evidence, several other key characteristics of receptor mediated endocytosis were tested; namely, membrane fluidity, protease degradability, and receptor saturation.

For the peptide selection and characterization, adherent cells are incubated with peptide for 1 hour at 37˚C, washed to remove any surface-bound peptide and analyzed by flow cytometry to assess peptide uptake. To determine whether or not membrane fluidity is an important parameter for peptide internalization, cells were incubated with HCC15.2-SAPE at 4˚C. The lower temperature increases the viscosity of the lipid bilayer and reduces the movement of proteins within the bilayer. Under these conditions HCC15.2 is not internalized indicating that membrane fluidity is key for peptide uptake and that internalization is not due to passive diffusion.

To determine whether or not peptide uptake is mediated by a proteinaceous cellular receptor, cells were incubated with trypsin for 2 minutes to degrade surface proteins before incubation with HCC15.2 at 37ºC. Peptide internalization was lost after trypsin treatment, suggesting the binding of HCC15.2 is mediated by a cell surface protein. However, cells become non-adherent after trypsin, which may alter cytoskeletal structure and impact peptide internalization. Yet lifting the cells by other means, such as EDTA treatment or scraping, reveals

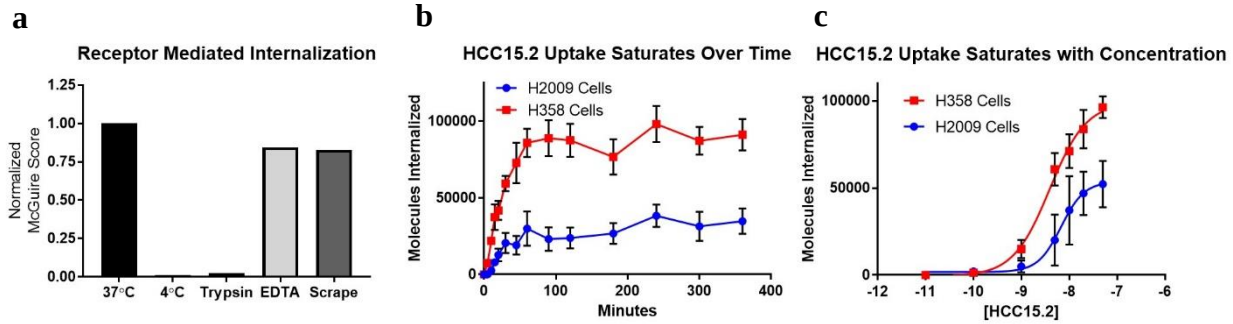

Figure 3-1 HCC15.2 Internalizes via Receptor Mediated Endocytosis
H1299 cells were incubated with HCC15.2 monomer at 37˚C and 4˚C, and with trypsin pretreatment. a) cells incubated at 4˚C and with trypsin pretreatment did not internalize HCC15.2. b) 50nM HCC15.2 dimer is incubated with H2009 and H358 cells for increasing amounts of time. Saturation is reached between 60–90 minutes. c) HCC15.2 dimer is serially diluted and incubated on H2009 and H358 cells for 1 hour and saturates at ~50nM. b and c made use of bead standards which allowed for quantification of internalization events. b), c) credit: Claire Gormley

no inhibition of HCC15.2 internalization (Figure 3-1 A). These data suggest that HCC15.2 internalization is mediated by a trypsin cleavable protein receptor. Internalization is also not due to diffusion or insertion into the cellular membrane nor is it mediated by binding to a cellular lipid.

HCC15.2 was also incubated with H2009 and H358 cells, and internalization was measured over time. With a constant incubation of 25 nM HCC15.2, peptide internalization levels off between 90–120 minutes and does not increase significantly over the next 4 hours. HCC15.2 also saturates at 1 hour, when the concentration is increased to approximately 50 nM (Figure 3-1 B and C). Taken together, these data demonstrate that peptide binding is saturable. HCC15.2 is binding to a cell surface protein and triggering endocytosis, resulting in peptide internalization.

3.2.2 HCC15.2 Receptor is not Recycled

To address the question of receptor recycling, cells were incubated with monomeric (50 nM) and dimeric (25 nM) HCC15.2 in the presence of the inhibitors chloroquine (10µg/µl, receptor recycling) or cycloheximide (10µg/µl, protein synthesis) or peptide alone for 24 hours. Additionally, cells were treated with HCC15.2 for 2 hours followed with a 22-hour chase in complete media. Interestingly, the monomer and dimer behaved differently. Cells incubated with both monomeric and dimeric HCC15.2 and no inhibitor for 24 hours accumulate ~2 fold more dye than cells treated for 2 hours. Internalization of monomeric HCC15.2 is partially inhibited by both chloroquine and cycloheximide over 24 hours. However, internalization of dimeric HCC15.2 is only inhibited by cycloheximide over 24 hours. This suggests that dimeric HCC15.2 binds the receptor more tightly due to avidity, and the receptor is pulled to the lysosome with the peptide. Whereas, the monomer likely releases some of the receptor in endosomes which can be

recycled back to the surface to bring in more peptide. Protein synthesis is required for continued uptake of both peptides, suggesting that the receptor is ultimately degraded in the lysosome in both cases.

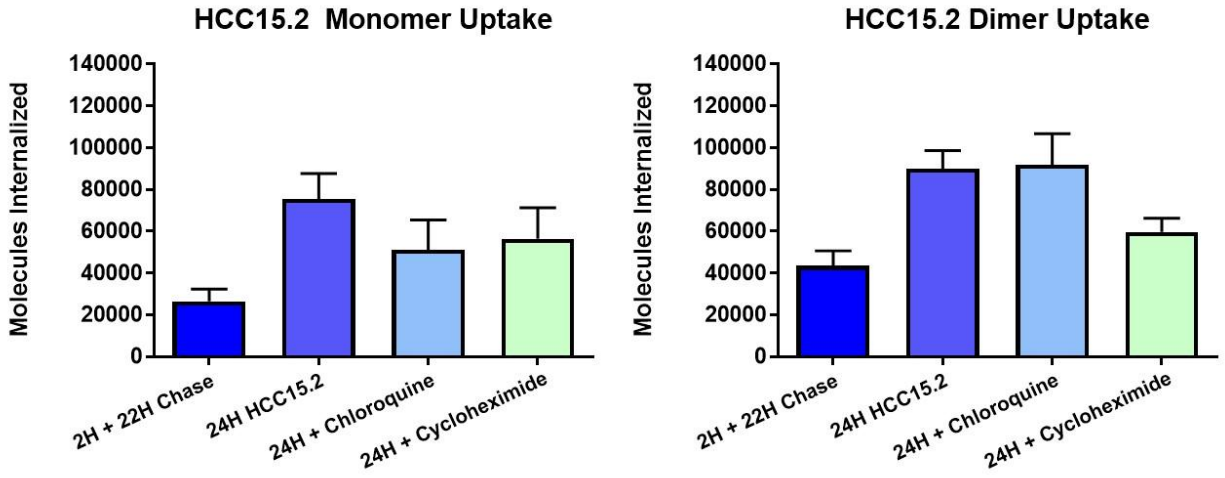

Figure 3-2 Receptor Recycling Depends on HCC15.2 Valency
H358 cells were incubated with HCC15.2 dimer for 2 hours (saturation) followed by a 22-hour chase, or for 24 hours with inhibitors of recycling (chloroquine) and new protein synthesis (cycloheximide). New protein synthesis is required for additional HCC15.2 internalization after initial saturation. There is no decrease in peptide internalization with inhibition of receptor recycling. Credit: Claire Gormley

3.2.3 HCC15.2 Mechanism of Endocytosis

Understanding the mechanism of endocytosis of HCC15.2 can assist in elucidating its receptor target and determining the appropriate therapeutic cargo for delivery. Mechanisms of endocytosis are still an active area of research and many of the mechanics are poorly understood. Cancer often misuses many pathways which complicates elucidation of the mechanism of internalization of HCC15.2 [1]. To address this question, at least two of three different types of approaches were used to block different pathways of endocytosis, looking for a reduction in HCC15.2 internalization. These approaches include chemical inhibition, siRNA, and dominant-negative constructs. Chemical inhibitors are often promiscuous, and siRNA often has off-target protein effects. Using two different reagents per pathway will aid in excluding off-target effect.

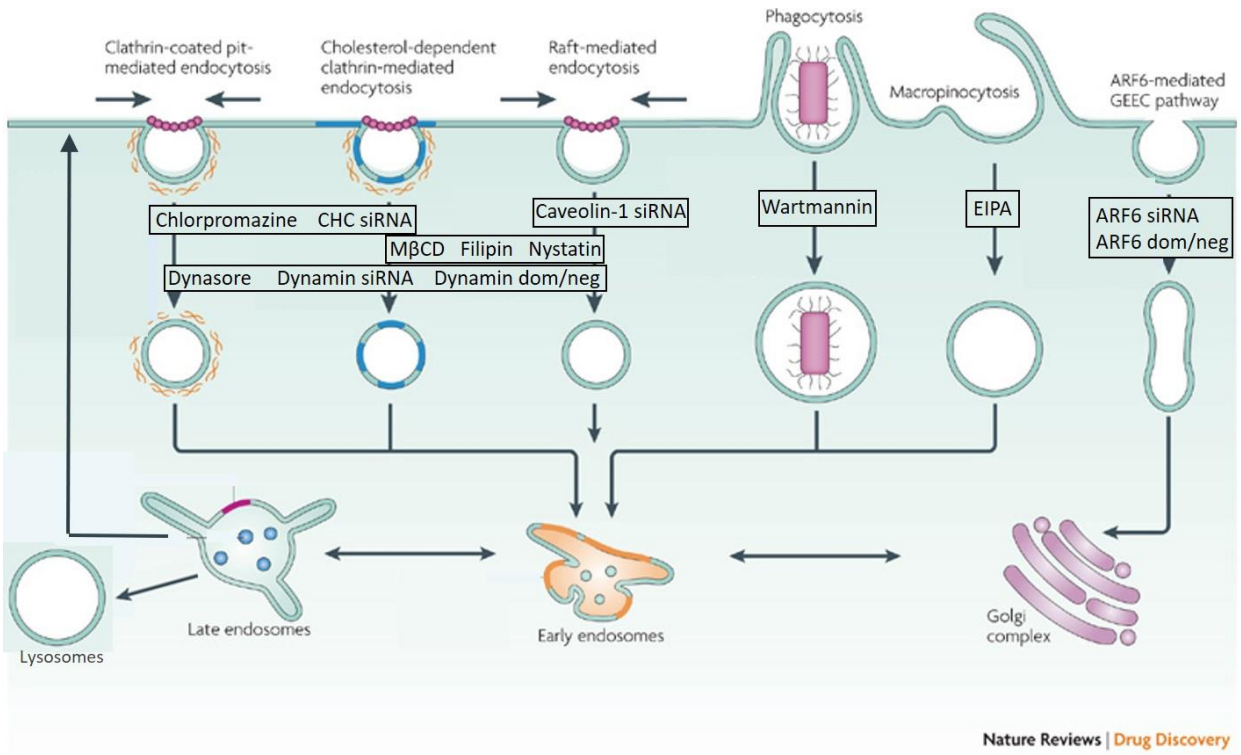

Figure 3-3 Possible Pathways of Endocytosis of HCC15.2
Figure adapted from Rajendran et al. doi: 10.1038/nrd2897 There are many pathways of endocytosis and methods to block them. Small molecule inhibitors, siRNA, and dominant/negative constructs have been used to determine which pathway is responsible for HCC15.2 internalization.

Each of the chemical inhibitors were titered to find the maximum tolerable dose on the cell line of interest. Inhibition of peptide internalization was then measured by flow cytometry and microscopy. Similarly, siRNA was electroporated into cells for the flow and microscopy assays, and western blot analysis was employed to determine knockdown efficiency. Dominant negative constructs are mutated proteins that bind like wild-type proteins in the cell but are nonfunctional. They compete with functional proteins for binding, substrate, etc., and the effect is similar to protein knock down by siRNA. Fluorescent protein-labelled dominant negative constructs were electroporated into H1299 cells for microscopy.

3.2.3.1 Clathrin-Mediated Endocytosis is not Involved in HCC15.2 Internalization

Chlorpromazine is thought to deplete clathrin from the plasma membrane, blocking clathrin-mediated endocytosis (CME) [2]. Chlorpromazine (50 µM) was preincubated with the desired cell type for 10 minutes prior to incubation with the peptide and was included during the 1-hour incubation of HCC15.2. Chlorpromazine treatment decreased HCC15.2 internalization by ~40% (Figure 3-4 b), but only in H1299 cells. Inhibition of HCC15.2 internalization was not observed in H2009 or H1993 cells. These data suggest that CME is not the pathway of HCC15.2 endocytosis, and that the inhibition seen in H1299 cells with chlorpromazine is likely due to off-target effects.

a

Chemical	Pathway	Conc	Preincubation
Chlorpromazine	Clathrin	50 µM	10 min
MβCD	Cholesterol Dependent	2 µM	10 min
Filipin	Cholesterol Dependent	5 µM	10 min
Nystatin	Cholesterol Dependent	10 µM	10 min
EIPA	Micropinocytosis	10 µM	30 min

b

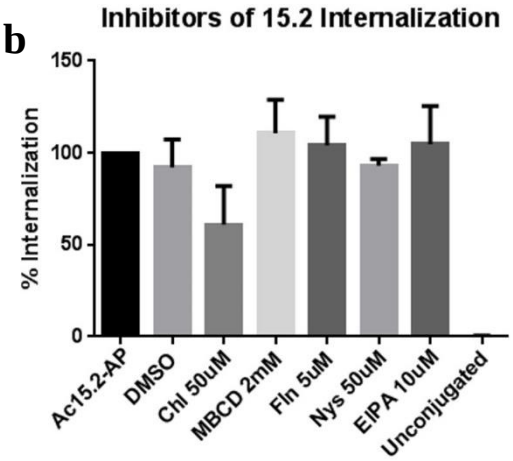

Figure 3-4 Chemical Inhibitors of Endocytosis do not Block HCC15.2 Internalization
a) Table of small molecule inhibitors, the pathway they block, the concentration used and the preincubation time. b) H1299 cells were incubated with inhibitor before and during 1-hour HCC15.2-SAPE incubation. Inhibition of HCC15.2 internalization was measured by flow cytometry. Chlorpromazine inhibited HCC15.2 internalization by ~40%; no other inhibitors had any measurable effect.

In order to validate that clathrin mediated endocytosis is not involved in peptide internalization, a different method of clathrin inhibition was used, specifically siRNA. Clathrin heavy chain 1 (CHC1) and clathrin heavy chain 2 (CHC2) were knocked down by electroporation of the appropriate siRNA into H1299 cells and plated in a 12 well culture plate.

The following day, cells were incubated with 25 nM HCC15.2-SAPE for 1 hour and peptide uptake was analyzed by flow cytometry. Knockdown cells were also treated with 50 nM HCC15.2-Alexa Fluor™ 555 for 1 hour (red), then washed, fixed, counterstained for cell membrane (green) and nuclei (blue), and analyzed by fluorescence microscopy. Clathrin knockdown had no effect on peptide internalization, as determined by flow cytometry (Figure 3-5 b), or microscopy (Figure 3-6) despite highly efficient protein reduction (Figure 3-5 a). This data supports that the modest inhibition seen with chlorpromazine treatment in H1299 cells was due to off-target effects.

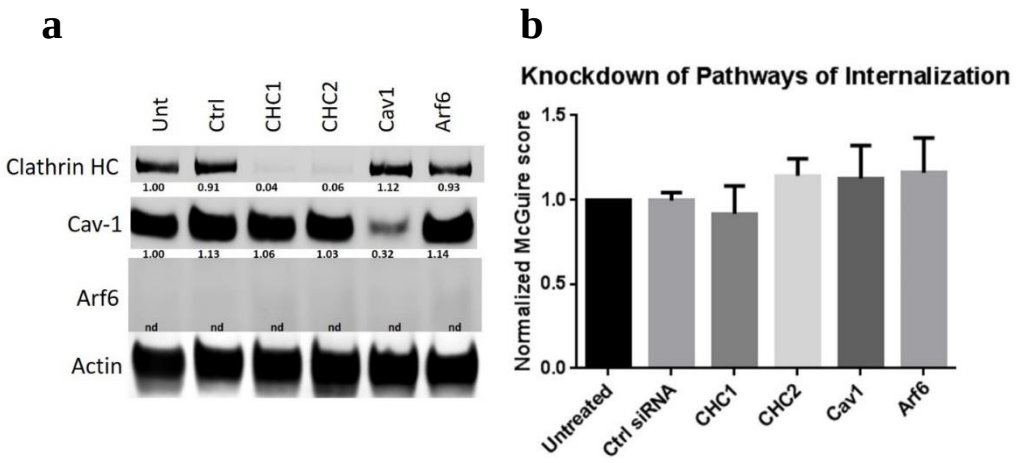

Figure 3-5 siRNA Knockdown of CHC1, CHC2, Cav1, and Arf6 does not Inhibit HCC15.2 Uptake by Flow Cytometry
a) Western blot analysis of protein knockdown in H1299 cells shows good knockdown of protein expression in CHC1, CHC2, and Cav1. Arf6 appears to be in very low abundance in these cells.
b) The second panel shows data from ≥3 flow experiments summarizing peptide internalization. No inhibition of peptide internalization was seen, despite good knockdown of protein expression.

3.2.3.2 HCC15.2 is not Dynamin Dependent

Dynamin is a protein vital in several pathways of endocytosis, including CME and some clathrin-independent endocytic (CIE) pathways (Figure 3-3). Dynamin is involved in scission of invaginated vesicles required for complete internalization. Dynasore is a small molecule drug thought to inhibit dynamin activity [3]. H1299 cells treated with dynasore show no inhibition of

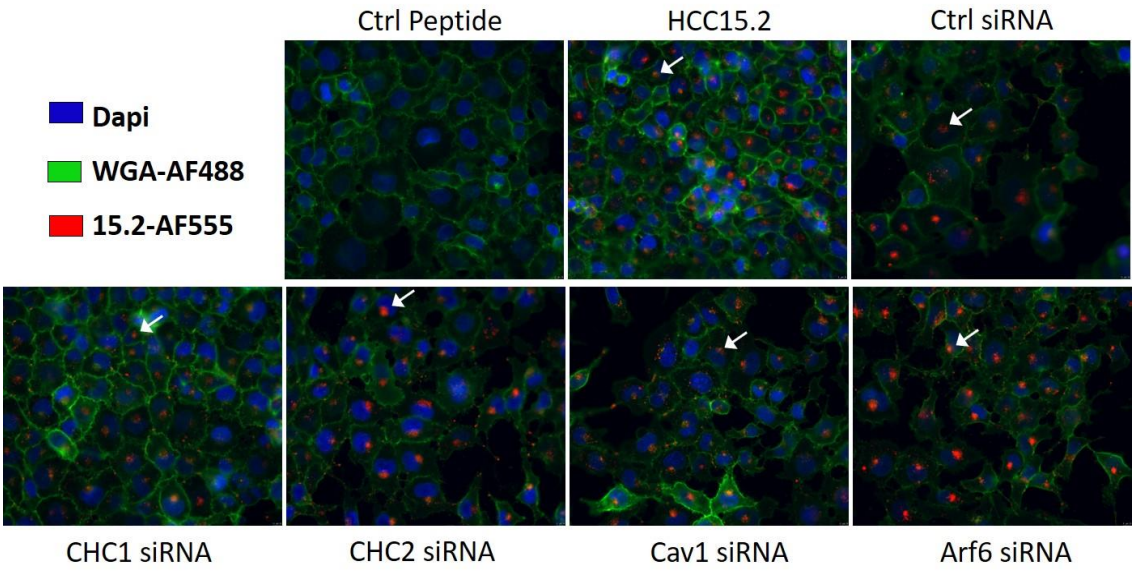

Figure 3-6 siRNA Knockdown of CHC1, CHC2, Cav1, and Arf6 does not Inhibit HCC15.2 Uptake by Fluorescence Microscopy
siRNA was delivered to H1299 cells via electroporation and cells were plated on an 8-well chamber slide. After 24 hours, 50nM HCC15.2-Alexa Fluor555 (red) was incubated with cells for 1 hour. Cells were fixed and counterstained with WGA-Alexefluor488 (cell membrane) and DAPI (nuclei). Representative images (n≥3) show no significant inhibition of peptide internalization. Punctate perinuclear peptide staining indicated by white arrows.

HCC15.2 uptake by the flow cytometry assay (Figure 3-4 b). Further, expression of the dominant negative dynamin construct in H1299 cells also showed no apparent inhibition of peptide internalization by microscopy (Figure 3-7). This supports the previous data that CME is not involved in HCC15.2 internalization. It also suggests that other pathways in which dynamin is involved, such as lipid raft/caveolin dependent endocytosis are also not responsible for peptide internalization.

3.2.3.3 Lipid Raft/Caveolin Mediated Endocytosis is not Involved in HCC15.2 Internalization

siRNA for caveolin-1 (Cav1) was electroporated into H1299 cells to determine whether or not caveolin dependent endocytosis played a role in HCC15.2 uptake. Despite a 70% knockdown of Cav1 as determined by western blot (Figure 3-5 a), endocytosis of HCC15.2 was unaltered, as measured by flow cytometry (Figure 3-5 b) and microscopy (Figure 3-6).

Cholesterol, like dynamin, plays a vital role in several pathways (Figure 3-3) Cholesterol is important in maintaining lipid rafts, which are involved in cholesterol dependent CME and in caveolin dependent endocytosis [4]. Methyl-beta-cyclodextrin (MβCD), filipin, and nystatin all work in a similar manner, by cholesterol depletion or sequestration, which inhibits cholesterol dependent (lipid raft) endocytosis [5]. These were used at 2 µM, 5 µM, and 50 µM respectively, with a 10-minute pre-incubation. No inhibition of HCC15.2 internalization was observed in any of these treatment groups (Figure 3-4 b).

3.2.3.4 HCC15.2 Binding does not Trigger Bulk Fluid Uptake

Peptide binding could also trigger bulk, nonspecific uptake of the surrounding fluid. Cells treated with 5 µM wortmannin, an irreversible phosphoinositide 3 kinase (PI3K) inhibitor which blocks phagocytosis [6], showed no inhibition of HCC15.2 internalization. EIPA (5-(N-Ethyl-N-isopropyl)amiloride) inhibits micropinocytosis by blocking NA^+/H^+ exchange across the plasma membrane [7]. Cells treated with 10 µM EIPA with a 30-minute preincubation also showed no inhibition of HCC15.2 internalization (Figure 3-4 b). Additionally, cells were incubated with peptide and unconjugated dye to see if HCC15.2 binding stimulates bulk fluid uptake. Under these conditions, no dye was observed inside the cell, indicating that peptide binding does not initiate uptake of the surrounding fluid and the free dye it contained. Taken together, these experiments suggest HCC15.2 binding does not trigger micropinocytosis or phagocytosis (Figure 3-4 b).

3.2.3.5 Arf6 is not Involved in HCC15.2 Internalization

ADP-ribosylation factor 6 (Arf6) is a small GTPase in the Ras superfamily which regulates endocytosis and recycling of membrane and membrane proteins. Dominant negative constructs for Arf6-CFP were electroporated into cancer cells. No selection marker was

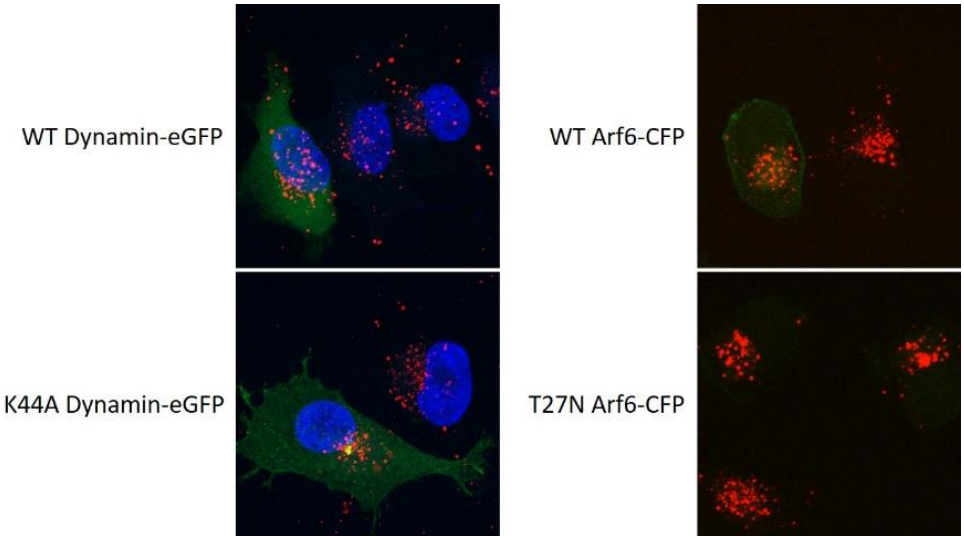

Figure 3-7 Dominant-negative Constructs do not Inhibit HCC15.2 Uptake
Wild type dynamin 1-pEGFP and dominant negative K44A-pEGFP (green, left) and wild type pARF6-CFP and dominant negative mutants pARF6(Q67L)-CFP and pARF6(T27N)-CFP (green, right) were transfected into H1299 cells and plated onto 8-well chamber slides. After 24 hours, cells were incubated with 50 nM HCC15.2-Alexa Fluor 555 for 1 hour and then washed, fixed, and counterstained with DAPI. Representative compressed images from confocal microscopy reveal no difference in peptide uptake or localization in dominant negative expressing cells.

available, so confocal microscopy was used to look for cells expressing the fluorescent protein labeled dominant-negative construct (green). Electroporated cells were incubated with 50 nM HCC15.2-Alexa Fluor™ 555 (red) for 1 hour, washed, fixed, and counterstained with DAPI (blue). No inhibition of HCC15.2 internalization was observed in dominant negative expressing cells compared to WT-Arf6 expressing cells and non-transfected cells (Figure 3-7). The role of Arf6 was also tested with siRNA. siRNA knockdown of Arf6 showed no inhibition of HCC15.2 internalization by flow cytometry (Figure 3-5 b). However, endogenous Arf6 expression is nearly undetectable by western blot (Figure 3-5 a), and is unlikely to be responsible for peptide internalization. Flow cytometry, microscopy and western blot data all suggest that Arf6-mediated endocytosis is not responsible for HCC15.2 internalization.

Endocytic Pathway	Reagent	Result	Method	Cell Line
Clathrin Mediated	Chlorpromazine CHC siRNA	~40% inh (H1299) No Change	Flow/Microscopy Flow/Microscopy	H1299/H2009/H1993 H1299/H2009
Lipid Raft / Cholesterol Dependent	MβCD Filipin Nystatin	No Change No Change No Change	Flow/Microscopy Flow/Microscopy Flow/Microscopy	H1299/H2009/H1993 H1299/H2009/H1993 H1299/H2009/H1993
Dynamin Dependent	Dynasore Dynamin Dom/ Neg	No Change No Change	Flow Microscopy	H1993 (1 repeat) H1299
Arf6 Dependent	Arf6 siRNA Arf6 Dom/Neg	No Change No Change	Flow/Microscopy Microscopy	H1299 H1299
Caveolin Dependent	Caveolin1 siRNA	No Change	Flow/Microscopy	H1299/H2009
Phagocytosis	Wartmannin	No Change	Flow	H1993 (1 repeat)
Macropinocytosis	EIPA	No Change	Flow/Microscopy	H1299/H2009

Table 3-1 Summary of Internalization Experiments
Summary of all the internalization experiments. Un-highlighted cells are chemical inhibition experiments, yellow highlighted cells are siRNA experiments, blue highlighted cells are dominant negative experiments. Most have 3 repeat experiments in 1 or more cell lines except dynasore and wartmannin, which are in process and have only 1 repeat.

Through this line of experimentation, a number of pathways of endocytosis can be ruled out as likely for HCC15.2 internalization (Table 3-1). The only inhibition observed was from chlorpromazine treatment, which blocked internalization of HCC15.2 by ~40%; however, neither clathrin knockdown nor dynasore treatment blocked internalization. This indicates CME does not play a significant role in HCC15.2 internalization. Phagocytosis, pinocytosis, cholesterol dependent endocytosis and caveolin dependent endocytosis can also be ruled out as likely pathways of HCC15.2 internalization. Arf6 dependent endocytosis is unlikely, as Arf6 is not expressed in these cells and neither siRNA nor dominant negative expression inhibited HC15.2 uptake. This leaves the CLIC-GEEC, flotillin, and RhoA pathways as possible routes of HCC15.2 internalization. More experimentation with inhibitors such as brefeldin A (CLIC-GEEG) and siRNA are in process.

3.2.4 HCC15.2 is Trafficked to and Accumulates in Lysosomes

3.2.4.1 HCC15.2 Colocalizes with Lysosomal Organelle Marker

Plasmids containing GFP-labelled, organelle specific proteins were electroporated into H1299 cells, and selected on G418. Labelled organelles included nuclei, ER, Golgi, lysosome, mitochondria, cytosol, and plasma membrane (green). When the labelled proteins were stably expressed, cells were plated in an 8 well chamber slide. The next day, the cells were treated with 50 nM HCC15.2-Alexa Fluor™ 555 (red) for 1 hour, washed, fixed and counterstained with DAPI (blue). HCC15.2 colocalization was only observed in lysosome labelled cells, seen as yellow pixels indicated by red arrows in Figure 3-8.

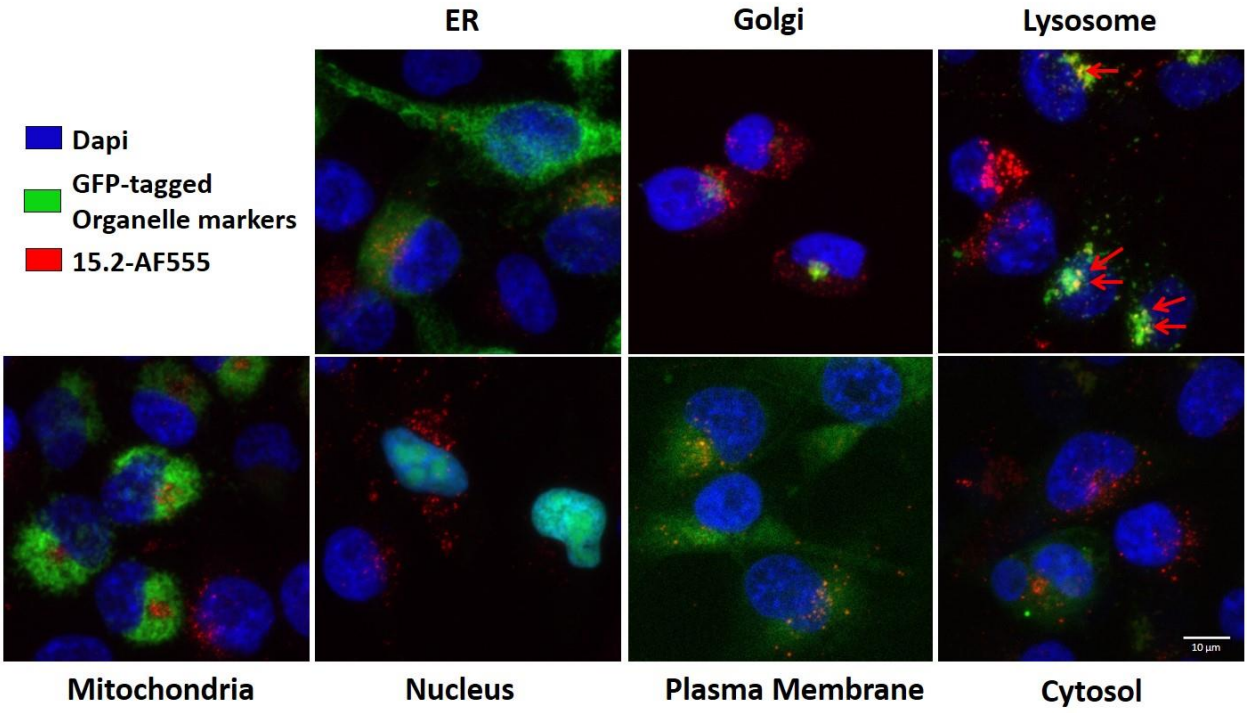

Figure 3-8 HCC15.2 Colocalizes with a Lysosomal Organelle Marker
H1299 cells were labelled with GFP-tagged organelle-specific proteins for ER, Golgi, lysosome, mitochondria, nucleus, plasma membrane, and cytosol (green). Cells were incubated with 50 nM HCC15.2-Alexa Fluor555 (red) for 1 hour at 37˚C. Cells were fixed and counterstained with DAPI (blue) and imaged on a Zeiss LSM 700 to look for colocalization of the peptide with any of the organelle markers. Representative compressed z-stacks show clear colocalization of HCC15.2 with labelled lysosomes (red arrows). No colocalization was observed in other groups.

3.2.4.2 HCC15.2 Accumulates in Lysosomes Over Time

A time-course experiment allowed for verification of lysosomal localization as well as observation of trafficking and accumulation. Lysosome-labelled cells (green) were treated with HCC15.2-Alexa Fluor™ 555 (red) for 30 minutes, 1 hour, 4 hours, or 24 hours, after which the cells were washed, fixed, and counterstained with DAPI (blue). Images were analyzed using ZEN colocalization software. Peptide-containing vesicles (red) are clearly seen at 30 minutes separate from the labeled lysosomes, which by 1 hour have started to colocalize with lysosomal vesicles (yellow). HCC15.2 remains colocalized with lysosomes out to 24 hours (Figure 3-9, top row).

The degree of colocalization was quantified for each slice using ZEN software (Figure 3-9, row 2). Thresholds were set for organelles (green, Y-axis) and peptide (red X-axis) on unlabeled (box 1) and untreated cells (box 2). Pixels in box 3 contain both peptide and organelle signal and are falsely colored yellow in the top row single slice images. At 30 minutes, most pixels are separate in boxes 1 and 2. By one hour many have moved to box 3, at 4 and 24 hours nearly all pixels are in box 3. This trafficking, accumulation and retention in the lysosomes is even more evident in the compressed maximally projected z-stack of the cells (Figure 3-9, row 3).

A Mander's colocalization coefficient was calculated based on the number of red pixels that contain green (Ch1) and the number of green pixels that contain red (Ch2), and averaged from all slices of 3 separate images (Table 3-2). The coefficient is given on a scale of 0–1, with 0 being no colocalization, and 1 being 100% colocalization. Again, at 30 minutes colocalization is only beginning; then it increases with time and is retained out to 24 hours.

Weighted Colocalization Coefficient

Hours	CH1	CH2
0.5	0.40	0.21
1	0.68	0.73
4	0.77	0.88
24	0.70	0.71

Table 3-2 Colocalization Quantification
In each slice, Mander's coefficients can be calculated which represent the proportion of red pixels that also have green (CH1) and vice versa (CH2). This table contains the averages from all the slices at the different time points. 0 is low correlation and 1 is perfect correlation.

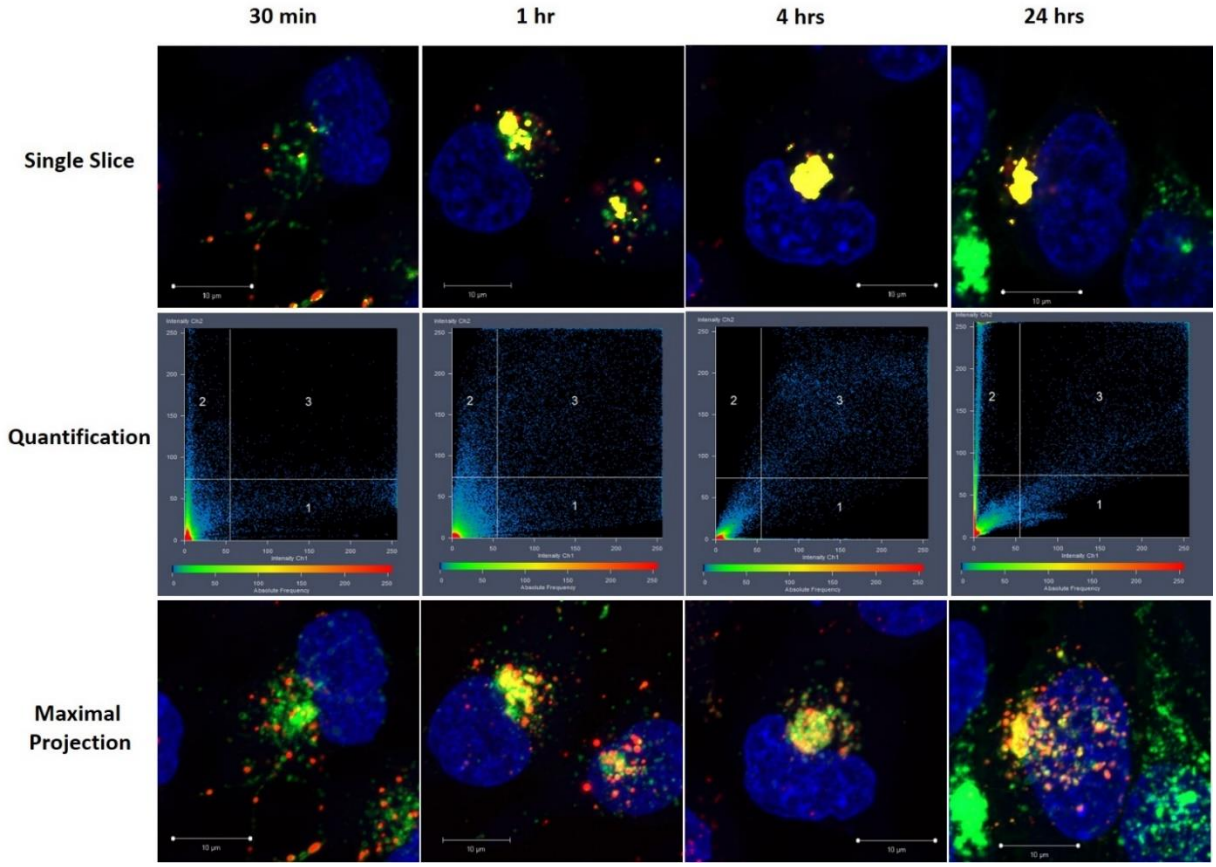

Figure 3-9 HCC15.2 Accumulates in Lysosomes Over Time
HCC15.2-AF555 (red) was incubated with lysosome-labelled (green) H1299 cells for 0.5, 1, 4, and 24. Cells were washed, fixed, and stained for DAPI (blue). Pixels from Representative single slice images (row 1) were plotted (row 2) based on intensity. Exclusively red pixels (box 1) are peptide-loaded vesicles, exclusively green pixels (box 2) are lysosomes, and box 3 contains both and pixels are falsely colored yellow in the single-slice images. Row 3 is the maximally projected compressed z-stack. Peptide-filled vesicles can be tracked heading towards the lysosomes at 30 minutes, with many already colocalizing by 1 hour. Practically all peptide is found within lysosomes by 4 hours and retained there out to 24 hours.

3.3 Discussion

Discovery of the mechanism of endocytosis and localization would not only lead to understanding of the biology behind peptide internalization, but would also help on two downstream aspects of the project. First it would narrow down the list of candidate receptors that could be responsible for peptide binding and internalization (Chapter 6). Second, it would help guide the choice of the therapeutic to deliver (Chapter 5). Several pathways of endocytosis have been conclusively ruled out as responsible for HCC15.2 internalization and other pathways are currently under experimentation. It was also found that HCC15.2 binds to a cellular receptor and traffics to and accumulates in lysosomes.

The case for internalization being mediated by a receptor is overwhelmingly supported by the data. HCC15.2 binding is sequence dependent, and specific to a discrete subset of cell lines. Internalization is temperature and protease sensitive as well as saturable over time and with increasing concentration. Internalization can also be blocked with excess unlabeled HCC15.2. Further, inhibition of protein synthesis decreases total peptide uptake by half over a 24-hour time period. All of these data support the theory of a limited proteinaceous cellular receptor as the binding partner for HCC15.2 that mediates internalization.

HCC15.2 clearly traffics to the lysosome and accumulates there over time. This is supported by the protein synthesis inhibition data. The receptor is not recycled back to the surface, but degraded in the lysosome, requiring new protein synthesis for additional peptide internalization. The colocalization barely begins to show after 30 minutes of HCC15.2 incubation, suggesting it also traffics through endosomes at earlier timepoints. Unfortunately, the endosomal marker did not work, but upon close examination of the 30-minute timepoint, the

peptide vesicles appear in line with lysosomes along a cytoskeletal strand. Trafficking through a lysosome is convenient for drug delivery, the subject of chapter 5. Lysosomes contain many proteases, among them Cathepsin B. Cathepsin B has a short recognition sequence after which it cleaves, valine citrulline (VC). There are many cathepsin cleavable reagents and therapeutics commercially available. Clinically approved ADC Adcetris utilizes a cathepsin linker to attach MMAE.

Failure to identify a pathway responsible for endocytosis could be due to a number of reasons: HCC15.2 most likely internalizes using a mechanism that has not been tested yet. Several pathways such as clathrin independent carriers, glycosylphosphatidylinositol-anchored protein (GPI_AP) enriched endosomal compartment (CLIC-GEEC), flotillin, and RhoA dependent endocytosis have yet to be tested. These pathways are less well-characterized than CME, but a number of proteins could be knocked down to block these pathways. CLIC-GEEC for example is dependent on cdc42, ARF1, and GRAF1, and would be susceptible to siRNA targeting any of these proteins. Similarly, Brefeldin A, a small molecule inhibitor of ARF1, also inhibits CLIC-GEEC endocytosis. These experiments are ongoing in the lab.

The CLIC-GEEC pathway is clathrin, dynamin, and caveolin independent, but is regulated by cdc42, which activity is cholesterol dependent [8, 9]. As the name suggests, this pathway serves as the major recycling mechanism for many GPI-APs (often associated with lipid rafts) and also accounts for a large fraction of bulk fluid uptake. There was no decrease in HCC15.2 internalization with cholesterol depletion, nor was there any observable uptake of unconjugated dye from the surrounding fluid with peptide treatment. Both of these results suggest that the CLIC-GEEC pathway is not likely to be responsible for HCC15.2 internalization.

RhoA dependent endocytosis relies on lipid rafts and dynamin and is the main internalization pathway for IL2 and botulinum toxin [10]. Cholesterol depletion (which disrupts lipid rafts) and dynamin knockdown both failed to inhibit HCC15.2 uptake in the previous studies. This pathway is unlikely to be involved in peptide internalization.

Flotillin dependent endocytosis is raft dependent and, depending on the cargo, can be dynamin dependent. Flotillin itself may not be involved in endocytosis, but of recruitment of proteins to invaginating regions. Proteoglycans, cholera toxin b, shiga toxin and some GPI anchored proteins are internalized through this pathway [11]. Knockdown of flotillin is ineffective at blocking internalization of some cargoes, so Fyn kinase may be a better target to inhibit this pathway [12].

There is also redundancy and overlap in the pathways, which leads to compensation[10]. In a systematic thorough study of mechanisms of endocytosis in NSCLC, Elkin et al. concluded that virtually all endocytic pathways in cancer are altered from normal [1]. Another study describes redundancy and overlap of the pathways using cholera toxin B (CTXB). CTXB normally internalizes via CIE, but was induced to internalize via CME with low CAV-1 expression [13]. This redundancy is more difficult to test as dual inhibition is often toxic to cells.

3.4 Conclusion

While the pathway of internalization has proved elusive as yet, experimentation in progress may yield results. HCC15.2 clearly accumulates in lysosomes which could facilitate rational peptide-drug conjugate design. Understanding the dynamics of endocytosis will also aid in treatment design. Short pulses that reach saturation days apart will work better than constant administration.

3.5 Materials & Methods

3.5.1 Materials

3.5.1.1 GFP-Labeled Constructs

Plasma membrane label Src-myrisylated-GFP, pmyr GFP was a gift from Kenneth Yamada (Addgene plasmid # 50528). Golgi label beta-1,4-galactosyltransferase 1-GFP, PA-GFP was a gift from Michael Davidson (Addgene plasmid # 57164). Lysosome Label Lamp-1-GFP, Emerald-lysosome-20 was a gift from Michael Davidson (Addgene plasmid # 56476). ER label SigPep-eGFP-KDEL, mEGFP-Endoplasmic Reticulum was a gift from Michael Davidson (Addgene plasmid # 56455). Mitochondria label mitochondrial import receptor subunit translocase of outer membrane 20 kDa subunit-GFP, mEmerald-TOMM20-N-10 was a gift from Michael Davidson (Addgene plasmid # 54282). Nucleus label SV40 NLS-GFP, mEmerald-Nucleus 7 was a gift from Michael Davidson (Addgene plasmid # 54206). Cytoplasm label Argonaut 3 isoform A-GFP, mEmerald-EIF2C3-C18 was a gift from Michael Davidson (Addgene plasmid # 54078). Golgi label Tyrosyl protein sulfotransferase 2, TPST2-EGFP was a gift from Michael Davidson (Addgene plasmid # 66618).

3.5.1.2 Chemical Inhibitors

Chemical inhibitors chlorpromazine, nystatin, filipin, and wortmannin were all purchased from Sigma Aldrich (Sigma Aldrich, St. Louis, MO). Dynasore was purchased from Tocris Bioscience (Bristol, United Kingdom). EIPA was purchased from Santa Cruz Biotechnology (Dallas, TX) siRNA was purchased from Invitrogen (Thermo Fisher Scientific, Waltham, MA).

3.5.1.3 Dominant negative mutants

Wild type pARF6-CFP was a gift from Joel Swanson (Addgene plasmid # 11382). Dominant negative mutant pARF6(Q67L)-CFP was a gift from Joel Swanson (Addgene plasmid # 11387). Dominant negative mutant pARF6(T27N)-CFP was a gift from Joel Swanson (Addgene plasmid # 11386). WT dynamin 1 pEGFP was a gift from Sandra Schmid (Addgene plasmid # 34680). K44A dynamin 1 pEGFP was a gift from Sandra Schmid (Addgene plasmid # 34681).

3.5.2 Methods

3.5.2.1 Flow Cytometry

As described in chapter 2.

3.5.2.2 Electroporation

Cells were grown to 90% confluency and removed from the growth plate using Trypsin + EDTA. Cells were washed and resuspended at a concentration of $1x10^7$ cells/mL in electroporation buffer 40. 100 µL of cells are mixed with 10 µL siRNA or plasmid then transferred to an electroporation cuvette with a 2 mm gap. The Eppendorf Electroporator 2510 (Eppendorf AG, Hamburg, Germany) was set to 500 volt and pulsed three times, checking the actual voltage to verify 210-220. Cells were diluted into 1 mL of RPMI + 5% FBS and plated for experiments. Buffer 40 for electroporation was made with 140mM Na_2HPO_4, 5mM KCl, and 10mM MgCl.

3.5.2.3 Confocal Microscopy

Plasmids with organelle-specific markers labeled with GFP were purchased from Addgene (Cambridge, MA) and electroporated into H1299 cells. After G418 selection, GFP-

labeled tumor cells were plated on 8-well chamber slides on the day previous to the study. Biotinylated peptide was conjugated to streptavidin-Alexa Fluor™ 555 (1:1) for 30 min at RT and quenched with RPMI, then added to the wells at 50 nM. After 1-hour incubation cells were washed for 5 min 3x with PBS, 2x acid rinses, and 1x PBS rinse. Cells were fixed in 2% formaldehyde for 10 min, washed with PBS, stained with DAPI in mounting media and coverslip was added. Microscopy was acquired on a Zeiss LSM 700 (Oberkochen, Germany) with a Pln Apo 63x/1.4 oil DIC III objective. Compressed images were obtained using ImageJ software, maximal intensity projections.

3.5.2.4 Colocalization Quantification

Thresholds were established for Ch1, representing the peptide in the red channel (75), and Ch2, representing the lysosome in the green channel (55). Each pixel of a single slice was evaluated for passing the threshold in red (box 1), green (box 2), or both (box3). Pixels found in box 3 are colored yellow in the confocal image. Mander's coefficients are calculated by the software for each slice. The number given (0–1) represents the proportion of positive pixels that are also positive for the other color. The higher the number the higher the correlation.

3.6 References

[1] Elkin SR, Bendris N, Reis CR, Zhou Y, Xie Y, Huffman KE, et al. A Systematic Analysis Reveals Heterogeneous Changes in the Endocytic Activities of Cancer Cells. Cancer research. 2015;75:4640-50.

[2] Wang LH, Rothberg KG, Anderson RG. Mis-assembly of clathrin lattices on endosomes reveals a regulatory switch for coated pit formation. The Journal of Cell Biology. 1993;123:1107.

[3] Macia E, Ehrlich M, Massol R, Boucrot E, Brunner C, Kirchhausen T. Dynasore, a Cell-Permeable Inhibitor of Dynamin. Developmental Cell.10:839-50.

[4] Brown DA, London E. FUNCTIONS OF LIPID RAFTS IN BIOLOGICAL MEMBRANES. Annual Review of Cell and Developmental Biology. 1998;14:111-36.

[5] Dutta D, Donaldson JG. Search for inhibitors of endocytosis: Intended specificity and unintended consequences. Cellular Logistics. 2012;2:203-8.

[6] Norman BH, Shih C, Toth JE, Ray JE, Dodge JA, Johnson DW, et al. Studies on the Mechanism of Phosphatidylinositol 3-Kinase Inhibition by Wortmannin and Related Analogs. Journal of Medicinal Chemistry. 1996;39:1106-11.

[7] Koivusalo M, Welch C, Hayashi H, Scott CC, Kim M, Alexander T, et al. Amiloride inhibits macropinocytosis by lowering submembranous pH and preventing Rac1 and Cdc42 signaling. The Journal of Cell Biology. 2010;188:547.

[8] Chadda R, Howes MT, Plowman SJ, Hancock JF, Parton RG, Mayor S. Cholesterol-Sensitive Cdc42 Activation Regulates Actin Polymerization for Endocytosis via the GEEC Pathway. Traffic. 2007;8:702-17.

[9] Sabharanjak S, Sharma P, Parton RG, Mayor S. GPI-Anchored Proteins Are Delivered to Recycling Endosomes via a Distinct cdc42-Regulated, Clathrin-Independent Pinocytic Pathway. Developmental Cell.2:411-23.

[10] Sandvig K, Pust S, Skotland T, van Deurs B. Clathrin-independent endocytosis: mechanisms and function. Current Opinion in Cell Biology. 2011;23:413-20.

[11] Doherty GJ, McMahon HT. Mechanisms of Endocytosis. Annual Review of Biochemistry. 2009;78:857-902.

[12] Otto GP, Nichols BJ. The roles of flotillin microdomains – endocytosis and beyond. Journal of Cell Science. 2011;124:3933.

[13] Singh RD, Puri V, Valiyaveettil JT, Marks DL, Bittman R, Pagano RE. Selective Caveolin-1–dependent Endocytosis of Glycosphingolipids. Molecular Biology of the Cell. 2003;14:3254-65.

Chapter 4 HCC15.2 Delivers Near IR Dyes to *In Vivo* Tumors for Whole Animal Imaging

4.1 Introduction

Clinical outcomes of cancer patients are far more favorable when the cancer is diagnosed early. Imaging and diagnostics are becoming increasingly important for earlier detection, especially in NSCLC. Nearly 60% of NSCLC patients are diagnosed with metastatic disease, which has a dismal 4% 5-year survival rate. If the tumor is already too advanced, treatment is only palliative. The current recommendation is to screen patients at high risk for developing lung cancer with yearly LDCT scans. In a large international screen, this was shown to improve survival in about 20% of the patients [1]. However, the study had a high false-positive rate, leading to more invasive biopsies. There is an urgent need for specific, reliable imaging diagnostics.

HCC15.2 has demonstrated high specificity for cancerous tissue, while delivering various cargoes into the cells. HCC15.2 also binds human NSCLC biopsy samples and not adjacent normal tissue. This suggests that HCC15.2 is a good candidate for specifically delivering high contrast imaging agents to tumors *in vivo*. This chapter describes testing of the ability of HCC15.2 to home to a human NSCLC xenograft in nude mice after systemic delivery for whole animal imaging. This serves as an *in vivo* validation for downstream drug delivery experiments, and also allows for evaluation of HCC15.2 as a clinical diagnostic marker and imaging agent.

4.2 Results

4.2.1 HCC15.2 Homes to In Vivo *Tumors After Systemic Delivery*

The ability of HCC15.2 to deliver a variety of cargoes to cancer cells *in vitro* has been previously demonstrated (Chapter 2), but to systemically administer a targeted dye *in vivo* and ask it to home to and accumulate in a tumor is a more relevant experiment. H2009 tumors were implanted on the flanks of female nude mice. H2009 cells establish more consistently sized tumors, and more quickly, than H1299 cells. When the tumors reached approximately 100 mm^3 in size, the mice were grouped and randomly assigned one treatment; HCC15.2-AF750, control -F15.2-AF750, or PBS. HCC15.2-AF750 (15 µg/100µl) or controls were injected via lateral tail vein.

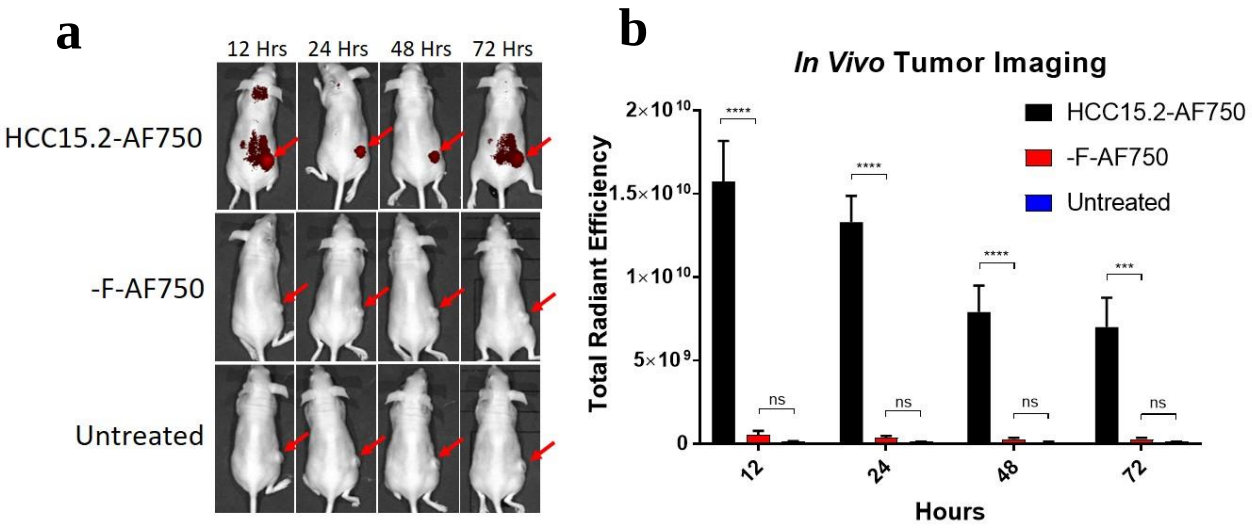

Figure 4-1 HCC15.2 Homes to Xenograft Tumor After Systemic Delivery
H2009 tumor bearing nude mice were injected with HCC15.2 labeled with NIR dye Alexa Fluor™ 750. 12, 24, 48, and 72 hours post injection, mice were anesthetized and imaged on an IVIS® (Perkin Elmer). a) A representative mouse (n=4) from each group is followed through all time points. Tumors are indicated by red arrows. ROIs were drawn around each tumor and the range (min–max) was applied to all animals at each time point, but varied between time points due to clearance: Range at 12 hours ($1.75e^9$–$5e^9$), 24 hours ($1.5e^9$–$4\ e^9$), 48 hours ($9e^8$–$4e^9$), and 72 hours ($5e^8$–$3e^9$). b) Quantification of the average total radiant efficiency over time. 15.2 peptide accumulates in tumor is 25–39 fold better than control peptide and the control peptide is statistically no different than untreated. **** p value < 0.0001, *** p value < 0.001

After 12 hours, mice were anesthetized with isoflurane, marked, and imaged in an IVIS® (Perkin Elmer). Mice were imaged again at 24, 48, and 72 hours.

One representative animal from each group was followed over time (Figure 4-1 a). The signal from the regions of interest (ROIs) of all four animals was quantified. At 12 hours, HCC15.2 targets dye to the tumors 30 times better than the control peptide. At 24, 48 and 72 hours, the targeting is 39, 30, and 25-fold better than control (Figure 4-1 b). It was also noted that the control peptide has no statistically significant accumulation compared to animals that received no dye at all.

4.2.2 Ex Vivo *Imaging of HCC15.2 Biodistribution*

After the 72-hour whole animal imaging was completed, the mice were euthanized and the organs were imaged and weighed. Figure 4-2a shows the organs and tumor from a

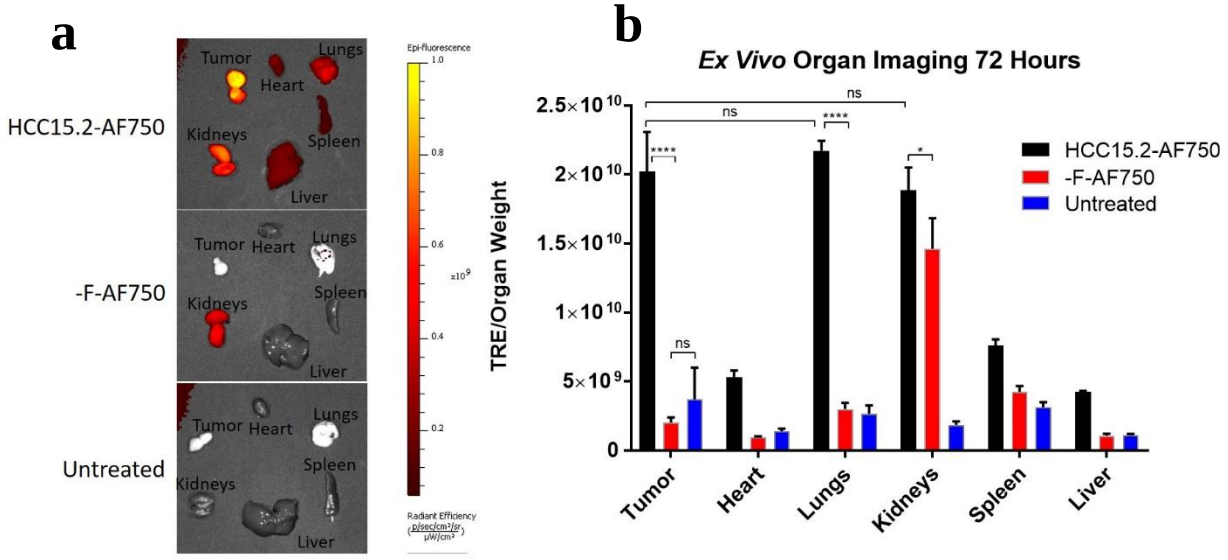

Figure 4-2 HCC15.2 Biodistribution in *Ex Vivo* Organ Imaging
The first panel shows representative e*x vivo* imaging of organs and tumors at 72 hours. ROIs were drawn around each organ/tumor and the total radiant efficiency was divided by the weight of the organ/tumor. The graph shows the quantification of *ex vivo* organs from all four animals 72 hours after injection. 15.2 targeting accumulated in the tumor 10-fold better than control peptide. Kidneys signal was high in targeted and nontargeted due to clearance. Lung signal was seen with HCC15.2 peptide and not with control. **** p value < 0.0001, * p value < 0.05

representative animal of each treatment group. Clear accumulation of the dye is seen in the tumor of HCC15.2-treated animals, while no accumulation is seen in group treated with the control peptide. The total radiant efficiency (TRE) of each organ, was divided by the weight of that organ, then averaged between all animals in the same group. With this *ex vivo* measurement, the HCC15.2 targeted tumors accumulated 10-fold more dye than the control -F15.2 nontargeted tumors. However, there was also a large specific signal in the lungs of HCC15.2 treated animals, which is likely due to the mouse model. The kidneys are the main clearance organs and as such, high signal was observed in both the targeted and nontargeted animal groups (Figure 4-2 b).

The tumors were fixed in formaldehyde, aligned according to treatment group, and imaged on a LICOR® Odyssey CLx (Figure 4-3 a). The HCC15.2 treated tumors show a 27-fold increase in dye accumulation (Figure 4-3b). This is similar to the 25-fold increase seen in the 72-hour whole animal imaging, but significantly more than what was seen in the previous *ex vivo* imaging in the IVIS®.

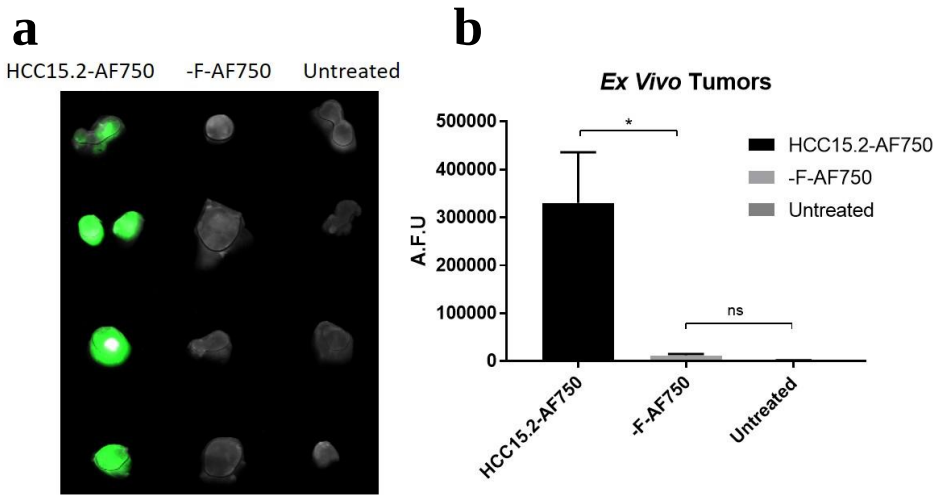

Figure 4-3 HCC15.2 Targeted Dye is Retained in Tumors Out to 72 Hours
Tumors were fixed in PBS + 4% formaldehyde and then imaged together on a LI-COR® Odyssey. ROIs were drawn around each tumor and the mean fluorescence intensity was graphed. Tumors treated with 15.2-AF750 show clear accumulation 27-fold greater than the control. The control peptide is statistically no different from untreated. * p value < 0.05

4.3 Discussion

HCC15.2 is ideal for delivering imaging agents. The peptide specifically homes to an *in vivo* tumor and quickly triggers internalization, resulting in ~25-fold more dye accumulating in the tumor than non-targeted dye. HCC15.2 has also demonstrated ability to bind 25% of tested human NSCLC biopsy samples and 50% of NSCLC lines (Chapter 2). These experiments serve as a validation that HCC15.2 performs *in vivo* for downstream drug targeting applications. They also show the potential of HCC15.2 for clinical diagnostics and imaging.

Mouse lungs displayed a high signal with the HCC15.2 peptide and not with the -F15.2 peptide. Lung signal was also observed with unoptimized HCC15.2 tetramer reported in previous work [2]. This suggests that the receptor is present in normal mouse lung tissue. However, two separate TMAs showed no HCC15.2 binding to normal human lung tissue (chapter 2). Further, two immortalized, non-transformed human bronchial epithelial cell lines (HBEC and Beas-2B) do not bind or internalize HCC15.2. This evidence shows that HCC15.2 does not bind to normal human lung tissue, and that the lung signal observed in the *in vivo* imaging experiment is likely mouse specific.

H2009.1 is another peptide in the lab that has been extensively tested in mice and on human tissue. H2009.1 binding was observed in variable amount between mouse models. Probing this question more deeply, it was discovered that αVβ6, the target of H2009.1, was expressed in mouse lung and not in normal human lung tissue. The HCC15.2 receptor is also likely expressed in mouse lung and absent in normal human lung tissue. From this data, it cannot be determined which cell types in the mouse lung bind HCC15.2 or if it is internalized. Follow up experiments staining human and mouse lung tissue for HCC15.2 receptor expression would

be ideal; however, the receptor for HCC15.2 has not yet been identified (Chapter 6). The next ideal experiment would be to section the lungs of treated mice to look for which cells internalize the peptide. However, HCC15.2 does not fix well, as it has no free amines.

Chapter 6 details *in vivo* drug delivery experiments in the same mouse model. There was no observable gross toxicity in mouse lung during these experiments, suggesting that the normal lung tissue does not internalize the peptide-drug conjugate. The high lung signal seen in the HCC15.2 *in vivo* imaging experiments is a limitation of the mouse model, likely due to the model, and doesn't necessarily reflect what would happen in human patients.

This mouse model is not ideal for HCC15.2 experimentation. H2009 cells internalize less peptide than other cell lines, but H2009 cells establish tumors more consistently. H2009 tumors also become scabby and necrotic if they grow too large. Future studies will likely involve a different animal model.

4.4 Conclusion

The clinic is in need of reagents capable of detecting lung cancer at earlier stages. HCC15.2 has remarkable *in vivo* delivery capabilities and biodistribution in mice, delivering a dye to a tumor 30-fold better than a control peptide. HCC15.2 could aid in earlier detection of lung cancer in patients to give them a chance of a better outcome.

4.5 Materials & Methods

4.5.1 Materials

Nude mice were purchased from Jackson Laboratory (Bar Harbor, ME). Maleimide-Alexa Fluor™ 750 was purchased from Thermo Fisher Scientific (Waltham, MA)

4.5.2 Methods

4.5.2.1 Tumor Implantation

H2009 tumor cells were lifted with trypsin, washed, and suspended at $1x10^6$ cells/100 µl sterile PBS and 100 µl were injected subcutaneously on the flank of female athymic nude mice (Jackson Labs.) Tumors were allowed to grow until measuring ~100 mm^3 in volume by caliper using the equation $(\pi/6)*(l*w)^{3/2}$.

4.5.2.2 *In Vivo* Imaging

Cysteine labeled peptides were conjugated to maleimide Alexa Fluor™ 750 C5 (1:1.1) in sterile PBS pH 7.4 for 1 hour. Peptide-dye conjugate was diluted in sterile PBS to 15 µg/100 µl, and 100µl were injected intravenously via lateral tail vein into 4 mice/group. Mice were anesthetized with Isothesia and whole animal images were collected on an IVIS (PerkinElmer, Waltham MA) at 12, 24, 48, and 72 hours. All ROIs were drawn and calculated using the IVIS software; statistical analysis was performed on GraphPad Prism®.

4.5.2.3 *Ex Vivo* Imaging

Ex vivo tumors and organs were weighed and imaged on the IVIS at 72 hours. ROIs were drawn and calculated using the IVIS software; statistical analysis was performed on GraphPad Prism®. Tumors were fixed in 4% formaldehyde and imaged again on an Odyssey® CLx (LI-COR, Lincoln NE). ROIs were drawn and calculated using the Odyssey software; statistical analysis was performed on GraphPad Prizm®.

4.6 References

[1] The National Lung Screening Trial Research T. Reduced Lung-Cancer Mortality with Low-Dose Computed Tomographic Screening. The New England journal of medicine. 2011;365:395-409.

[2] McGuire MJ, Gray BP, Li S, Cupka D, Byers LA, Wu L, et al. Identification and Characterization of a Suite of Tumor Targeting Peptides for Non-Small Cell Lung Cancer. Scientific Reports. 2014;4:4480.

Chapter 5 HCC15.2-Saporin Efficacious Against *In Vitro* and *In Vivo* Tumors

5.1 Introduction

HCC15.2 delivers many different cargoes specifically to tumor *in vivo*, by binding a receptor expressed specifically on cancer cells and triggering internalization. Internalization is quick, most events happening within 1 hour; then HCC15.2 and its cargo traffic to and accumulate in the lysosome. The lysosome is a convenient localization point because it can be used for drug release, similar to the ADC Adcetris.

Figure 1 is a diagram of a currently used ADC, brentuximab vedotin (Adcetris) mentioned in chapter 1. Even though it uses an anti-CD-30 antibody, the therapy does not rely on inhibition of CD30. Rather, it binds to CD30 to gain entry into the cell. After internalization, the conjugate is trafficked to the lysosome where the valine-citruline (VC) linker is cleaved by cathepsin B, a lysosomal enzyme. This releases the toxic auristatin molecule to home to

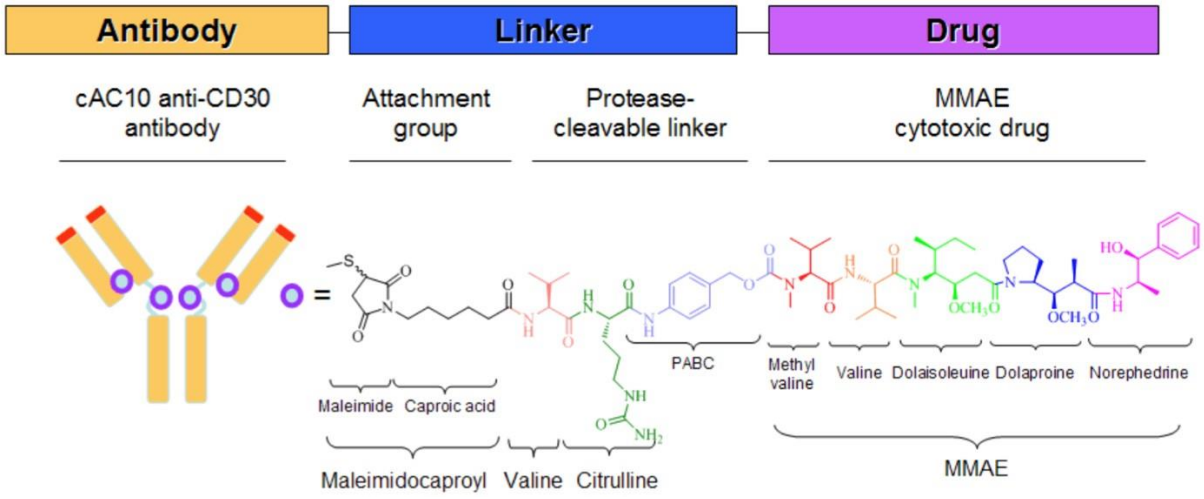

Figure 5-1 Structure of Antibody-Drug Conjugate Adcetris
Details of the antibody drug conjugate Adcetris. Contains targeting antibody, cathepsin b cleavable linker, and the toxic auristatin drug MMAE.

microtubules, causing destabilization and cell cycle arrest. Kadcyla is an ADC approved for metastatic HER2-positive breast cancer. An anti-HER2 antibody (trastuzumab) is linked to DM1, another microtubule inhibitor. The linker in this case is non-cleavable, and the antibody is degraded in lysosomes to release the drug. These two approved ADCs provide precedent for efficient drug release in lysosomes with and without cleavable linkers. In this chapter, we address the potential of HCC15.2 to deliver therapeutics to NSCLC cells and tumors as a targeting therapy.

5.2 Results

5.2.1 In Vitro *Delivery of Microtubule Destabilizers*

In targeting therapies, the choice of the drug is critical. It must be extremely potent, only requiring a low concentration of intracellular molecules to kill the cells. At the same time, it should not be able to get into cells without the targeting moiety. These two criteria ensure high efficacy in the tumor and low side effects in healthy cells. Auristatins are a related family of microtubule destabilizers that meet these two criteria. They are derived from dolastatin, a natural product from sea sponges, and display wide anticancer activity [1].

We initially conjugated the HCC15.2 monomeric peptide to monomethyl auristatin F (MMAF) via a maleimide caproic acid (mc) linker. MMAF inhibits tubulin polymerization but is modified to contain a carboxylic acid which reduces the cell permeability. The monomeric peptide was employed instead of the dimeric version as it retains high affinity and specificity while being easier to synthesize. As such, it is a suitable lead targeting agent with which to begin drug delivery experiments. The resultant conjugate (Figure 5-3) was incubated with H1299 NSCLC cells for 1 hour, after which the drug conjugate was removed and complete media

replaced. After 72 hours, cell viability was read by CellTiter-Glo® Assay. Unfortunately, there was only a 20–30% reduction of cell viability even at concentrations as high as 200 nM. Disconcertingly, the reduction of cell viability is not dependent on the HCC15.2-mc-MMAF concentration (Figure 5-2 a). Additionally, cell cytotoxicity experiments were performed in which the cells were exposed to the conjugate for a full 72 hours (data not shown). No effect was observed and the cells remained viable.

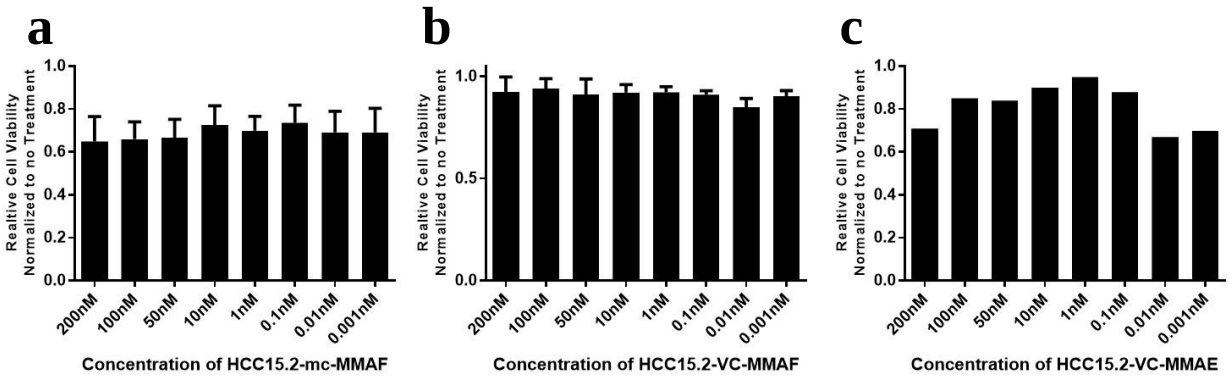

Figure 5-2 Peptide-Auristatin Conjugates do not Kill Cancer Cells
H1299 cells were incubated with a concentration gradient of HCC15.2 conjugated to mc-MMAF, VC-MMAF, and VC-MMAE. After 1 hour, the conjugate was removed and complete medium replaced. After 72 hours, viability was measured by CellTiter-GLO®. None of the conjugates killed H1299 cells in a dose dependent manner up to 200 nM.

It is possible that MMAF is not released from HCC15.2 in the lysosome, which may adversely affect its biological potency or prevent MMAF from reaching the cytoplasm where it can inhibit microtubules. Since HCC15.2 traffics its cargo to the lysosome, HCC15.2 was coupled to MMAF using a valine-citrulline-para-amino benzyl alcohol (VC-PAB) linker with the hopes that upon delivery to the lysosome, the linker would be cleaved by cathepsin B, a lysosomal protease. This is a self-immolative linker, which upon cleavage results in release of an unmodified MMAF. However, the data show this conjugate to be less potent than the first non-cleavable linker (Figure 5-2 b). Finally, the auristatin derivative, MMAE, which is used clinically in Adcetris, was attached through the same VC-PAB linker. As MMAE is less polar

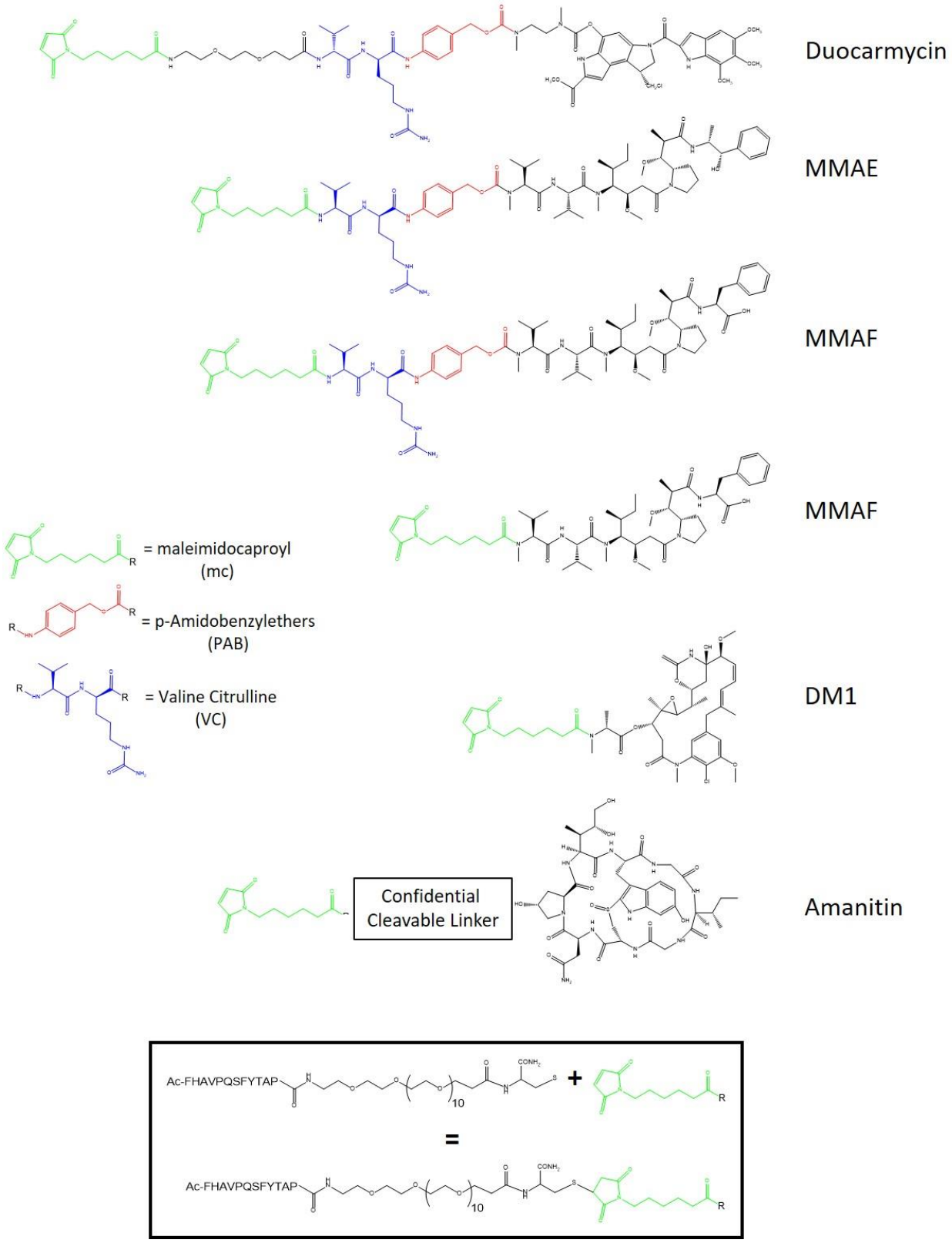

Figure 5-3 Structures of Small Molecule Drugs and Their Linkers
Chemical structures of the small molecule drugs and linkers conjugated to HCC15.2. Box) The conjugation scheme of the cysteine labelled peptide to the maleimide group of the drug linkers.

and more cell permeable than MMAF, we reasoned that it might be released from the lysosome more effectively, if that were the issue that was impeding efficacy. Unfortunately, this switch did not dramatically improve the efficacy. While it is more potent than the analogous MMAF conjugate, no more than 30% reduction in cell viability is observed at concentrations as high as 200 nM and it is not dose dependent (Figure 5-2 c). In sum, the antimitotic auristatin derivatives failed to show significant anticancer activity when delivered to cells via HCC15.2.

In an attempt to understand why the HCC15.2 conjugates were not working, fluorescence microscopy was used to visualize the conjugates inside cancer cells. H1299 cells were incubated with 50 nM of the two HCC15.2-MMAF conjugates for 1 hour. Cells were then washed, fixed, permeabilized and stained with antibody to MMAF. Unfortunately, HCC15.2 and the small molecule drugs fix poorly because they lack free amines, and no staining of any of the small molecule drugs was observed (data not shown). As such, poor delivery cannot be ruled out as a reason for the low efficacy.

Drug	Linker	Target
MMAE	mc-VC-PAB	Tubulin
MMAF	mc	Tubulin
MMAF	mc-VC-PAB	Tubulin
DM1	mc	Tubulin
Amanitin	Confidential Cleavable	RNA Pol II
Duocarmycin	mc-VC-PAB-DMEA-(PEG2)	DNA alkylator
Saporin	Biotin-Streptavidin	Ribosome

Table 5-1 Table of Therapeutics
Table of therapeutic molecules which were used in cell viability assays. A variety of cleavable or non-cleavable linkers and varying mechanisms of action are listed.

We also tested another microtubule destabilizer, DM1. This is a highly potent maytansine derivative with a different tubulin binding site than the auristatins. DM1 is known to be functional without release of its targeting agent removing a number of variables in the system.

Conjugation of DM1 to the HCC15.2 monomer was accomplished via a non-cleavable mc linker. Under the conditions described above, cell viability was reduced by 40–60% (Figure 5-4 a). However, we again observed a lack of concentration dependence. To determine whether or not the incubation time is an issue, the cell viability assay was performed under constant exposure to the HCC15.2-DM1 conjugate for 72 hours with H2009 NSCLC cells. Under these conditions the HCC15.2-DM1 conjugate significantly reduced the cell viability, demonstrating an IC50 of 40 nM (Figure 5-4 b). Although encouraging, this is significantly higher than the IC50 observed with other DM1-conjugates, such as clinically approved Kadcyla®, under the same conditions, most of which are sub-nanomolar [2].

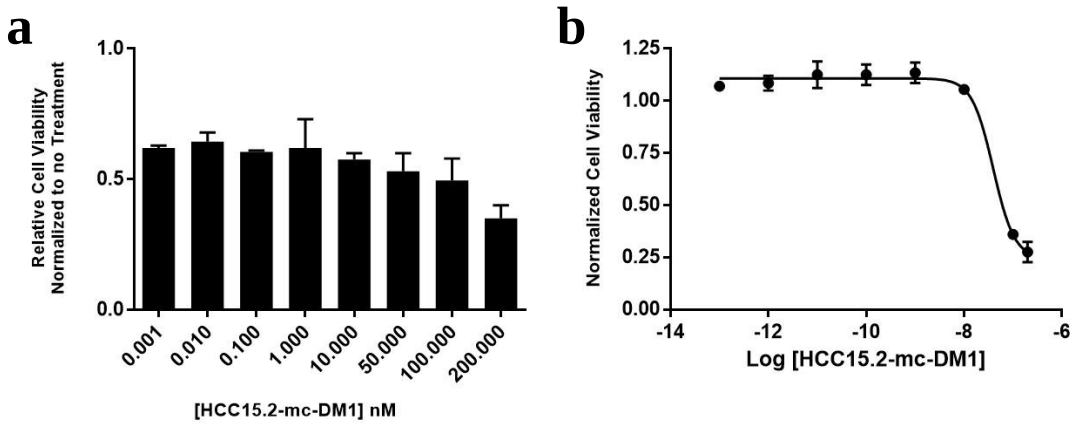

Figure 5-4 HCC15.2-DM1 is Effective with 72-Hour Treatment
H2009 cells were incubated with serial dilutions of HCC15.2-DM1 for 1 hour with a 71-hour chase, or constantly for 72 hours. Cell viability was read by CellTiter Glo®. HCC15.2-DM1 has an IC50 of 40 nM with the 72-hour treatment.

5.2.2 In Vitro *Delivery of Other Small Molecule Therapeutics*

Two other small molecule drugs were explored for use as peptide-drug conjugates (Table 5-1). Amanitin is derived from the deathcap mushroom and is a potent selective inhibitor of RNA polymerase II [3]. Duocarmycin is a DNA minor groove alkylator derived from Streptomyces bacteria [4]. The HCC15.2-Amanatin conjugate was inactive and resulted in no cell death when tested on H1299 NSCLC cells with either a 1 hour or 72-hour exposure to the

drug conjugate. Efficacy was observed with HCC15.2-duocarmycin under the 72-hour incubation (Figure 5-5) on H1299 cells, resulting in an IC50 of 57 nM. By comparison, free duocarmycin does not affect cell viability. HCC15.2-duocarmycin is also effective on H2009 and H1993 NSCLC cells with IC50s of 68 and 94 nM respectively. However, under the same conditions, H460 cells (which do not bind the HCC15.2) are also sensitive to HCC15.2-duocarmycin (IC50 41 nM). This suggests that uptake of the conjugate is nonspecific although it requires the peptide for efficacy. Further studies are needed to better understand the loss of cell-specificity; but due to the moderate IC50 of the HCC15.2-Duocarmycin conjugate, it was decided to focus on drug-conjugates with better efficacy and likelihood of proceeding to the clinic (see next section).

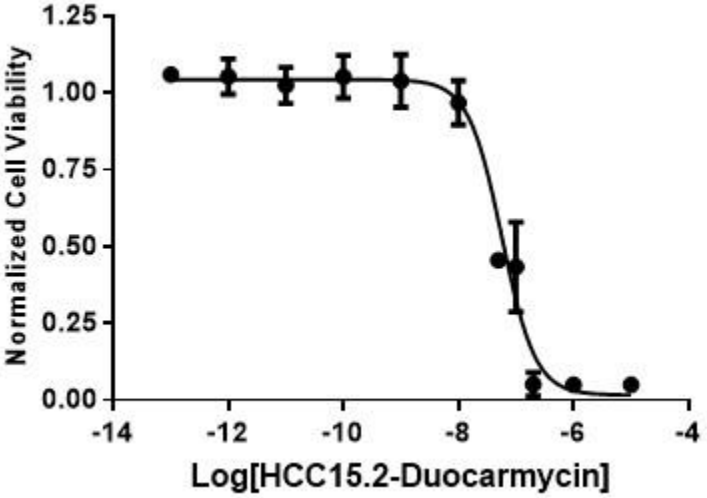

Figure 5-5 Hcc15.2 Duocarmycin is Effective with 72 Hour Treatment
H1299 cells were incubated with a concentration gradient of HCC15.2-Duocarmycin for 72 hours. Viability was analyzed by CellTiter Glo®. IC50s on H1299, H2009, and H1993 cells were 54 nM, 68 nM, and 94 nM respectively. However, H460 cells, which do not bind HCC15.2, were also sensitive, with an IC50 of 41 nM

5.2.3 In Vitro *Delivery of Protein Toxin Saporin*

Rate of uptake data from Chapter 2 show an average of ~50,000 molecules/cell are internalized over an hour. However, the drug delivery data suggests that the drugs used are not

reaching effective intracellular concentrations at their respective targets. Likely, they are internalized but remain trapped in vesicles such as the lysosome and are unable to reach their targets. In addition to the criteria of potency and inability to internalize by itself, the next drug chosen for delivery would now have a third criterion added. It must be able to escape from intracellular vesicles. In the search for a compound to overcome this unexpected hurdle, saporin was tested.

Saporin is a protein toxin isolated from the seeds of saponaria officinalis and is a member of a family of related ribosome-inactivating proteins (RIPs). RIPs function by cleaving the ribosomal 28S rRNA, halting protein synthesis [5]. The enzymatic activity of saporin is catalytic, requiring few molecules to inactivate the ribosomes in a cell. Saporin lacks the internalization domain found on ricin; therefore, it contains no tropism for human cells and cannot internalize

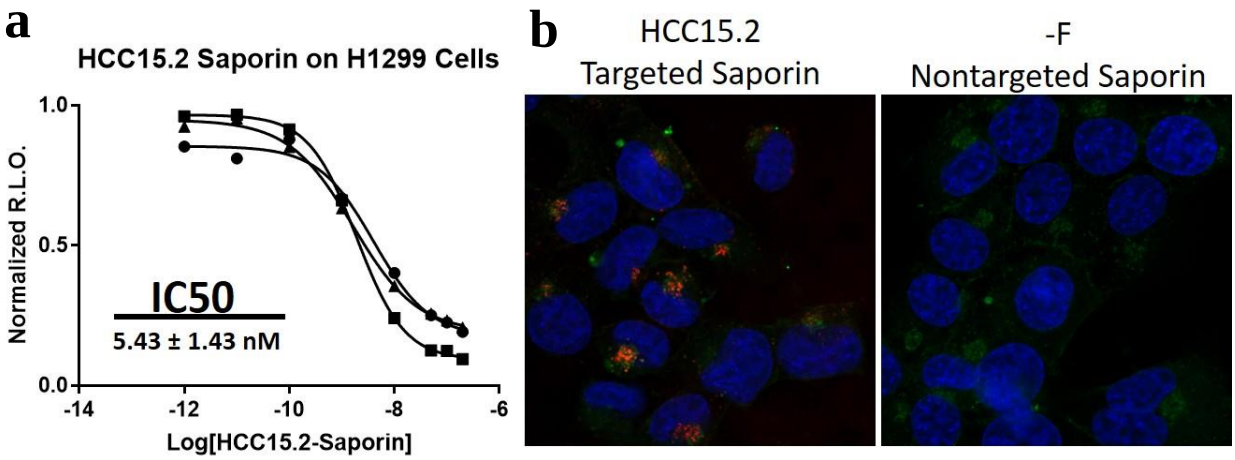

Figure 5-6 HCC15.2 Targets Saporin to Cancer Cells
a) Biotinylated HCC15.2 was conjugated to streptavidin-saporin and a concentration gradient of conjugate was incubated on H1299 cells. After 1 hour, the conjugate was removed and complete growth media replaced to the wells. After 72 hours, viability was measured by CellTiter Glo®. HCC15.2-saporin had an IC50 of 5.43 ± 1.43 nM. b) HCC15.2-saporin was incubated with H1299 cells for 1 hour. Cells were washed, fixed, permeabilized, and stained with an anti-saporin antibody (red), WGA (green), and DAPI (blue). HCC15.2 delivers saporin into H1299 cells, while the control peptide does not.

by itself. These qualities meet the first two criteria for drug choice in a targeting therapy. While it contains no internalization domain, saporin can escape from membrane bound vesicles.

Streptavidin-labelled saporin was conjugated to biotinylated HCC15.2 monomer and tested in the viability assay. HCC15.2-saporin killed the cells with an IC50 of 5.4 nM, the only conjugate to do so with a 1-hour incubation (Figure 5-5 a). Microscopy confirms that HCC15.2 successfully delivers saporin into cancer cells, while a control peptide cannot (Figure 5-5 b).

5.2.4 Internalized Saporin is able to Escape Lysosomal Trafficking

The saporin staining in the microscopy experiment looked strikingly similar to previous HCC15.2 staining; punctate and perinuclear. This is worrisome, as HCC15.2 traffics to the lysosome, and saporin is a protein and would be degraded if trafficked to lysosomes. Yet cell killing is still observed with HCC15.2 delivery. This is likely due to endosomal escape before trafficking to lysosomes. To observe endosomal escape, a time-course was performed to look for loss of saporin colocalization with lysosomes. HCC15.2 was conjugated to Qdot605 or to saporin, and the conjugate (red) was incubated with H1299 cells for 30 minutes, 1 hour, 1 hour with a 3-hour chase, or 1 hour with a 23-hour chase. Cells were then washed, permeabilized and counterstained for lysosomes (green) and nuclei (blue). Both saporin (row1) and Qdots (row 3) traffic to and accumulate in lysosomes (yellow) over time (Figure 5-7). However, there is a discrete population of saporin loaded vesicles (red) that seem to evade trafficking to the lysosome, which are not present in the Qdot sample (Figure 5-7, Row 2, Box 1). This is especially evident in the 1-hour timepoint. These non-colocalizing, saporin containing vesicles are also evident in the quantification of the Mander's coefficient. Saporin shows less colocalization compared to Qdots at 1 hour (0.334 vs 0.549 respectively) and 24 hours (0.657 vs 0.758 respectively) (Table 5-2). These data suggest that a fraction of saporin is

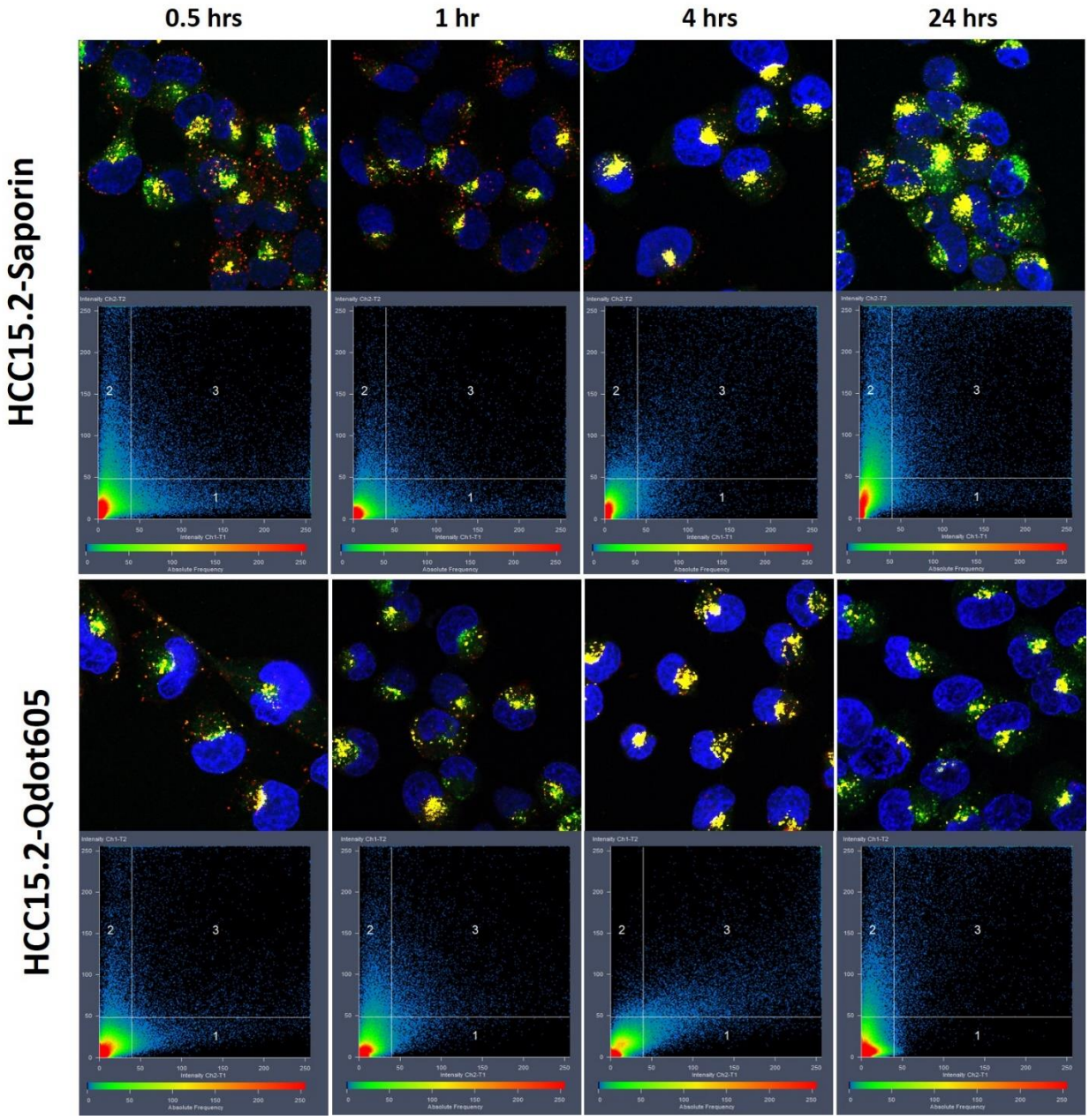

Figure 5-7 The Majority of Saporin Colocalizes with the Lysosome.
HCC15.2 was conjugated to Qdot605 or saporin via biotin/streptavidin and incubated with H1299 cells for 0.5 or 1 hour, or for 1 hour with a 3- or 23-hour chase. Cells were washed, fixed, and stained with DAPI (blue), anti-Lamp1 (green), and anti-Saporin (red). Rows 1 and 3 contain representative slices from each time point. Rows 2 and 4 plot the pixels from the images above based on intensity in the red channel (Ch2) and green channel (Ch1). Box 1 is exclusively peptide conjugate, Box 2 is exclusively lysosomes, and Box 3 is colocalization of the peptide and lysosomes and are falsely colored yellow in rows 1 and 3. The majority of the saporin still traffics to the lysosome. However, a discrete subpopulation of saporin-containing vesicles remains distinct from lysosomal signal, which is not observed in the Qdot-treated groups.

escaping from lysosomal trafficking and getting into the cytosol to exert cell killing. As the activity of saporin is catalytic, a fraction is enough for an IC50 of 5.4 nM, which is 3-fold less than the affinity of HCC15.2.

5.2.5 HCC15.2-Saporin Slows In Vivo *Tumor Growth*

Previous experiments have demonstrated the ability of HCC15.2 to deliver NIR dye to tumors *in vivo* after systemic administration and that HCC15.2 conjugated to saporin effectively kills cancer cells *in vitro.* The obvious next experiment is to test the efficacy of HCC15.2-saporin conjugate *in vivo* in a tumor growth assay.

Hours	Qdots	Saporin
0.5	0.228 ± 0.024	0.207 ± 0.015
1	0.549 ± 0.015	0.334 ± 0.017
4	0.660 ± 0.026	0.646 ± 0.021
24	0.758 ± 0.018	0.657 ± 0.016

Table 5-2 Colocalization Calculations
The average and standard error of the weighted Mander's coefficient were calculated from all slices in three images per treatment group. A Mander's coefficient of 0 is no correlation of red pixels to green pixels (HCC15.2 conjugate to lysosomes). Coefficient of 1 is perfect correlation of red pixels to green pixels. The visible subpopulation of distinct saporin-containing vesicles from Figure 5-4 drops the Mander's coefficient value at the 1-hour and 24-hour time-points.

In previous clinical trials, administration of RIPs often had serious dose limiting toxicities. Before testing of the tumor efficacy, the maximum tolerable dose was established in nude mice. Saporin was given as a single dose in 3 mice; 50 µg, 25 µg, and 10 µg were administered in 100 µl via tail vein injection. The animals were watched for signs of distress, weight loss, grooming, movement etc. The mouse which received the 50-µg dose died two days after the injection. The animals given the lower doses tolerated the treatment well with no signs of distress.

H2009 tumors were subcutaneously implanted on the flanks of female nude mice. When the tumors reached 100 mm^3, the mice were injected with 7.5 µg of HCC15.2-saporin, 7.5µg of saporin conjugated to control peptide, or nothing via tail vein, 2x/week for a total of 5 injections (red arrows). HCC15.2-saporin significantly slowed the tumor growth compared to non-targeted saporin.

Tumors were measured by a blinded researcher every other day starting on day 0. HCC15.2-targeted saporin significantly slowed tumor growth compared to control peptide (Figure 5-8). The control non-targeted saporin treatment is no different from the untreated tumors. Figure 5-8 represents 8–9 mice/group from two separate trials.

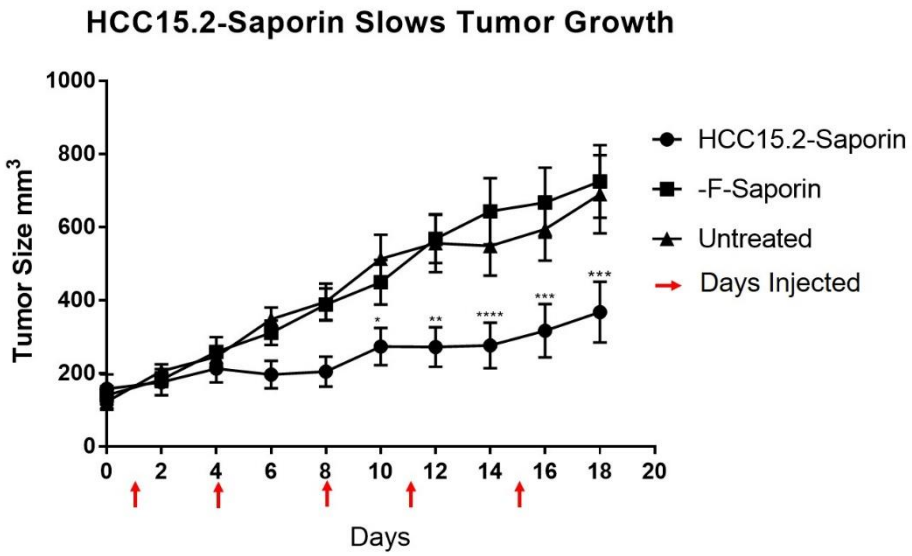

Figure 5-8 HCC15.2-Saporin Treatment Slows Xenograft Tumor Growth
H2009 cells (10^6) were implanted subcutaneously on the flank tumors of female nude mice. Saporin was conjugated to either targeting HCC15.2 or nontargeting -F15.2. When tumors reached 100 mm^3, 7.5 µg of the conjugate was injected IV into mice via lateral tail vein 2 times per week for 2.5 weeks (red arrows). Tumors were measured every other day by an independent blinded researcher. This represents 8–9 mice per group from two separate repeat experiments. HCC15.2-targeted saporin clearly slows tumor growth, while nontargeted saporin has no effect. * p-value < 0.05, ** p-value < 0.01, p-value < 0.001, p-value < 0.0001.

5.3 Discussion

Most of the HCC15.2-drug conjugates, failed to kill cancer cells effectively. This effect could be due to a number of scenarios. First, not enough conjugate is delivered to the cells. Second, enough conjugate is delivered, but is not released from the vesicular compartment in sufficient cellular concentrations to be effective. Third, it iss delivered and released, but in an inactive form. The answer is likely a combination of the first two scenarios. Some conjugates began working with a constant 72-hour incubation, but this result is less relevant, as in clinical settings, a PDC is not likely to be in circulation for long time periods, being quickly cleared from circulation. The saporin-conjugate solved these problems and worked fantastically *in vitro* and *in vivo*.

While there have been no clinical trials of saporin conjugates for cancer treatment since 2002 [6], there is a current trial of a saporin conjugated to substance P for pain management in terminal cancer patients (NCT02036281). The earlier saporin conjugate trials did not progress further than phaseI/II clinical trials, because of several hurdles that have since been partially addressed. Vascular leak syndrome (VLS), which causes interstitial edema, was the main dose limiting side effect. Vitetta et al. have identified a motif in ricin toxin A, which if mutated relieves VLS in mice while retaining activity against the tumor [7]. The motif is conserved in saporin but located in 2 different regions. Mutagenesis of these motifs in saporin may reveal a similar decrease in VLS, but have yet to be tested [6]. Another major hurdle, especially in solid tumor treatment is the development of neutralizing antibodies or anti-toxin antibodies (ATA) in most patients after a single treatment [5]. Some work with other RIP proteins has identified potential antigenic sites, which sites are conserved in saporin [6]. Mutagenesis in these sites may decrease immunogenicity.

Many other toxins are currently in phase I clinical trials, mostly in the form of immunotoxins (targeting therapies). Ricin and gelonin are RIPs similar to saporin. 2 ricin and 1 gelonin immunotoxins are currently in phase I trials for hematologic cancers. Pseudomonas exotoxin A (PE) immunotoxins are currently being tested in dozens of phase I trials. PE, like RIPs, halts protein synthesis, but by inhibition of EF2 instead of ribosome inactivation [8]. Diphtheria toxin also inhibits EF2 and is currently being tested in 2 phase I trials for bladder and pancreatic cancers as an immunotoxin.

HCC15.2-targeted saporin successfully slowed tumor growth in an *in vivo* xenograft mouse model. The animals handled the treatments well and no gross toxicity was observed in any organs. This was encouraging, as the *in vivo* imaging data suggested some targeting of mouse lung tissue. These experiments serve as proof of principle of the potential of HCC15.2 as a targeting therapy in the clinic. A highly toxic molecule that is unable to enter cells on its own was delivered by HCC15.2 to slow tumor growth *in vivo*.

The next two major experiments needed in the development of HCC15.2-saporin for clinical use involve optimization of the conjugate and testing in immunocompetent animals. The current conjugation is less than ideal as streptavidin is larger than the saporin and peptide combined. Cloning the peptide onto either terminus of saporin for expression would not only remove the need for conjugation altogether, but it would be significantly less expensive. Cloning would label saporin with HCC15.2 monomer 1:1 with no bulky linkers or messy conjugations. During cloning, the regions responsible for VLS and immunogenicity could also be mutated, further optimizing saporin for clinical use.

As was mentioned in Chapter 4, this *in vivo* tumor model is less than ideal. To more closely mimic clinical applications, HCC15.2 will be tested in a syngeneic tumor model with

immunocompetent mice. Patient development of ATAs ground several saporin clinical trials to a halt. This will be a critical barrier to overcome in the future.

5.4 Conclusion

Data have shown that HCC15.2 delivers many cargoes, including toxins, specifically to cancer cells *in vitro* and *in vivo*. This capability has been harnessed to slow tumor growth by delivering the toxin saporin to human cancer cells *in vivo*. HCC15.2 could be the first of a new class of targeting therapies, peptide-drug conjugates.

5.5 Materials and Methods

5.5.1 Materials

Nude mice were purchased from Jackson Laboratory (Bar Harbor, ME). CellTiter-GLO® was purchased from Promega (Madison, WI). VC-MMAE, mcMMAE, VC-MMAF, DM1, Duocarmycin, and Amanitin toxins were purchased from Levena Biopharma (San Diego, CA). Streptavidin Saporin and anti-saporin antibody were purchased from Advanced Targeting Systems (ATS Bio, San Diego, CA).

5.5.2 Methods

5.5.2.1 In Vitro Drug Delivery

Cysteine labelled HCC15.2 was conjugated to maleimide toxins at 1:1 ratio. Biotinylated peptide was conjugated to streptavidin-saporin 1:1. Cells were seeded on the inner 6x10 wells of a 96-well plate for 4-day growth to confluence. The next day, increasing doses of peptide-drug conjugate in triplicate or free drug were incubated on the cells for 1 hour at 37˚C. The drug was

removed and the wells were filled with growth media. After 72 hours, CellTiter-GLO® was added to each well and cell viability was measured by luminescence.

5.5.2.2 In Vivo Drug Delivery

H2009 cells (10^6) were implanted subcutaneously on the flank of female nude mice, and the mice were sorted when the tumors reached 100 mm^3. Biotinylated HCC15.2 or the control - F15.2 were conjugated to streptavidin-saporin and administered via tail-vein injection (7.5µg/100µl) 2x/week for 2.5 weeks (n=5). A blinded researcher measured tumor volume with calipers every other day and volume was calculated with the equation $(\pi/6)*(l*w)^{3/2}$. Statistical analysis was performed on GraphPad Prism®.

5.6 References

[1] Doronina SO, Toki BE, Torgov MY, Mendelsohn BA, Cerveny CG, Chace DF, et al. Development of potent monoclonal antibody auristatin conjugates for cancer therapy. Nature Biotechnology. 2003;21:778.

[2] Singh R, Setiady YY, Ponte J, Kovtun YV, Lai KC, Hong EE, et al. A New Triglycyl Peptide Linker for Antibody–Drug Conjugates (ADCs) with Improved Targeted Killing of Cancer Cells. Molecular Cancer Therapeutics. 2016;15:1311.

[3] Moshnikova A, Moshnikova V, Andreev OA, Reshetnyak YK. Anti-proliferative effect of pHLIP-amanitin. Biochemistry. 2013;52:1171-8.

[4] Yasuzawa T, Iida T, Muroi Ki, Ichimura M, Takahashi K, Sano H. STRUCTURES OF DUOCARMYCINS, NOVEL ANTITUMOR ANTIBIOTICS PRODUCED BY STREPTOMYCES SP. CHEMICAL & PHARMACEUTICAL BULLETIN. 1988;36:3728-31.

[5] Polito L, Bortolotti M, Mercatelli D, Battelli MG, Bolognesi A. Saporin-S6: A Useful Tool in Cancer Therapy. Toxins. 2013;5:1698-722.

[6] Giansanti F, Flavell D, Angelucci F, Fabbrini M, Ippoliti R. Strategies to Improve the Clinical Utility of Saporin-Based Targeted Toxins. Toxins. 2018;10:82.

[7] Smallshaw JE, Ghetie V, Rizo J, Fulmer JR, Trahan LL, Ghetie M-A, et al. Genetic engineering of an immunotoxin to eliminate pulmonary vascular leak in mice. Nature Biotechnology. 2003;21:387.

[8] Yates SP, Merrill AR. Elucidation of eukaryotic elongation factor-2 contact sites within the catalytic domain of Pseudomonas aeruginosa exotoxin A. Biochemical Journal. 2004;379:563-72.

Chapter 6 Receptor Identification

6.1 Introduction

Antibody and small molecule development, require a known target and lots of optimizations. Our limited knowledge of crucial receptors to target is reflected in the small number of different proteins targeted in the clinic. Only 16 protein targets across all types of cancer have clinically approved antibody therapies[1]. Further, many of these targets are only present on a fraction of cancer cases. HER2 has several clinically approved antibody treatments, but only represents ~20% of breast cancer patients[2]. EGFR activating mutations have two small molecules inhibitors and an inactivating antibody in clinical use[3], but these treatments only apply to ~10% of NSCLC patients[4]. These treatments are quite effective, but only impact a small portion of cancer patients. This highlights a need for ways to quickly identify novel biomarkers and ligands.

Peptides selected on cancer can act as surrogate biomarkers and be used to develop the receptor as a biomarker. Peptide selection through phage display on live cancer cells in our lab has yielded more than 10 distinct peptides that together can recognize more than 75% of NSCLC lines tested[5]. Phage display biopanning on live cancer cells allows for biasing the selection towards binding, internalization, and even subcellular trafficking. The selection is not limited to the biomarkers currently known, but everything that is expressed on the surface of cells. Our peptidic ligands not only recognize cancer cells vs normal, but they are able to trigger internalization, drag in up to nanoparticle sized payloads and deliver them to specific subcellular localizations.

Identification of the cellular receptor responsible for peptide binding and internalization has proved to be a significant roadblock. While peptides work great for many applications such as imaging, and solid tumor penetration, it would be ideal to know the cellular receptor to develop other classes of molecules and understand the underlying biology. This has been a significant problem in the field and presents a non-trivial challenge. One contributing factor is that it is difficult to find a database of proteins that are expressed on the cell surface, that is further exacerbated by the change in protein profiles in cancerous cells. A second difficulty is that membrane proteins are notoriously difficult to isolate, especially with the native tertiary and/or quaternary interactions intact.

Attempts have been made in the lab to identify receptors with little success. This chapter details efforts to develop a robust technique that could be used to identify the receptor of all the current peptides as well as new peptides that will be selected in the future. Experiments involving classic pulldowns, cross-linking, and near western blotting, then using mass spectrometry for final protein identification was attempted, to create a list of candidate receptor proteins for HCC15.2 to be tested further.

6.2 Results

6.2.1 Development and Testing of HCC15.2 Cross-Linking Construct

6.2.1.1 Building the Crosslinking Construct

Choosing a crosslinking reagent was the first decision to be made. Classic aldehyde crosslinking reagents often fix peptides poorly as they have few free amines. HCC15.2 contains only one, the N-terminus. GGH is a tripeptide that binds Ni with a very high affinity and, when exposed to a strong oxidizing reagent, such as magnesium monoperoxyphthalate hexahydrate

(MMPP), GGH-Ni facilitates highly efficient cross-linking of interacting proteins with little nonspecific background reaction [6]. This crosslinker can easily be incorporated into the synthesis of any peptide.

GGH-Ni needs to be close enough to the peptide to enact cross-linking, but it also needs to be distant enough to not effect peptide binding. These two parameters were tested different sized linkers between the peptide and the crosslinker.

The smallest linker (GG) did not allow the petide to bind to its target and no internalization was observed (data not shown). The (PEG_3) linker allowed for binding of the peptide (green), until Ni was complexed (blue) (figure 6-1 Left). The large square planar complex significantly reduced peptide binding. The (PEG_{11}) linker did not interfere with peptide binding (Figure 6-1 Right).

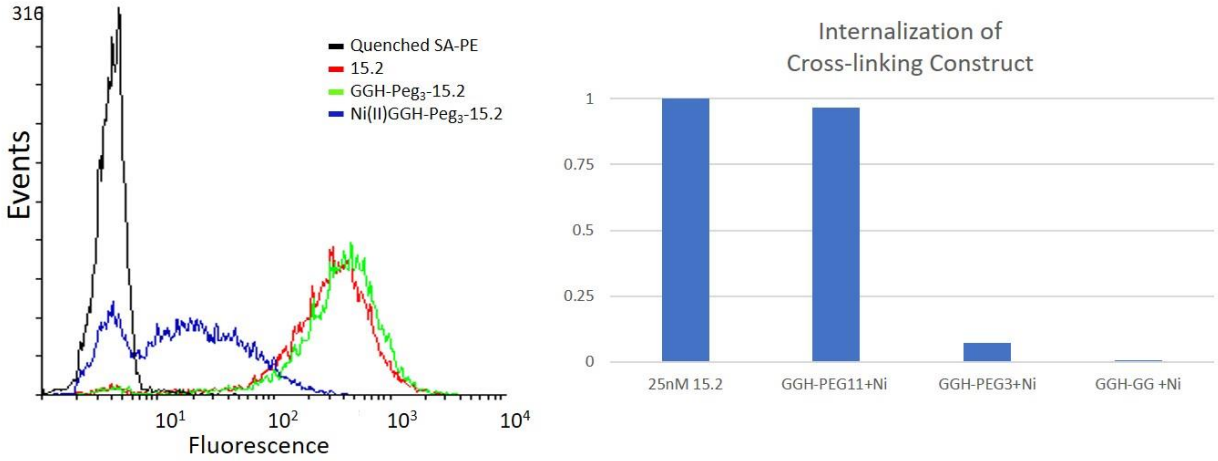

Figure 6-1 A PEG_{11} Linker is Required Between the Cross-Linker and HCC15.2 Peptide
Flow histogram depicting internalization of cross-linking constructs. The PEG3 linker retains binding until the Ni complex is formed. Only the PEG11 linker is able to bind to cells when the Ni complex required for crosslinking is formed.

To assess whether crosslinking was occurring, the construct was first affixed to magnetic beads and then crosslinked to cells. This provides a visible link that can be qualitatively observed under a microscope. The construct was affixed to M-280 dynabeads via biotin-streptavidin

interactions. Leftover streptavidin sites were quenched with excess biotin. The beads were then incubated with EDTA lifted H1299 cells for 10 min at 37˚C and exposed to the cross-linking catalyst MMPP. Cells were then washed with acid to disrupt non-covalent binding and incubated with excess HCC15.2 peptide or control peptide, then imaged on an inverted light microscope at 10x. With Crosslinking, the beads remain associated with the cancer cells despite excess free peptide. Without crosslinking, the beads are displaced from the cell surface by excess free peptide. This experiment showed that the PEG_{11} linker worked well to both retain the

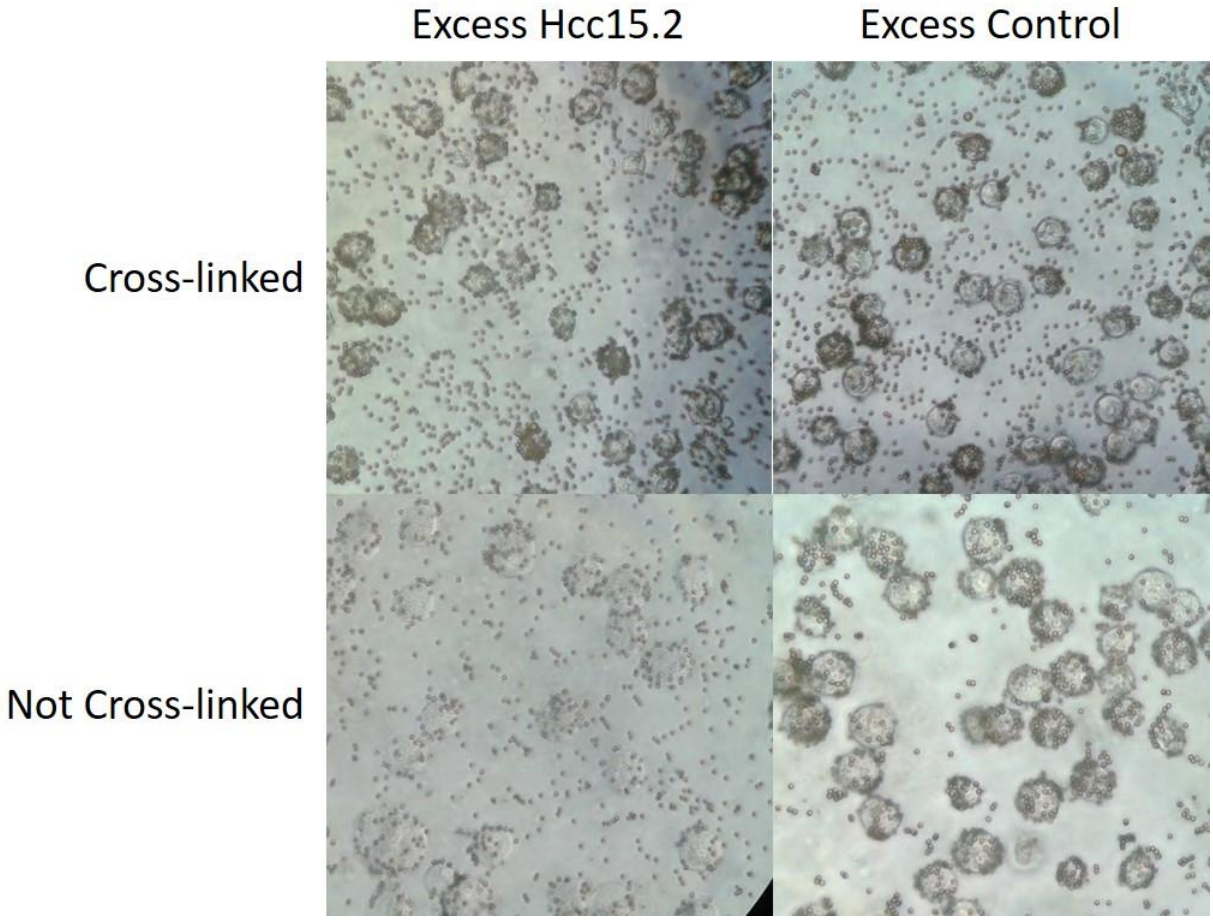

Figure 6-2 Construct Facilitated Cross-linking of Cancer Cells to Magnetic Beads.
H1299 cells were incubated with magnetic beads labeled with the crosslinking construct, then crosslinked, washed, and incubated with excess HCC15.2. Excess HCC15.2 peptide does not displace the beads in the crosslinked group(top left), but does displace beads that have not been crosslinked to cells (bottom left).

peptide binding and the crosslinking ability of the tripeptide GGH-Ni(III). The optimized construct is modeled in Figure 6-3

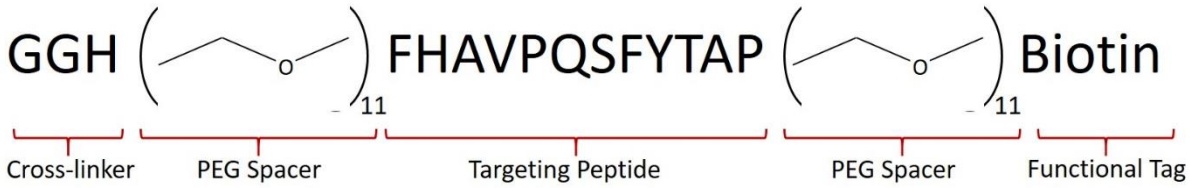

Figure 6-3 Model of Optimized Crosslinking Construct
Optimized crosslinking construct contains PEG_{11} between the peptide and both the crosslinker (N-terminus) and functional group (C-terminus)

6.2.1.2 Crosslinked Pulldowns Failed to Identify Potential Receptors

HCC15.2 triggers internalization upon binding, which complicates the experiment by actively removing the complex from availability to crosslinking by the MMPP.. This gives only a short window of time to add MMPP, when the peptide has bound the receptor, but not yet internalized. Membrane proteins require membrane fluidity to internalize. At lower temperatures, membrane is no longer fluid and receptor mediated endocytosis halts. To aid in catching the peptide receptor interaction on the cell surface, the beads were loaded with the peptide and they were incubated with the cells at 4˚C for 1 hour. Then cold MMPP was added and the cells were imaged. Unfortunately, it appears that the lower temperature also decreases peptide binding to its target and hardly any beads were associated with cells under these conditions.

A potential solution to this problem was found in a head and neck cancer cell line PC-15A. This cell line binds HCC15.2, but has very slow internalization as measured by flow cytometry (data not shown). This would allow for cross-linking to occur on the surface of live cells. PC-15A cells were incubated with 10 nM construct for 30 minutes at 37˚C in serum free media. Cells were rinsed with PBS, then 100µM MMPP was added. As controls, some cells were pretreated with trypsin (which abrogates peptide binding), and some were never crosslinked. All cells were lysed, run on denaturing gel, and blotted to nitrocellulose. Or cells were lysed and

streptavidin magnetic beads were used to pull out biotinylated complexes, then run on SDS gels and blotted for analysis. Anti-biotin, avidin-HRP and streptavidin-dye probes were used to search for biotinylated proteins present in the cross-linked sample and not in the controls. Figure 4 shows the blot that was probed with SA-800CW and imaged on a LICOR Odyssey. No unique protein bands were identified in the cross-linked sample.

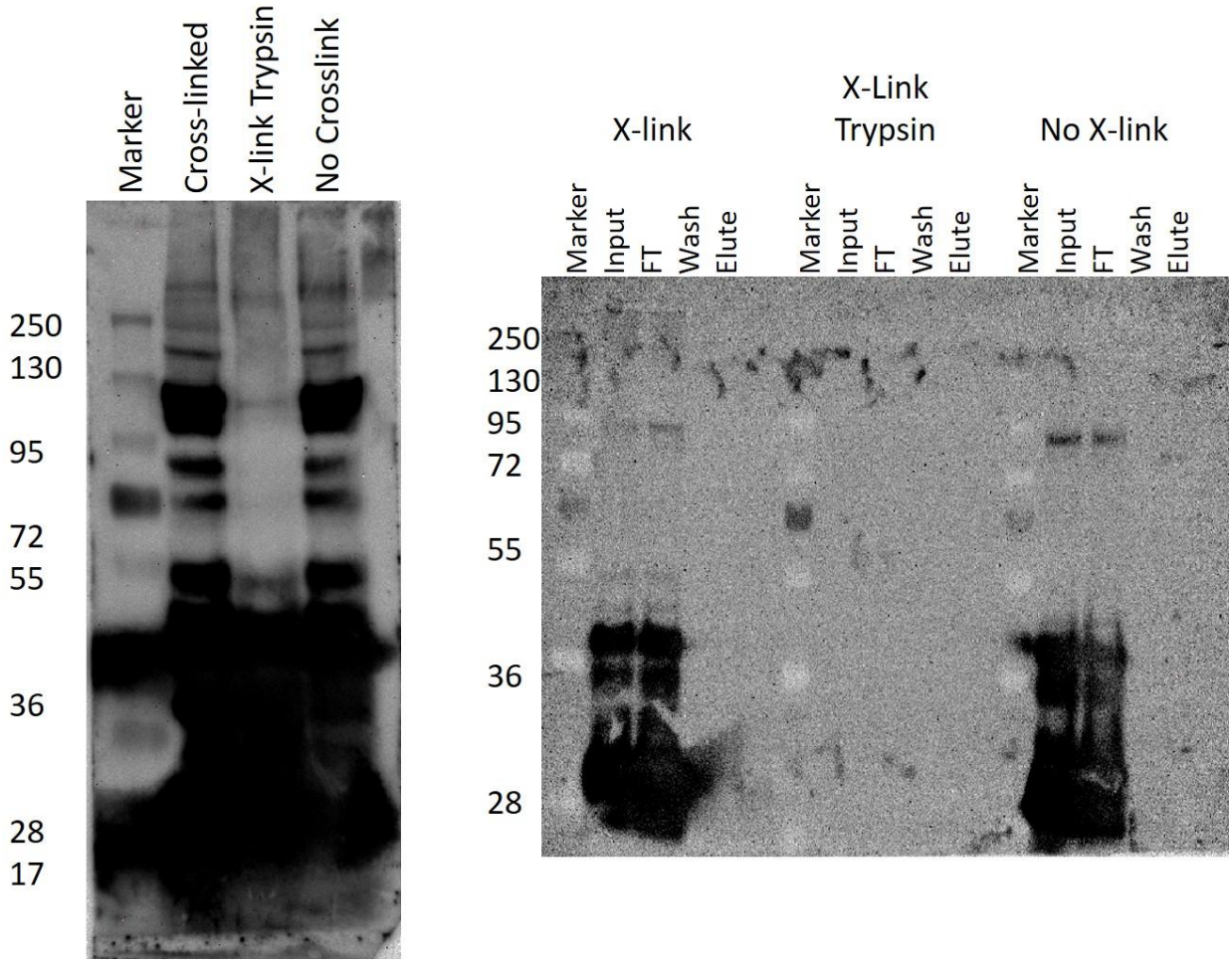

Figure 6-4 Cross-Linking Revealed No HCC15.2 Specific Bands by Western Blot
The first blot is of PC-15A cells that were incubated with crosslinking construct, for 30 minutes, then crosslinked, then the cells were lysed. Lysates were run straight onto SDS PAGE protein gel without a pull down, blotting for the biotin tag on the construct with SA-800CW and imaged on a LI_COR Odyssey CLx. There were no unique bands in the cross-linked

Unfortunately, this was the case for practically every different iteration. Experiments were run with live cells, whole cell lysates, plasma membrane extracts, different conjugation schemes to magnetic beads, varying incubation times and temperatures, and different detection methods all failed to produce any unique bands in the cross-linked group.

The last cross-linking experiment returned to the 4˚C incubation. $1x10^7$ H1993 cells (high HCC15.2 binders) were lifted with EDTA washed with PBS+ and resuspended in cold 20nM construct. These cells were left incubating at 4˚C for 2 hours, then the cells were spun down at 4˚C and resuspended in cold 100µM MMPP for 20 minutes. Cells were washed once with PBS then resuspended in warmed trypsin and incubated at 37˚C for 2 minutes then trypsin inactivating solution was added. The cells were pelleted and the supernatant was removed to a microcentrifuge tube and again cooled to 4˚C. Streptavidin magnetic beads were incubated with the supernatant overnight at 4˚C. The beads were washed with PBS 3x and boiled in loading buffer and run about 4 mm into an 8% sds polyacrylamide gel. The entire sample was cut out of the gel and prepped for mass spectrometry using in gel digest protocol [7]. The sample was submitted to the MS core for peptide analysis on an LTQ Orbitrap XL™ Hybrid Ion Trap-Orbitrap Mass Spectrometer (Thermo Fisher Scientific™, Waltham, MA). No relevant proteins were identified from that experiment.

6.2.2 Classic Pulldown

While the GGH constructs were still being made and tested, classic pull down experiments could be started with the peptides already in hand. Whole cell lysates with protease inhibitors were incubated with HCC15.2 loaded SA-magnetic beads or biotin quenched beads at 4˚C overnight. The beads were then washed with lysis buffer and bound protein was eluted by adding excess HCC15.2 to the sample, then afterwards boiling the beads in SDS loading buffer.

SDS PAGE polyacrylamide gel was run and Coomassie stained, destained then silver stained. A single new band is in the sample from the HCC15.2 loaded beads as indicated by the red arrow (Figure 6-5).

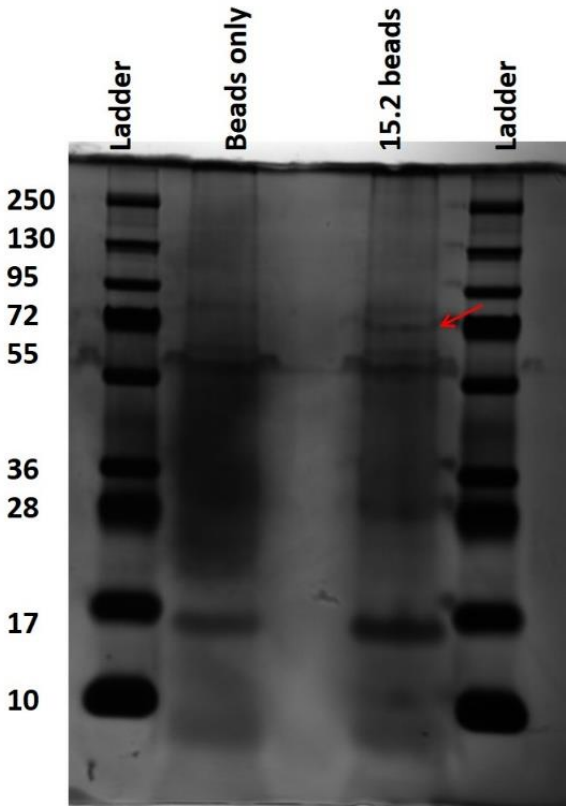

Figure 6-5 Pull down Revealed HCC15.2 specific band in Silver Stained Gel
Silver stained protein gel from a pull down with HCC15.2 conjugated to magnetic beads in H1299 whole cell lysates. Specific band identified at ~72 KDa (red arrow).

Unfortunately this particular experiment was run before the MS collaboration was fully established and was not analyzed further. This particular result was not replicable, but it was encouraging that new bands could be seen.

Membrane proteins are generally in low abundance compared to other intracellular proteins. In order to enrich for the protein of interest, different methods to isolate plasma membrane were tried. Pull downs from isolated membrane lysates of positively binding cells were compared to lysates from negatively binding cells. A band with the same apparent molecular weight from figure 5, was seen indicated by a red arrow (Figure 6-6). This band ~70 KDa was excised from the gel from positive and negative cell line samples. In gel trypsin digestion and peptide extraction was run for MS analysis. Unfortunately, this analysis also yielded no meaningful results. Of note, there were many mitochondrial protein contaminates, showing that the plasma membrane isolation kit was not very pure. As one would expect, it is very difficult to isolate one type of membrane from another.

Things went poorly after this for the rest of the pull down experiments. Changing many other parameters including different magnetic beads, different cell lysis conditions, diverse ways of isolating plasma membrane, failed to yield any results.

6.2.3 Near Western

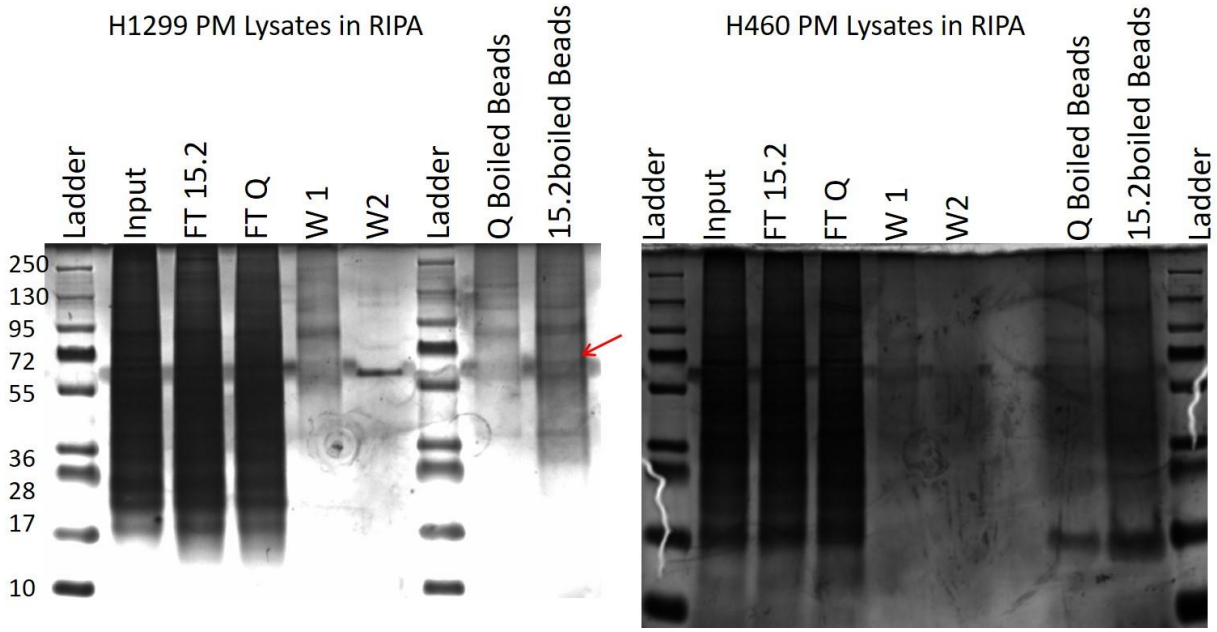

Figure 6-6 Pull Down from Plasma Membrane Lysates Revealed HCC15.2 Specific Band
Plasma membranes were isolated from ~40x10^6 H1299 cells (positive binders, left gel) and H460 cells (negative binders, right gel) and resuspended in RIPA buffer. HCC15.2 loaded beads were incubated with the lysates overnight at 4˚C. The beads were washed and eluted by boiling in loading buffer, then loaded onto SDS gels and silver stained. There was a single band ~65 kDa that was not present in either the quenched (no peptide) beads or the H460 beads.

HCC15.2 shows incredible affinity for its target, on the same order of magnitude as many monoclonal antibodies. What if it could be used to detect proteins on a blot like antibodies? It was not likely to work as a peptide might have a difficult time binding to linearized protein, but it was a very cheap and quick experiment to try. Whole cell lysates and plasma membrane lysates from positive binding cell line and cell lysates from a negative binding cell line were run in duplicate on an SDS-PAGE gel. Biotinylated HCC15.2 was conjugated streptavidin-800CW dye then quenched or free dye was quenched with biotin. Surprisingly, many protein bands were

observed in the HCC15.2 blot that were not present in the quenched dye blot. There were also differences in the band pattern between the positive and negative binding cell lines (Figure 6-7).

There were too many bands present to be specific for HCC15.2. Plasma membrane lysates for both H1993 and H460 cells were run in duplicate on an SDS PAGE gel and half were blotted to nitrocellulose and blocked with 2.5% BSA + 100 nM scrambled HCC15.2 peptide. The blot was then incubated with HCC15.2-SA800CW. 2 bands were identified at about 65 kDa and 110 kDa highlighted by red arrows in the H1993 lane of Figure 6-9. The other gel was then Coomassie stained and the corresponding segments ~60-70 and ~105-115 for both H1993 cells and H460 cells, were carefully and cleanly excised from the gel, digested, extracted, and

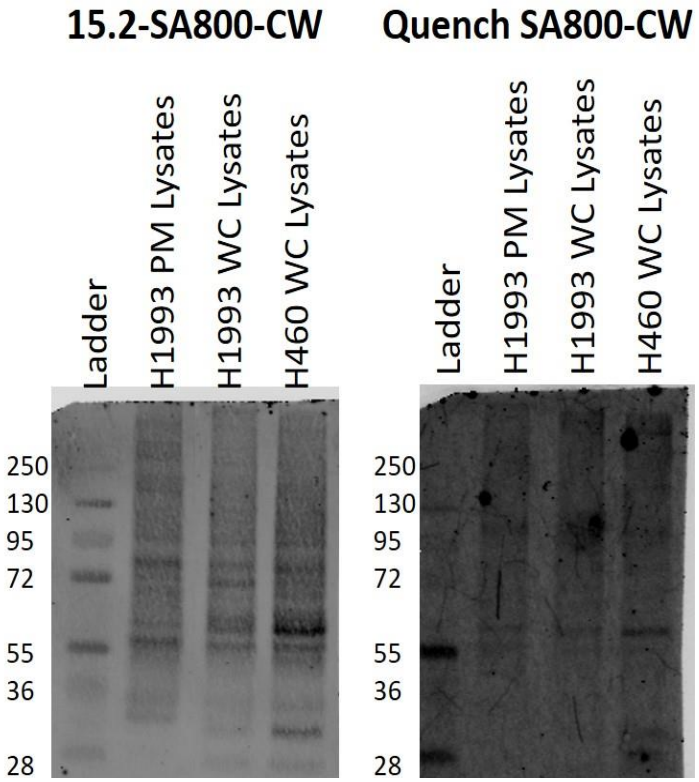

Figure 6-7 Near Western Blot
Near western blots probed with HCC15.2-SA800CW or quenched SA800CW. Differences are seen between the samples in the peptide probed blot. H1993 (positive binder) plasma membrane and whole cell lysates vs H460 (negative binder) whole cell lysates. While the quenched streptavidin blot is messy, it seems to have fewer bands.

prepared for mass spectrometry. The data that was returned was curated to exclude proteins found in the H460 samples, contaminates such as trypsin and keratin and proteins that are significantly outside the range that was excised. The score is calculated based on a number of parameters including the number of unique peptides, the percentage of the protein that was covered, and how abundant a particular fragment was. The higher the score, the more likely it is that that protein was actually present in the band. The table in figure 9 lists the proteins that were identified and the yellow highlighted rows are proteins that have precedence for being found on the extracellular leaflet of the plasma membrane in the literature. Most of the applicable proteins had very low scores, only protein disulfide-isomerase (PDI) is within the MW range of the excised band and is found on the membrane. This is the first protein to add to the list of candidates to be further tested.

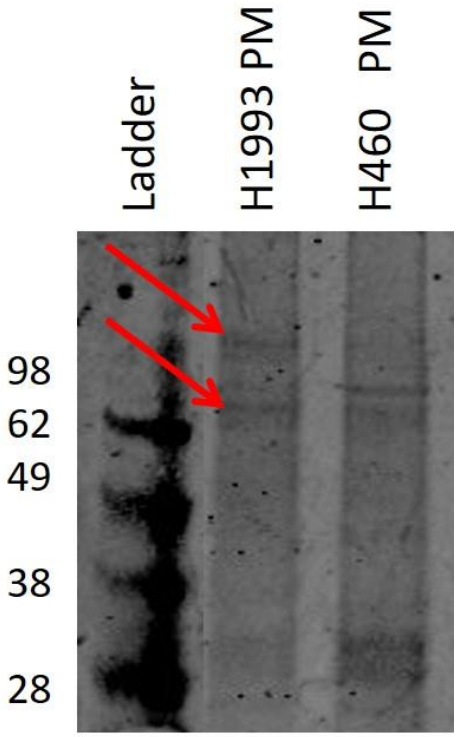

Figure 6-8 Near Western for MS Analysis
H1993 and H460 cells were run in duplicate on an SDS gel and one was blotted to nitrocellulose and probed with HCC15.2-800CW. Two bands not in the H460 were identified (red arrows) They were cut out of the other gel and prepped for MS

Many other permutations of this experiment were tried. To identify peptide specific bands, two identical blots were run side by side with HCC15.2-SA800CW, one also contained 10x excess HCC15.2 specific peptide and bands that disappeared were later cut and analyzed in the same manner. Plasma membrane was collected from cells pretreated with trypsin and run

High Band ~105-115 kDa

Accession	Description	Score	Coverage	# Unique Peptides	# PSMs	# AAs	MW [kDa]
Q13985	Carcinoembryonic antigen (Fragment)	7.60	27.66	2	2	141	15.5
Q8N1C0	CTNNA1 protein	6.04	5.41	1	2	536	59.5
Q96HE7	ERO1-like protein alpha	4.05	3.63	1	1	468	54.4
Q562L5	Actin-like protein (Fragment)	4.00	17.48	1	1	103	11.5
Q53QD5	Putative uncharacterized protein HSPD1 (Fragment)	3.99	32.73	1	1	55	6.0
P05556	Integrin beta-1	3.97	2.63	1	1	798	88.4
A6NJJ0	Putative uncharacterized protein PRDX4	3.74	7.03	1	1	185	21.3
Q96HX3	Similar to ribophorin I (Fragment)	3.66	2.64	1	1	568	64.5
A6QKW0	SHINC3	3.21	4.86	1	1	247	27.9
B7ZB78	cDNA, FLJ79442, highly similar to Ras-related protein Rap-1b	3.13	10.17	1	1	118	13.5

Low Band ~60-70 kDa

Accession	Description	Score	Coverage	# Unique Peptides	# PSMs	# AAs	MW [kDa]
P07237	Protein disulfide-isomerase	126.91	22.64	13	42	508	57.1
P23368	NAD-dependent malic enzyme, mitochondrial	11.95	7.36	3	4	584	65.4
Q5SZE2	LAG1 homolog, ceramide synthase 2 (Fragment)	8.66	12.40	1	2	129	15.4
B3KUR6	cDNA FLJ40471 fis, clone TESTI2042508, highly similar to Nucleobindin-1	8.54	31.45	3	3	124	14.2
Q9HCC0	Methylcrotonoyl-CoA carboxylase beta chain, mitochondrial	8.52	6.75	3	3	563	61.3
B4DDM5	cDNA FLJ53298, highly similar to Peroxisomal multifunctional enzyme type 2	7.04	3.77	2	2	717	77.4
P35232	Prohibitin	6.93	8.82	2	2	272	29.8
Q13985	Carcinoembryonic antigen (Fragment)	6.74	9.22	1	2	141	15.5
B4DKM5	cDNA FLJ60120, highly similar to Voltage-dependent anion-selective channel protein 2	6.54	12.94	2	2	255	27.5

Figure 6-9 Mass Spectrometry Results
MS results from Figure 8, after curation of data. Proteins identified in the H460 negative sample, and contaminants were excluded from the list. Higher score means the protein was more likely truly in the sample. Score is calculated from the number of unique peptides in that protein found, the percent of the protein that those peptides covered, and the number of times the peptides showed up. Yellow highlights proteins that are found on the plasma membrane. The only likely hit in this experiment is protein disulfide isomerase

alongside non-treated cells, to look for loss of binding as well. This near western method was also combined with other methods, such as the pull down. After many of these experiments, MS was run with little to add to the list. Interestingly, a different splice variant of protein disulfide isomerase did show in another experiment, but with a much lower score.

6.2.4 Other Experiments

With the planned methods failing to yield results, new experiments were devised in an attempt to isolate the protein of interest. Surface proteins were irreversibly biotinylated before or after HCC15.2 incubation. The cells were lysed, run on SDS-PAGE, blotted to nitrocellulose, and probed with streptavidin-800CW. Peptide treatment would trigger internalization of the receptor, protecting it from biotinylation. Disappearance of a band in the peptide treated sample

would signify the receptor. Loss of signal experiments are not sensitive and I was unable to observe any changes on the blot (data not shown).

A different but related approach was to incubate cells with peptide for an hour, then lyse the cells without detergent to leave the internalized vesicles intact. Cells were treated with PE labeled HCC15.2 for 1 hour at 37˚C. The cells were lysed on a French press and vesicles were isolated through a 15% optiprep layer onto a 60% optiprep cushion. Cell lysates were carefully pipetted on top of the 15% optiprep and spun at 22,000 g in an ultracentrifuge for 2 hours. 1 mL at a time was carefully pipetted from the top of the tube and put into its own sample vial. Each vial was then tested for fluorescence which would indicate the presence of peptide. The vesicles were found close to the 60% optiprep in sample 18 (Figure 6-10).

Combining the elements from the two above experiments yielded better results. Surface proteins of live cell were reversibly biotinylated under oxidative conditions. HCC15.2-dye was incubated after biotinylation for 1 hour. Then all biotinylation sites left on the cell surface were removed with reducing conditions. The cells were lysed, centrifuged on the gradient and . Fraction 6 (green arrow) was from the supernatant and contains cytosolic proteins. Fraction 17 (orange arrow) was from the 15% optiprep just above the boundary line between the 15% and 60% layers. Fraction 18 (purple arrow) was the boundary between 15% and 60% optiprep layers and contained intact vesicles containing peptide-dye conjugate as observed by the high fluorescent signal. Fraction 25 (black arrow) was well into the 60% layer and contained no fluorescence, indicated by black arrow. These four samples were run in duplicate on non-reducing and reducing gels.

It was found that four bands disappeared from fraction 18 in the reducing gel at around 28 kDa, 40 kDa, 60 kDa and 85 kDa as indicated by red arrows in figure 10. These were reversibly biotinylated proteins that had been protected from the reduction at the cell surface by peptide stimulated internalization. These proteins also co-sedimented in the gradient with the vesicles containing peptide dye, fraction 18. Unfortunately, at this point in time, my mass spectrometry collaborator accepted a new position at a different facility and left me without means to easily obtain mass spec.

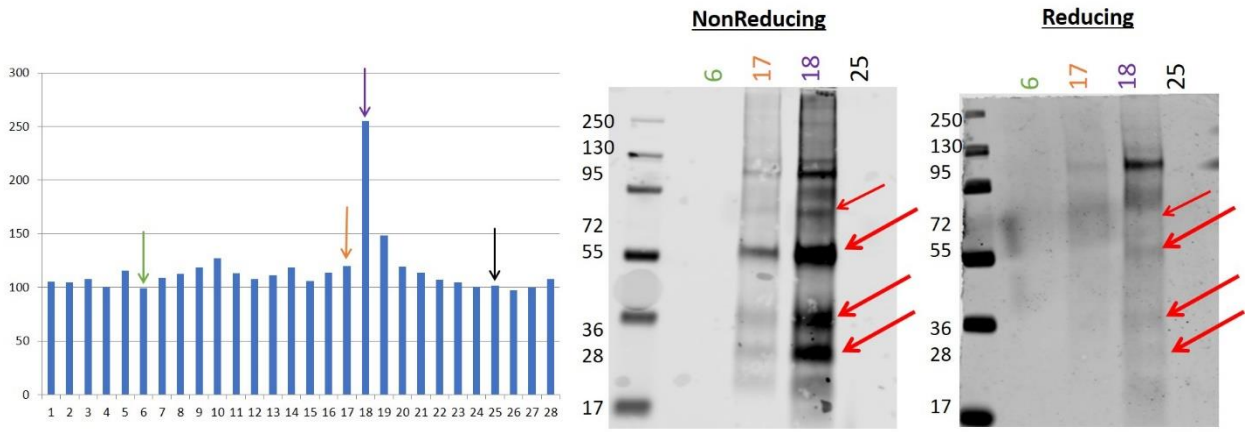

Figure 6-10 Vesicle Isolation
Cells were treated with reversible biotin label then incubated with HCC15.2-SAPE and incubated with cells for 1 hour at 37˚C. The biotin left on the cell surface was removed and the cells were lysed by French press. The lysates were centrifuged for 2 hours at 22,000 g on an optiprep discontinuous gradient and1 mL fractions were collected. The first panel is the fluorescence of the fractions and the colored arrows correspond to the colored lanes in the reducing (right panel) and the nonreducing (middle panel) blots. Red arrows on the blots are reversibly biotinylated proteins that co-sedimented with peptide containing vesicles.

6.3 Discussion

The first question always asked is “What is the receptor?” Identifying the receptor for peptides selected from large libraries has posed a significant hurdle for the field. Of 75 cancer targeting peptides isolated, only 15% have identified the receptor responsible for binding, even fewer have made steps to confirm [8]. Only one peptide in our lab has an identified receptor. It

closely matched a viral protein in a BLAST search and was confirmed by antibody blocking, and by ectopic expression. Identifying the receptor for HCC15.2 has proven more difficult. Protein BLAST reveals virtually nothing, even with the newer truncation data. HCC15.2 internalization data was compared to protein expression levels in a reverse phase protein array to look for correlation of any protein with HCC15.2 binding. No possible targets were identified.

After explaining that we do not know the receptor, the follow up question most frequently asked is “With such a great affinity, why don’t you just use IP/MS?” Part of the problem with this new assay development, is that there is no way to optimize. To optimize we need to follow the receptor, but the purpose of the experiments is to identify the receptor.

A comprehensive analysis of the transcriptome of cancer lines, including many of the NSCLC lines we tested, was recently published. Cell lines that bind HCC15.2, were sorted from non-binders and peptide internalization and gene expression were plotted, looking for linear correlation. Several biologically relevant proteins, Integrin α3, Integrin α6, Axl, HCAM, EphA2, N-cadherin, and CDCP1, have been identified as possible receptors in this manner. Experiments to knockdown protein expression to look for a decrease in peptide internalization are currently underway.

If the above proteins are not the receptor, another approach under consideration, would be to buy siRNA libraries to cell surface proteins, and screen for loss of peptide binding and internalization. Looking for loss of signal is less sensitive than gain of signal and this method is labor intensive and expensive.

A different screen, using CRISPR technology could be performed in a similar manner. CRISPR gene knockout libraries are becoming more widely available and cheap. This library would be used in binding cell lines, and then challenged with peptide incubation. Wells that no

longer internalized peptide could be pooled and deep sequenced looking for related proteins responsible for internalization. While the libraries are relatively cheap, deep sequencing is not.

Outsourcing is the most expensive option. RetroGenix is a company that has built a library of human plasma membrane proteins. This library is expressed in cells in an array, then exposed to the labelled ligand. This approach rapidly screens ~4,500 membrane proteins in a gain of signal assay and claims to be 4x more effective than typical proteomics/MS approaches.

6.4 Conclusion

The first question asked after a presentation is, “What does the peptide bind to?” or some variation of the question. Despite a plan and proper execution the receptor remains unidentified. Following the receptor along with HCC15.2 would allow for deeper probing of the biology of cancer and development of other reagents. The identified receptor will likely be a novel biomarker or even target for targeted molecules. I feel that I gave it my best effort for the time and resources available to me. The last experiment I ran with isolating the vesicles was probably the closest I came, and when we have MS capabilities again, I hope to repeat the experiment The benefits of identifying the receptor are even more important as IP for this peptide and its applications have been filed.

6.5 Materials & Methods

6.5.1 Methods

6.5.1.1 Cross-linking

GGH binds Ni(II) as a square planar complex, and in the presence of a strong oxidizer such as magnesium monoperoxyphthalate hexahydrate (MMPP), GGH-Ni facilitates highly

efficient cross-linking of interacting tyrosines with little nonspecific background reaction [6]. GGH-linker-15.2-PEG_{11}-Biotin was synthesized with 3 different linkers by standard FMOC solid phase peptide synthesis. GG, PEG_3, and PEG_{11} and tested by flow cytometry for target binding. GGH labeled peptide is pre-incubated with Nickel (II) Acetate (1:1) for 10 minutes at room temperature. Solution is diluted in phosphate buffered saline PBS to final concentration and the acetate precipitates with phosphate. The solution is centrifuged at 16,000 g for 5 minutes and the supernatant is added to the cells under different conditions. 100µM MMPP is added for 10 minutes and cells are spun down at 1000 g for 5 min and washed once with PBS

6.5.1.2 SDS-PAGE Protein Gel

8% Bis-tris acrylamide 1.5 mm SDS gels were casted using Bio-Rad casting materials. Protein was quantified using Pierce BCA Protein Assay Kit (Thermo Fisher Scientific, Waltham MA). 10-20µg of protein was mixed with NuPAGE™ LDS Sample Buffer (4X) and NuPAGE™ Sample Reducing Agent (10X) (Thermo Fisher Scientific, Waltham MA) before adding samples to wells. Gels were run at 100 V for 60 min in NuPAGE MOPS SDS running buffer in Bio-Rad electrophoresis chambers (Bio-Rad, Hercules CA).

6.5.1.3 Peptide synthesis

As previously described.

6.5.1.4 Coomassie stain

After protein gel has completed its run, remove from glass and incubate it in Coomassie stain for 30 minutes at room temperature. Remove stain and rinse gel in destain (30% acetic acid, 10% methanol) to remove leftover Coomassie. Incubate in copious amounts of destain overnight at room temperature while agitating on a rocker. If needed, knot kimwipes and place them into the destain to remove Coomassie stain from solution.

6.5.1.5 Western Blot

Gels were removed from glass plates and stacking gel was removed. In the Invitrogen blotting system, soak filter paper, nitrocellulose, and gel in MES Running buffer +10% methanol. Stack first filter paper then the gel then pre-wetted nitrocellulose, then filter paper. Making sure the leads are in the right direction, the machine is set for 30 volts for 1 hour.

6.5.1.6 Near Western

Same as western blot but probing with HCC15.2 conjugated to streptavidin-800CW for the protein of interest. Or after crosslinking experiments, blotting with SA-800CW for the biotinylated peptide cross-linked onto the target protein. The protein is run on an sds gel first, then blotted on nitrocellulose, probed with the peptide conjugated to 800CW dye, then wash in TBS + 0.2% Tween20 at least 3 times for 5 minutes each. Blot was imaged on a LICOR Odyssey CLx.

6.5.1.7 Magnetic beads on cells

GGH(Ni)-HCC15.2 was incubated with magnetic streptavidin labelled beads for 30 min at RT and quenched with RPMI. Peptide loaded beads were then incubated with cells for 10 min at 37˚ C. cells and beads were exposed to MMPP for 10 min at RT, then washed with acid rinse and PBS. Pictures were obtained on and inverted light microscope. Or cells were lysed, the beads were washed with PBS, acid, and the crosslinked peptide eluted for further study.

6.5.1.8 Classic Pull-down with Magnetic beads

Cells were lysed in RIPA, or other detergent with protease inhibitor cocktails. Magnetic beads were preloaded with HCC15.2 or quenched with free biotin then incubated with cell lysates at 4˚C overnight on a tumbler. The beads were removed from the lysates and washed 3 times with the RIPA, then eluted with excess HCC15.2 and/or boiled in SDS loading buffer.

6.5.1.9 Plasma Membrane Isolation

Plasma membrane was isolated using Minute™ Plasma Membrane Protein Isolation Kit. Another method to isolate plasma membrane is to expose the cells to hypotonic solution for 10 minutes on ice, rupture cells in a Dounce, then use increasing centrifugation.

6.5.1.10 Vesicle Isolation

H1299 cells were incubated with 50 nM HCC15.2-Alexa Fluor™ 488 for 1 hour at 37˚C. Cells were then lifted off the plate with trypsin and washed once with PBS. Cells were resuspended in cold PBS and put on ice. The French press cell was chilled in the fridge overnight then loaded with cells. The press was pressurized to 2500 lbs and the release valve was turned slowly until the cells began dripping slowly into a 15 mL centrifuge tube on ice. A 50 mL ultracentrifuge tube was loaded with 5 mL of 60% OptiPrep™ then 15 mL of 15% OptiPrep™ was carefully added on top of the 60% layer. This was cooled to 4˚C and lastly, the cell lysates were added on top of the 15% layer. The tubes were balanced and centrifuged at 22,000 g for 2 hours. The tubes were carefully removed and the fractions were collected by aspiration from the top down. Each fraction was collected into microcentrifuge tubes and sampled for fluorescence on a SpectraMax Plus 384 (Molecular Devices, Sunnyvale, CA)

6.6 References

[1] Shepard HM, Phillips GL, Thanos CD, Feldmann M. Developments in therapy with monoclonal antibodies and related proteins. Clinical Medicine. 2017;17:220-32.

[2] Parakh S, Gan HK, Parslow AC, Burvenich IJG, Burgess AW, Scott AM. Evolution of anti-HER2 therapies for cancer treatment. Cancer Treatment Reviews. 2017;59:1-21.

[3] Jackman D, Pao W, Riely GJ, Engelman JA, Kris MG, Jänne PA, et al. Clinical Definition of Acquired Resistance to Epidermal Growth Factor Receptor Tyrosine Kinase Inhibitors in Non–Small-Cell Lung Cancer. Journal of Clinical Oncology. 2010;28:357-60.

[4] Boch C, Kollmeier J, Roth A, Stephan-Falkenau S, Misch D, Grüning W, et al. The frequency of EGFR and KRAS mutations in non-small cell lung cancer (NSCLC): routine screening data for central Europe from a cohort study. BMJ Open. 2013;3:e002560.

[5] McGuire MJ, Gray BP, Li S, Cupka D, Byers LA, Wu L, et al. Identification and Characterization of a Suite of Tumor Targeting Peptides for Non-Small Cell Lung Cancer. Scientific Reports. 2014;4:4480.

[6] Brown KC, Yu Z, Burlingame AL, Craik CS. Determining Protein−Protein Interactions by Oxidative Cross-Linking of a Glycine-Glycine-Histidine Fusion Protein. Biochemistry. 1998;37:4397-406.

[7] Shevchenko A, Tomas H, Havlis J, Olsen JV, Mann M. In-gel digestion for mass spectrometric characterization of proteins and proteomes. Nat Protocols. 2007;1:2856-60.

[8] Brown KC. Peptidic Tumor Targeting Agents: The Road from Phage Display Peptide Selections to Clinical Applications. Current pharmaceutical design. 2010;16:1040-54.